Winter 2008

Tool wear monitoring for milling by tracking cutting force model coefficients

Yanjun Cui
University of New Hampshire, Durham

TOOL WEAR MONITORING FOR MILLING BY TRACKING CUTTING FORCE MODEL COEFFICIENTS

BY

YANJUN CUI

Bachelor of Science, Shandong University, 1997

THESIS

Submitted to the University of New Hampshire
in Partial Fulfillment of
the Requirements for the Degree of

Master of Science
in
Mechanical Engineering

December, 2008

This thesis has been examined and approved.

Thesis Director, Dr. Robert B. Jerard
Professor of Mechanical Engineering

Thesis Co-Director, Dr. Barry K. Fussell
Professor of Mechanical Engineering

Dr. Brad L. Kinsey
Associate Professor of Mechanical Engineering

12-08-2008
Date

ACKNOWLEDGEMENTS

I wish to thank my supervisor, Dr. Jerard, for the support, encouragement and guidance that allowed me to complete my graduate studies. I would also like to thank my committee members, Dr. Fussell and Dr. Kinsey, for their thorough review of this paper and many constructive suggestions.

I would like to acknowledge all of my lab partners for their support and friendship. Min, Bennett, Chris, Jeff, and Raed have been great coworkers. I would also like to thank Donald Esterling for his time and input.

The support of the National Science Foundation under grants DMI-0620996 and IIP-0810434 is gratefully acknowledged.

Most of all, I would like to thank my wife, Jing, and my daughter, Linda, for all of their love and support. Without them, I would not have made it through.

TABLE OF CONTENTS

TABLE OF FIGURES

LIST OF TABLES

LIST OF SYMBOLS

a	----	axial depth, (mm)
b	----	radial depth, (mm)
V	----	Cutting speed (mm/min)
f	----	Feed rate (mm/min)
f_t	----	feed per tooth (mm/tooth)
r	----	radius of tool (mm)
ω	----	spindle speed (rpm)
$h(\Phi)$	----	chip thickness at Φ (mm)
h_{avg}	----	average chip thickness (mm)
Ft	----	tangential cutting force (N)
Fr	----	radial cutting force (N)
K_{TC}	----	model parameter for tangential shearing force component (N/mm^2)
K_{TE}	----	model parameter for tangential rubbing force component (N/mm)
K_{RC}	----	model parameter for radial shearing force component (N/mm^2)
K_{RE}	----	model parameter for radial rubbing force component (N/mm)
P	----	average cutting power (N*mm/sec)
$\dot{Q}$	----	average material removal rate (mm^3/sec)
$\dot{A}_c$	----	contact area rate (mm^2/sec)
VB	----	flank wear land width (mm)

ABSTRACT

TOOL WEAR MONITORING FOR MILLING BY TRACKING CUTTING FORCE MODEL COEFFICIENTS

By

Yanjun Cui

University of New Hampshire, December 2008

This study establishes a way to monitor tool wear in end milling using a tangential force model coefficient method. An experimental investigation of the characteristics of tangential force model coefficients, K_{TC} and K_{TE}, under different cutting conditions is presented. Experimental results indicate that the coefficients are relatively insensitive to the cutting conditions and quite sensitive to tool wear. Several tool wear experiments were performed on AISI 1018 steel. The tool wear was examined using an optical measurement inspection system. The results indicate that K_{TE} increases proportionally with tool flank wear while K_{TC} stays relatively constant until close to the end of tool life. Other possible wear indicators were studied, specifically the radial coefficients (K_{RC} & K_{RE}) and vibration signals. It was found that K_{RC} & K_{RE} are proportional to K_{TC} & K_{TE}, and the vibration signal magnitude is related to flank wear.

Chapter 1

INTRODUCTION

In metal cutting operations, it is important to select machining conditions that balance the compromise between product quality and production costs. Therefore, a tool condition monitoring (TCM) system can play a critical role in guaranteeing a reliable and stable cutting process. A significant amount of tool monitoring research has been performed to identify tool wear status and two comprehensive surveys of various methods were published by Prickett [1] and Rehorn [2]. Altintas [3] and Li et al. [4] developed intelligent tool wear monitoring systems based on the cutting force using inexpensive current sensors. Kim and Klamecki [5] investigated the tool wear in the end milling process using spindle shaft torsional vibration. Acoustic emission has been proposed as an indicator of tool wear [6, 7], especially for operations where spindle current or force measurement is ineffective. Cutting force is often the most reliable information source; however, its characteristics, in addition to tool wear, vary with change in cutting conditions. Xu [8] and Jerard [9] proposed a new energy based cutting force model, which uses an inexpensive and non-invasive spindle motor power sensor for in-process force estimation over a wide variety of cutting conditions. The tangential force model coefficients K_{TC} and K_{TE} show correlation with tool wear exhibiting a steady increase in K_{TE} as wear continues and a sharp increase in K_{TC} near the end of tool life.

Over the last few decades, TCM systems may be divided into two main groups, i.e. direct methods [10, 11] which measure the tool surface directly, and indirect methods

[12–16] which measure physical phenomena that are correlated with the tool wear such as force, vibration, power, etc.

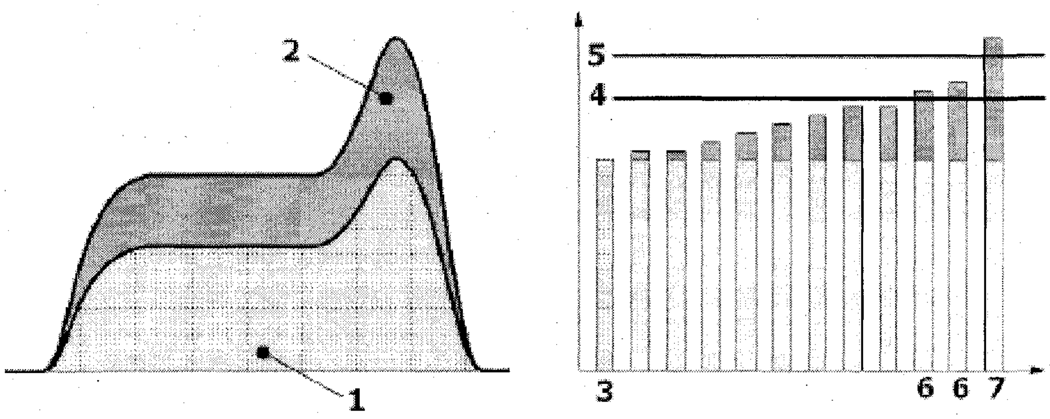

Figure 1-1. Tool-wear-monitoring strategy used in most TCM systems [6]: 1, area signal learned 100 percent; 2, larger area signal (e.g. through worn tools); 3, learned area (bar diagram); 4, pre-alarm limit (e.g. 130 per cent), wear limit (e.g.150 per cent); 6, pre-alarm (area exceeds wear limit); 7, wear alarm (area exceeds wear limit)

For most existing TCM systems, the monitoring strategies are largely based on limits and envelope functions. The sensor signal of the typical machining operation is measured and stored in the database as the reference pattern. During subsequent machining operations, online decision making is implemented by comparing sample signals with the reference pattern. **Figure 1-1** presents a typical strategy for tool wear monitoring.

The major limitation of the above monitoring strategy is that if any process variables are changed, (e.g. spindle speed, tool material, radial/axial depth) then the threshold of the signal which corresponds to a worn tool will change, and it therefore becomes necessary to retrain the system, as shown in **Figure 1-2**. Thus, using a percentage increase of the signal amplitude to assess tool condition is only viable when both the cutting conditions and the tool failure mode are identical. This imposes a severe limitation on the existing commercial TCM systems.

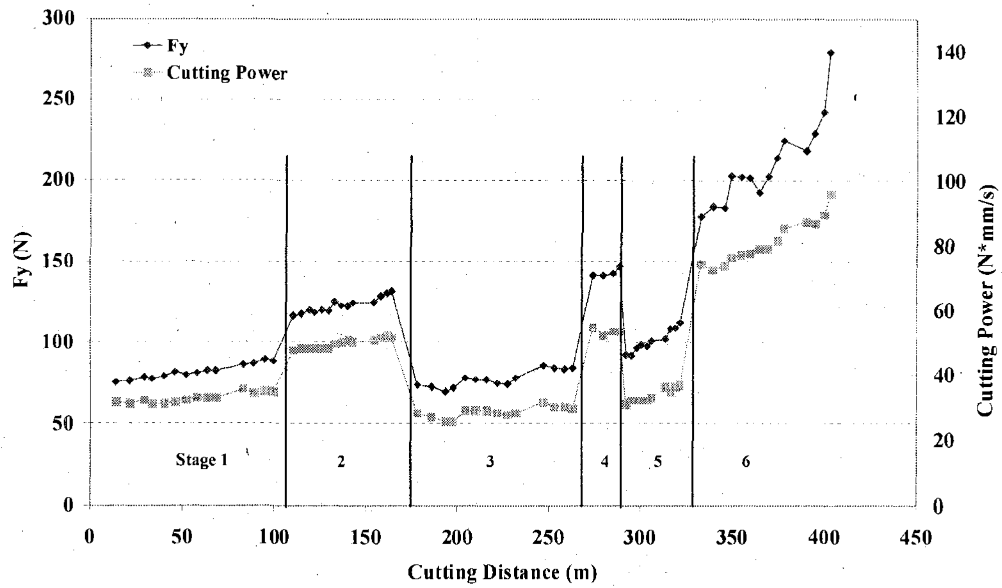

Figure 1-2. Cutting stages with varied cutting parameters

In this research we use an approach based on the threshold of coefficients of the tangential cutting force model, K_{TC} and K_{TE}, to estimate the tool wear state. This method has the potential to estimate tool wear without the necessity of a retraining process. The model is calibrated by measuring spindle motor power over a variety of cutting geometries. The influences of tool wear mode and cutting conditions on the characteristics of the tangential force model coefficients in flat-end milling are investigated. A variety of wear tests using high-speed steel cutters, carbide cutters and coated inserts are used to develop and evaluate this TCM system. Experiments show that K_{TC} and K_{TE} have a high sensitivity to tool wear and are insensitive to cutting conditions, and it is therefore simpler and more convenient to monitor the tool wear than existing traditional TCM systems.

1.1 Tool Wear

Tool wear in machining is defined as the amount of volume loss of tool material on the contact surface due to the interactions between the tool and workpiece. Because of its effects on both the economics of cutting and the quality of the resultant machined surface, tool wear is usually undesirable and should be minimized. A wide variety of factors are involved in tool wear, such as tool and workpiece material, tool geometry, cutting environment, and cutting conditions like cutting speed, feedrate, and depth of cut.

Wear may be classified into several types as follows:

- Abrasive wear (due to the cutting action of hard material)
- Adhesion wear (a part of the tool forms a bond with the chip and is carried away)
- Erosive wear (cutting action of particles in a fluid)
- Diffusion wear (due to high surface temperature and stress)
- Corrosive wear (due to chemical attack of a surface)
- Fracture wear (chipping of brittle surface)
- Delamination wear (subsurface microcracks join up to produce laminar wear particles)

Wear is an intricate phenomenon influenced by a multitude of these types of wear that may occur simultaneously, or one of them may dominate the process. For example, in milling, adhesive wear is found mainly at low temperatures (Gu et al. [18]) due to the formation of the unstable Build-Up Edge (BUE) formed at the chip–tool interface, which breaks away in small pieces or fractures. When higher cutting temperatures are reached, the adhesive strength between the work material and the tool is increased by diffusion and recrystallization of work material, and the conditions for this phenomenon are largely reduced due to the reduced probability of BUE being detached from the tool. Therefore, the types of wear on a tool depend on the relative roles of these mechanisms. In general, the wear behavior of a cutting tool can be identified as either: (1) gradual wear: *flank wear*; or (2) catastrophic wear: *chipping* or *groove wear* on the cutting edge, see **Figure 1-3**, Kalpakjian [19].

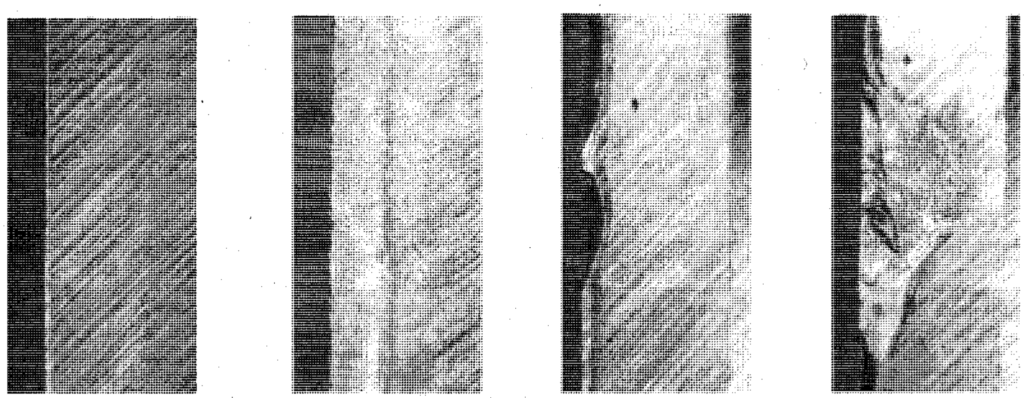

(a) No wear **(b) Flank wear** **(c) Chipping** **(d) Groove wear**

Figure 1-3. Common wear types

1.1.1 Flank Wear

Flank wear is commonly caused by abrasive wear of the cutting edge against the machined surface, which has detrimental effects on part surface integrity including surface finish, residual stress, microstructure, etc. The flank wear land is measured as the average width of the wear land (VB) on the primary clearance face, as shown in **Figure 1-4 (a) [12] and (b)**. Flank wear is widely used as the accepted tool life criteria in industry.

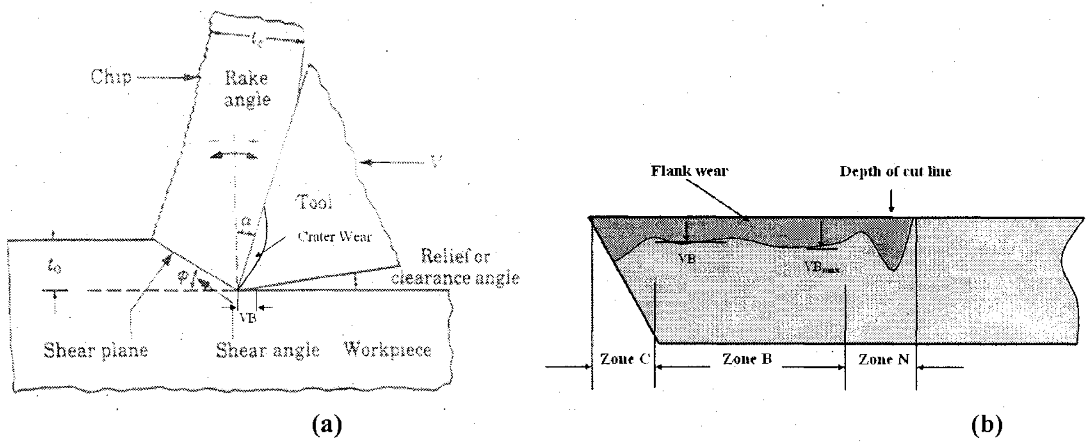

Figure 1-4. Cutting Geometry and Typical profile of flank wear

The tool life criterion is entirely concerned with the profile of the leading edge in zone **B,** as shown in **Figure 1-4(b).** According to ISO 8688-2:1989 (E) [32], if the profile is uniform, the average width (VB) of the wear land is measured and a tool can be used until VB exceeds 0.3 mm. In the case of uneven wear, the maximum peak land width of the groove VB_{max} is taken as the tool life criterion and its limit is 0.6 mm.

1.1.2 Chipping

In general, tool chipping in milling occurs at about half or less of the chip thickness in continuous cutting due to ***Mechanical Shock*** and ***Thermal fatigue*** when the maximum principal tensile stress reaches a critical value. Chipping results in a sudden loss of tool material and gives a wide dispersion of tool life.

Chipping by mechanical shock has to do with the stress distribution when the tool enters and exits the cutting zone, as shown in **Figure 1-5**. During these stages, the loading on the tool changes; increased tensile stresses arise in the tool and the shear stress at the cutting edge increases. This can lead to chipping at a chip thickness much smaller than in continuous cutting. The entry damage plays a significant role in milling hard material, while the exit damage is more decisive for the ductile and softer materials [20].

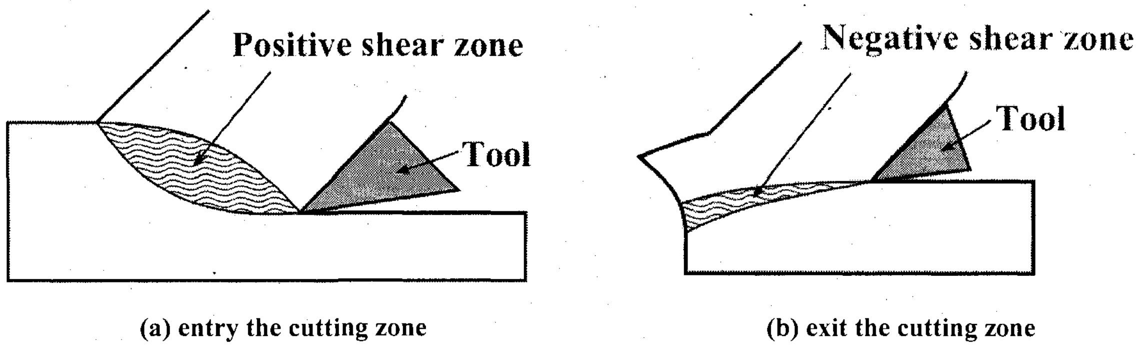

Figure 1-5. Formation of shear zone at the entry and exit from the cutting [20]

Meanwhile, the tool is heated during cutting and cooled after it leaves the cutting zone. The periodic thermal cycling causes alternating expansion and contraction of the tool leading to the formation of comb cracks, which progress toward the tool edge and weaken it, causing chipping [21].

1.1.3 Groove Wear

Deep groove wear frequently occurs when machining high temperature alloys, very soft steels, or other materials having a strong tendency to strain harden. Shaw et al. [22] investigated the main source of groove wear in turning and concluded that the flow of chip material at the cutting edges was the main cause (see **Figure 1-6**).

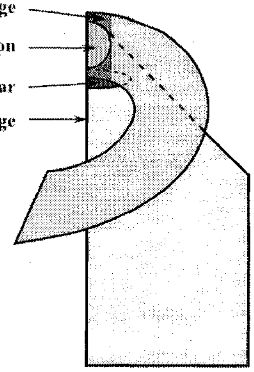

Figure 1-6. Groove wear formed at glowing edge of chip [22]

When a high temperature alloy was being turned under normal conditions, the edges of the chip glowed while the central region did not. Since the rate of heat transferring from edges of the chip is much greater than the central region, the observed red-hot edges can only mean that more energy was expended in chip formation in the vicinity of the edges of chip than elsewhere [22].

Other reasons for groove formation have been proposed as below [22]:

- Formation of thermal cracks due to the steep temperature gradient at the cutting edges.
- Stress concentration due to the stress gradient at the cutting edges.
- Presence of a burr at the edge of the freshly machined surface.

1.2 Factors Affecting Tool Wear

In 1907, F. W. Taylor [20] first introduced the famous tool-life equation that showed a relationship between the rate of tool wear and the cutting speed for machining various steels. Through the years a great number of studies on tool life have been proposed to describe the effects of various cutting variables on the tool life.

1.2.1 Temperature and Cutting Environment

Because of the major influence of temperature on the physical and mechanical properties of material, the variation of thermal stress is a major contributor to tool wear in milling. When the tool periodically enters and exits from the workpiece, it is heated during cutting and cooled after it leaves the cutting zone. In each thermal cycle, during the heating-up period the faces of the tool are hotter than the inside and compressive stresses arise on the tool surface. During the cooling-off period, faces are cooler than the inside, and tensile stresses occur. This variation of thermal stress accelerates flank wear.

Traditionally, cutting fluids have been seen as a solution to reduce workpiece temperature and distortion, friction and wear, hence improving tool life and surface finish. However, in milling the use of cutting fluid can be detrimental. The cooling actions increase the extent of the thermal cycle which leads to more severe thermal stresses. Trent and Wright [23] concluded that coolant cannot act directly on the heat source which is the thin flow-zone on the tool/work interface. The coolant removes heat from the surfaces of the chip, the workpiece and the tool but has little effect on the temperature at the tool/work interface. Childs et al. [24] also stated that flood-cooling is most effective in reducing the bulk temperature of the tool and holder, but is less effective in reducing the tool flank temperature and least effective in reducing tool/chip contact temperature. Billatos and Basaly [25] reported that cutting fluids were responsible for the reduction of crater wear and the increase of the groove wear.

1.2.2 Tool Geometry

Based on the discussion of *Section 1.1*, the effective ways to prevent or at least diminish chipping or groove wear are to strengthen the brittle cutting tools by a chamfered/honed edge or using the largest permissible side cutting edge and negative rake angle , as shown in **Figure 1-7 [20]**.

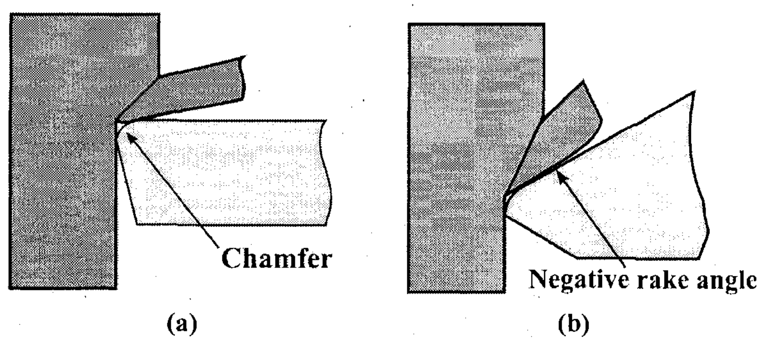

Figure 1-7. Tool geometry to strengthen the cutting edge

Rech [26] showed that when comparing a standard ground end-mill and a tool "mechanically treated" with a radius of 10μm, one can observe the impressive improvements of between 400 to 500% in the tool life, as shown in **Figure 1-8**.

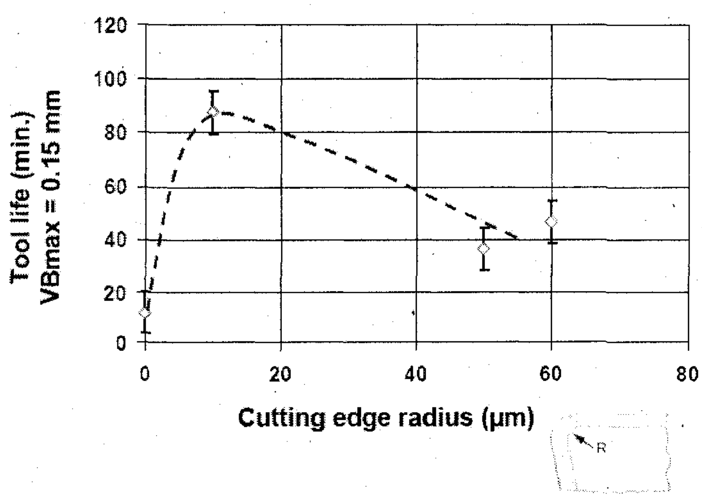

Figure 1-8. Influence of the cutting edge radius with a PM-HSS end-mill (Rech [26])

1.2.3 Cutting Path

Since the variation of shear stress has a great effect on tool life, as discussed in Section *1.1.2*, it is necessary to find an optimal exit angle to minimize the stress variation. The exit angle (ε_2) is defined as the angle that the motion of the cutting edge makes with the workpiece as shown in **Figure 1-9**. Tulsty [20] and Peklharing showed that down milling with $\varepsilon_2 = 0$ gives the most number of cuts before chipping. It was also found that as the exit angle increases the number of cuts dramatically decreases till $\varepsilon_2 = 105°$. For half immersion up-milling, i.e. $\varepsilon_2 = 90°$ to $105°$, is worst. For quarter immersion up-milling, $\varepsilon_2 = 60°$, is considerably better. When $\varepsilon_2 \geq 120°$, cutting is safe from breakage, but a large burr was created.

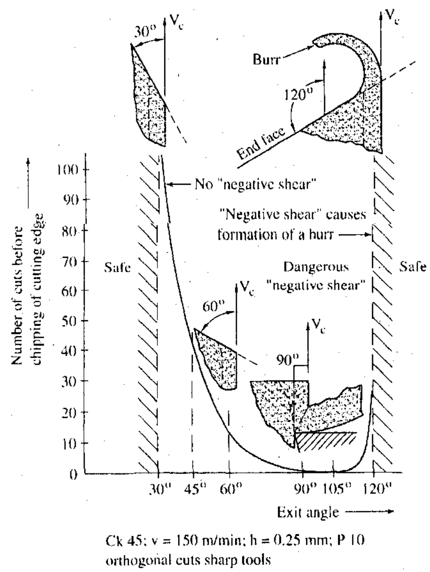

Figure 1-9. Safe exit angles – Tlusty [20 pg 484]

1.2.4 Material

The hardness of the work material plays a critical role in the flank wear rate. The lower hardness is associated with the annealed condition and the higher with the hardened and tempered state. In general, a harder work material will result in higher cutting force and tool temperatures, leading to greater tool wear, as shown in **Figure 1-10**. However, the hardness of the workpiece material may not be the only factor affecting the flank wear rate. The composition and microstructure are also important considerations.

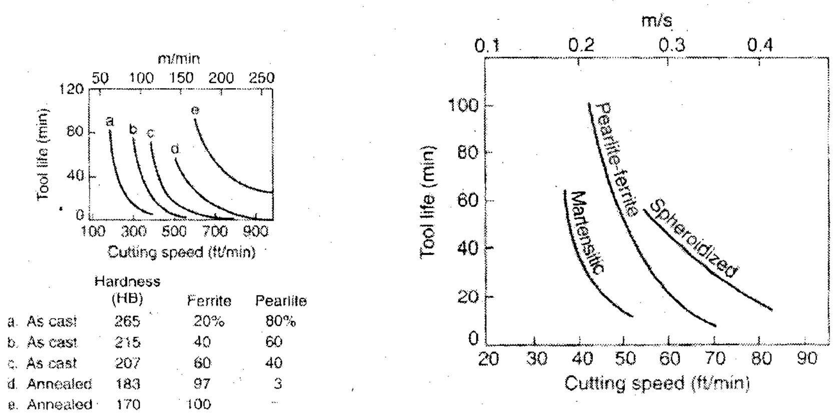

Figure 1-10. Effect of workpiece hardness and microstructure on tool life (Kalpakjian[17])

1.2.5 Cutting Speed and Feedrate

Experimental investigations have shown that cutting speed is the most significant variable in tool wear (see **Figure 1-11(a)**), followed by the feedrate (see **Figure 1-11(b)**) and depth of cut. As shown in **Figure 1-11**, at lower cutting speeds (stage "b-o") the wear rate increased due to the development of BUE and at higher cutting speed (stage "o-d") the wear rate increased due to increased temperature in the cutting zone.

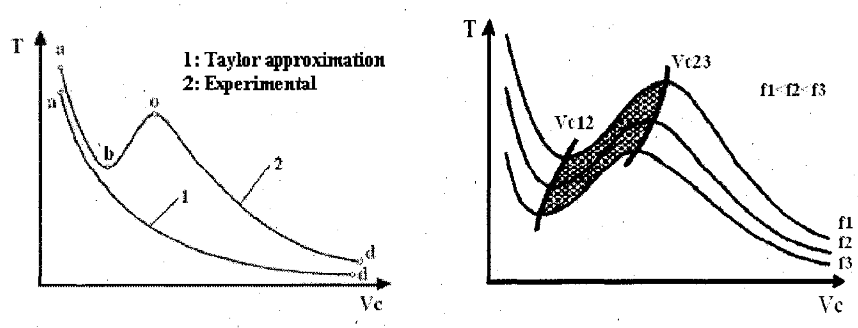

(a) Typical tool life curves **(b) Tool life vs. feedrate**

Figure 1-11. Tool life curves using Taylor's expansion equations (Kalpakjian [17])

1.2.6 Thesis Outline

This investigation explores the feasibility of using cutting force model coefficients to estimate the magnitude and type of wear during milling. In Chapter 2 the models of our research and experimental methods will be described. In Chapter 3 the results of the calibration experiments will be presented. Experimental results show that changing cutting conditions, e.g. cutting speed, feedrate and radial immersion, do not affect K_{TC} and K_{TE}. The tangential cutting force model coefficients (K_{TC} and K_{TE}) are highly correlated to tool wear. In Chapter 5 wear test experiments on cutting AISA-1018 steel were performed with three typical cutting tool types: a) coated carbide inserts, b) High Speed Steel (HSS) and c) solid uncoated carbide. It was found that the behavior of the coefficients as a function of cutting distance is almost identical for all tools types. These observations are used in Chapter 6 to formulate a new method for online TCM in which K_{TC} is assumed constant and K_{TE} is estimated by a simple spindle power measurement. In Chapter 7 other possible wear indicators were studied, specifically the radial coefficients of a cutting force model (K_{RC} & K_{RE}) and vibration signals. It was found that K_{RC} & K_{RE} are proportional to K_{TC} & K_{TE}, and the vibration signal magnitude is related to flank wear.

Chapter 2

METHODOLOGY

2.1 Tangential Force Model

In milling, the cutter is subjected to tangential, radial and axial forces. The cutting force components are derived as projections of the resultant cutting force F, which is formed by the friction force on the rake face and normal force to the rake (see in **Figure 2-1**).

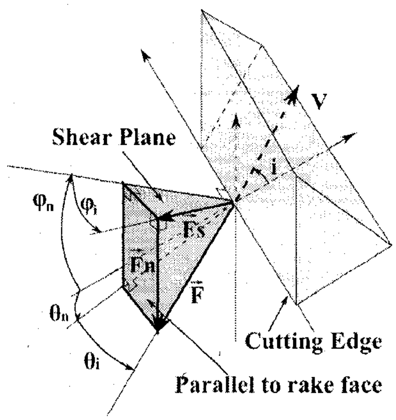

Figure 2-1. Force diagram in oblique cutting [12]

The average tangential force for a flank end mill cut can be shown to be [12, Pg 24]:

$$F_t = F(\cos\theta_i \cos\theta_n \cos i + \sin\theta_i \sin i)$$

$$= \frac{\tau_s a h(\cos\theta_n + \tan\theta_i \tan i)}{[\cos(\theta_n + \varphi_n)\cos\varphi_i + \tan\theta_i \sin\varphi_i]\sin\varphi_n} \tag{2-1}$$

It is convenient to express the tangential cutting force in the following form:

$$F_{t_{avg}} = K_{TC} \cdot h_{avg} \cdot a + K_{TE} \cdot a \tag{2-2}$$

where K_{TC} and K_{TE} represent the cutting coefficient and edge coefficient, respectively, a is the axial depth of cut and h_{avg} is the average chip thickness, as shown in **Figure 2-2**, which is defined as the average value over the angular increments where the cutting edge is engaged with the workpiece. It can be shown that [9]:

$$h_{avg} = \frac{1}{\phi_{eng}} \int_{\phi_{ent}}^{\phi_{ext}} f_t \cdot \sin(\phi) \cdot d\phi = \frac{\dot{Q}}{\dot{A}_c} \tag{2-3}$$

where f_t is the feed per tooth, $\dot{Q}$ is the is the material removal rate and $\dot{A}_c$ is the contact area rate, both of which are determined by the cutting conditions and can be pre-calculated for each tool move [8]. The contact area rate is simply the area of contact between the tool and the workpiece divided by the tooth passing period [9, 13].

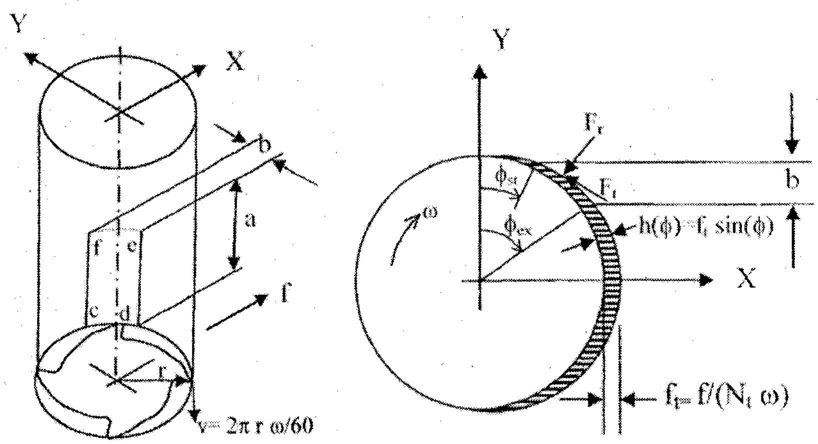

Figure 2-2. Geometry of milling process

For constant axial and radial depth, the average chip thickness in **Equation 2-3** can be simplified to:

$$h_{avg} = \frac{f \cdot b}{r \cdot \omega \cdot n \cdot \Delta\varphi} \tag{2-4}$$

where b is the radial depth, r is the cutter radius, ω is the cutting speed (rpm), n is the number of teeth, $\Delta\varphi$ is the difference of the entry and exit angle of cuts. For example, a half immersion up milling cut has an entry angle of zero and an exit angle of 90 degrees (note that this is a different definition for exit angle than as used in Section 1.2.3).

The average cutting power is proportional to the torque caused by tangential forces and can be easily measured with inexpensive power sensors. From energy principles [8, 9, 13] we obtain the general relationship:

$$P_{avg} = K_{TC} \cdot \dot{Q} + K_{TE} \cdot \dot{A}_c \tag{2-5}$$

The average tangential force is related to the average power and h_{avg} by **Equations 2-2** and **2-6**:

$$\frac{F_{t-avg}}{a} = \frac{P_{avg}}{\dot{A}_c} = K_{TC} \cdot h_{avg} + K_{TE} \tag{2-6}$$

By separating the power into two components it is possible to discriminate between the energy used in cutting the material from the energy dissipated in rubbing. Our research indicates that the rubbing energy correlates well with flank wear and by isolating this term the tool wear effect on power is isolated.

To calibrate the tangential force model coefficients (K_{TC} & K_{TE}), the average power at a minimum of two different h_{avg} values must be measured. The slope and intercept of the graph shown in **Figure 2-3** are found by linear regression. Therefore, a calibration data point requires measurement of power and knowledge of the volumetric removal rate and the contact area between the cutter and the workpiece. Power is easily measured via an inexpensive, non-invasive power sensor and the other two quantities can be estimated by a geometric modeling program (e.g. Predator Software [33]).

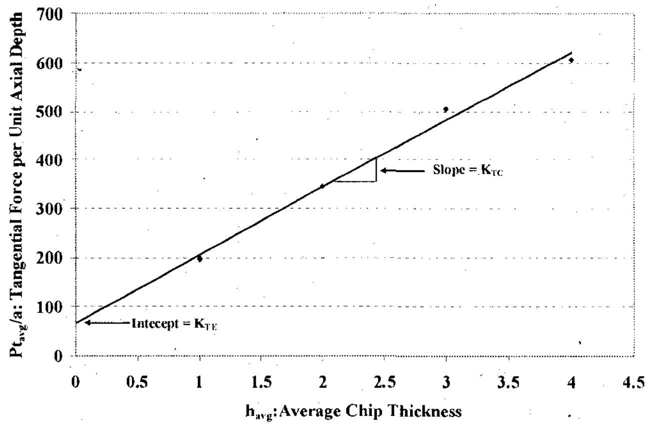

Figure 2-3. Model predicted tangential force plot

2.2 Radial Force Model Coefficients - K_{RC} & K_{RE}

In **Figure2-2**, the horizontal and normal components of the cutting forces acting on the cutter are derived as:

$$dF_x(\phi) = -dF_t \cos\phi - dF_r \sin\phi \tag{2-7}$$

where $dF_t(\phi, z) = (K_{TC} h(\phi, z) + K_{TE})dz$, $dF_r(\phi, z) = (K_{RC} h(\phi, z) + K_{RE})dz$

The average force in the x direction is:

$$\overline{F}_x = \frac{N}{2\pi} \int_{\phi_{ent}}^{\phi_{ext}} F_x(\phi) d\phi$$

$$= \left\{ \begin{array}{l} \dfrac{Naf_t}{8\pi}\left[K_{TC}\cos 2\phi - K_{RC}(2\phi - \sin 2\phi)\right] \\ + \dfrac{Na}{2\pi}\left[-K_{TE}\sin\phi + K_{RE}\cos\phi\right] \end{array} \right\}_{\phi_{ent}}^{\phi_{ext}} \tag{2-8}$$

where N is the total number of teeth, and f_t is the feed per tooth. Since K_{TC} & K_{TE} can be calculated by the method discussed in the previous section and other variables can be estimated by a geometric modeling program, K_{RC} & K_{RE} are derived from **Equation 2-9**:

$$[B_1]=[A_1 \quad A_2]\begin{bmatrix}K_{RC}\\K_{RE}\end{bmatrix} \tag{2-9}$$

where,

$$\begin{aligned}
A_1 &= -\frac{Naf}{8\pi}(2\phi_{ext} - 2\phi_{ent} - \sin 2\phi_{ext} + \sin 2\phi_{ent}) \\
A_2 &= -\frac{Na}{2\pi}(\cos\phi_{ext} + \cos\phi_{ent}) \\
B_1 &= \bar{F}_x - \frac{Naf}{8\pi}(\cos 2\phi_{ext} + \cos 2\phi_{ent})K_{TC} + \frac{Na}{2\pi}(\sin\phi_{ext} + \sin\phi_{ent})K_{TE}
\end{aligned} \tag{2-10}$$

2.3 Tool Wear Experiments and Setup

As previously discussed, for conventional Tool Condition Monitoring (TCM) systems, if any process variables are changed during cutting, e.g. spindle speed, feedrate or cutting depth, the threshold of the signal feature will vary greatly. Therefore, an ideal tool wear indicator should have the following characteristics:

- Insensitive to cutting conditions
- High correlation to tool wear
- Measurements don't interrupt the cutting process
- Non-invasive sensors which do not affect system compliance.

For experimental verification of the hypothesis that tangential force model coefficients are reliable indicators of tool wear, a number of calibration and tool wear experiments were performed as listed in Table 2-1. Four kinds of cutters, i.e. uncoated carbide, HSS

Flat End Mill, HSS Ball End Mill, and coated carbide inserts were used to investigate the characteristics of the cutting coefficients K_{TC} & K_{TE}. Table 2-1 summarizes the experimental conditions and procedures as discussed in Appendix A and B. Tables of experimental data can be found in Appendix C.

- Calibration experiments C1 - C4 (see Table 2-1) were designed to verify that the coefficients are relatively insensitive to cutting speed, average chip thickness (feedrate), and radial depth, while they are affected by the helix angle.
- Experiments W1 and W2 (see Table 2-1) investigated the influence of flank wear on the coefficients while using both conventional and artificial methods to wear tools. W2 was performed with an artificial method to wear the coated carbide insert as shown in **Figure 2-4**.

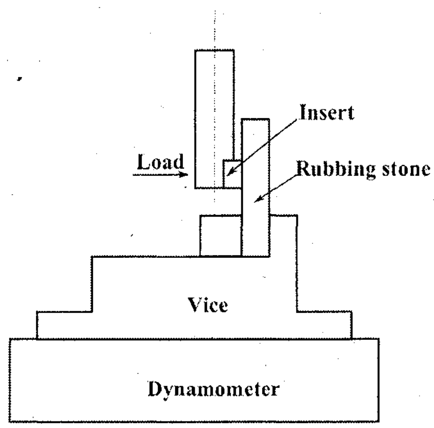

Figure 2-4. Artificial method to wear the tool

The insert tool rotated in the counterclockwise direction, and was worn by a rubbing stone with a constant cutting speed of 500 rpm, and a constant side loading, f = 89 N, was measured by a Kistler dynamometer. The repeated period of wearing was 2 minutes, then the insert was calibrated on an AISI-6061 aluminum block at the cutting speed V = 125 m/min and feedrates f = {0.03, 0.04, 0.05, 0.06} mm/tooth (see Appendix A).

Table 2-1. Experiment Description

			Spindle Speed (rpm)	feed per tooth (mm)	Feedrate (m/min)	Entrance/ Exit Angles (deg)	Radial Depth (mm)	Tool Life Cutting Distance (m) 40%	80%
Experiments	Calibration	C1	2500	0.01/0.02/0.03/0.04 /0.05/0.06/0.07 /0.08/0.09/0.10/0.11	0.15/0.2/0.3/0.43 /0.55/0.67/0.76 /0.89/1.02/1.14/1.27	0/90	6.35		
		C2	1500/2000/2500 /30003500/4000 /4500/5000	0.03/0.05/0.08/0.10	0.12/0.22/0.36/0.48	90/180	6.35		
		C3	3000	0.00635/0.00127 /0.03/0.05/0.08/0.10	0.07/0.12/0.24 /0.36/0.48/0.64	90/180	12.7/9.525 /6.35/3.175		
		C4	2500	0.0025/0.0038 /0.0044/0.0051	0.26/0.39 /0.45/0.52	0/68.9	5.08		
	VB	W1	880	0.01/0.02/0.03/0.04	0.04/0.10/0.12/0.17	0/90	6.35		
		W2	2500	0.02/0.03/0.04 /0.05/0.08	0.09/0.15/0.22 /0.26/0.44	0/68.9	5.08		
	Wear (Crabide)	TC1	2500	0.04	0.15	90/180	6.35	1016	1143
		TC2	2500	0.05	0.18	90/180	6.35	750	934
		TC3	2500	0.03	0.10	90/180	6.35	931	1071
		TC4	2000	0.04	0.12	90/180	6.35	1064	1380
		TC5	3000	0.04	0.18	90/180	6.35	1081	1270
		TC6	2500	0.04	0.15	90/180	6.35	820	1181
		TC7	2500	0.04	0.20	120/180	3.18	662	748
		TC8	2500	0.04	0.15	0/90	6.35	1016	1355
	Wear (HSS)	TH1	880	0.03	0.04	90/180	6.35	508	755
		TH2	880	0.05	0.06	90/180	6.35	576	1037
		TH3	1100	0.03	0.05	90/180	6.35	506	823
	Wear (Insert)	TI1	2500	0.04	0.18	0/68.9	5.08	1685	
		TI2	2500	0.08	0.38	0/68.9	5.08	2022	
		TI3	4000	0.04	0.29	0/68.9	5.08	1811	
		TI4	2500	0.04	0.18	111.1/180	5.08	1785	

1. Experiments C1-C3 and W2 were performed on 6061 aluminum blocks, and C4 was performed on 6061 aluminum thin plate.
2. Wear Experiments and W1 were performed with AISI 1018 steel blocks.
3. Experiments W2 was performed with one SANDVIK 15.875mm, 21-degree helical, carbide insert;

   Experiments C1 was performed with 12.7mm diameter, 2 flutes, 30-degree helical, carbide flank end mill cutters.

   Experiments C4 was performed with 19.05mm diameter, 2 flutes, ball-end mill cutters.
4. Other experiments were operated wit 1 flute cutters.
5. In-process calibrations were performed periodically in tool wear experiments.
6. The axial depth of all experiments: AD = 5.10mm.
7. Except Experiment TC6, all other experiments were performed with coolant

- Tool wear experiments (TC, TH, and TI) explored the relationship between the coefficients and tool wear induced by a variety of cutting conditions. Nominal uncoated carbide end mills, HSS flat end mills, and coated carbide inserts were employed for all tool wear experiments. In order to eliminate the effect of runout, all tool wear experiments were performed with one-flute cutters.

The tangential force model coefficients, K_{TC} & K_{TE}, were calibrated based on the cutting power and were used to estimate tool wear. The test bed was a Fadal EMC CNC milling machine fitted with an open architecture MDSI Controller. The workpieces were aluminum alloy AISI-6061 and low-carbon steel AISI-1018. The electrical spindle motor power was measured with a UPC power sensor from Load Control Inc. Tare power was subtracted to determine the mechanical cutting power based on motor efficiencies under different cutting speed [8]. All the data was collected with an A/D board sampling every 3 degrees of rotation for 30 revolutions. The tool wear was examined using an optical measurement inspection system (Mitutoyo) and an LCD capturing microscope (ESPA D3).

Chapter 3

INFLUENCES ON TANGENTIAL FORCE MODEL COEFFICIENTS

As discussed in the previous section, in the machining process, an ideal tool wear indicator should be acceptable and reliable at various cutting conditions without a retraining process and with the following characteristics:

- Insensitive to cutting conditions
- High correlation to tool wear
- Measurements don't interrupt the cutting process
- Non-invasive sensors which do not affect system compliance.

This chapter presents methods for determining tangential force model coefficients for a general helical end mill from milling tests at an arbitrary radial immersion. The experimental results verify that the tangential force model coefficients, K_{TC} and K_{TE}, satisfy the necessary requirements and can be used as reliable indicators of tool wear.

3.1 Influences of feedrate on K_{TC} & K_{TE}

Coefficients were calculated from 50% radial immersion up-milling tests C1 (see Table 2-1) using an uncoated carbide FEM cutter, D = 12.7 mm, and AISI 6061 aluminum. These were repeated six times at an axial depth a = 5.08 mm and feedrates f = {0.01, 0.02, 0.03, 0.04, 0.05, 0.06, 0.07, 0.08, .09, 0.10, 0.11} mm/tooth. The mean estimates of K_{TC} & K_{TE} are plotted in **Figure 3-1**, which shows that the tangential model accurately predicts the average tangential force and that there is a generally linear relationship between the tangential force and the average chip thickness over the typical range of chip thicknesses. The data also shows that K_{TC} & K_{TE} are insensitive to the average chip thickness for the range of chip thicknesses used in this study.

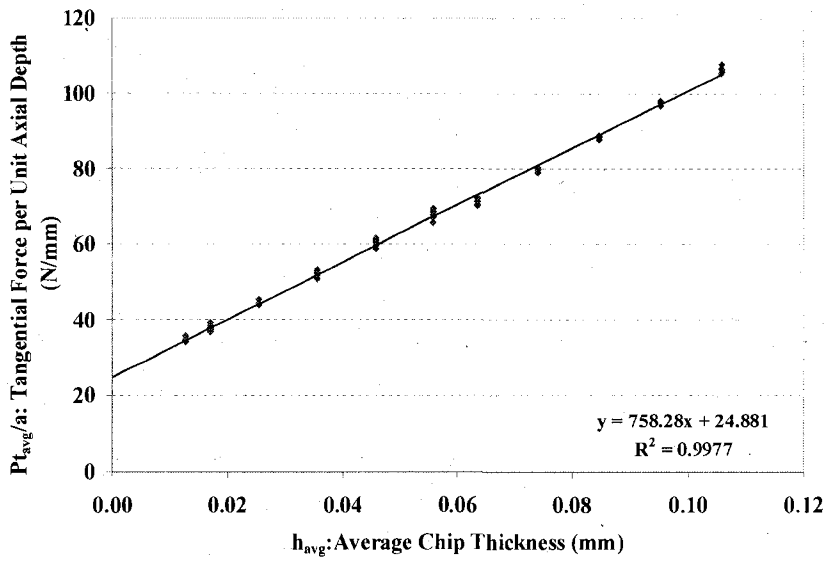

Figure 3-1 K_{TC}&K_{TE} vs. Average Chip Thickness (Experiment C1 - two flutes carbide cutter)

3.2 Influences of cutting speed on K_{TC} & K_{TE}

Experiment C2 with 50% radial immersion down-milling was carried out at eight cutting speeds V = {1500, 2000, 2500, 3000, 3500, 4000, 4500, 5000} rpm using the same cutter and workpiece as Experiment C1. The cutting coefficients K_{TC} (slope) & K_{TE} (intercept) under different cutting speeds are plotted in **Figure 3-2**. It can be seen that values of K_{TC} & K_{TE} are almost constant over this range of cutting speeds. The main reason for the deviation of K_{TE} is the fluctuation of the measured cutting power. **Equation 2-6** and **3-1** show that if the contact area rate ($\dot{A}_c$) is very small and K_{TC} is constant, even a little change in the cutting power would cause a large deviation from the normal results.

$$\frac{P_{avg} + \Delta P}{\dot{A}_c} = K_{TC} \cdot h_{avg} + (K_{TE} + \Delta K_{TE}) \longrightarrow \frac{\Delta P}{\dot{A}_c} = \Delta K_{TE} \tag{3-1}$$

It indicates that in order to get stable and reliable results, the calibration tests should be performed with large cutting depth or cutting speed to make the contact area as large as possible. It also should be noted that a slight change in K_{TC} may produce a large percent change in K_{TE}, and we have dubbed this the “see-saw” effect.

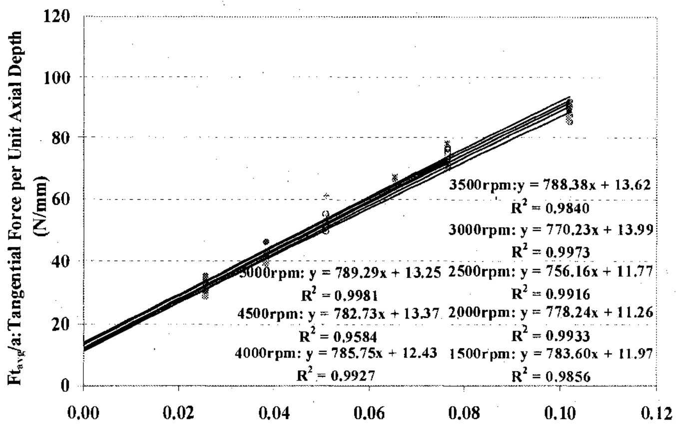

Figure 3-2. K_{TC}&K_{TE} vs. Cutting Speed (Experiment C2 - one flute carbide cutter)

Table 3-1. Variation of K_{TC} (N/mm^2) and K_{TE} (N/mm) with cutting speed

	Cutting Speed (rpm)									Standard	Coeff of
	1500	2000	2500	3000	3500	4000	4500	5000	Average	Deviation	Variation
Ktc	783.60	778.24	756.16	770.23	788.38	785.75	782.73	789.29	779.30	10.45	0.0134
Kte	11.97	11.26	11.77	13.99	13.62	12.43	13.37	13.25	12.71	0.92	0.0726

3.3 Influences of radial immersion on K_{TC} & K_{TE}

Experiments C3 was carried out at a series of radial depth b = {100%, 75%, 50%, 25%} using the same cutter and workpiece as Experiment C1. The influence of changing radial immersion is summarized in **Figure 3-3**. As expected, despite of the fluctuation of the tare cutting power, no systematic variations of K_{TC} & K_{TE} are observed as the radial immersion changes so the cutting coefficients are insensitive to the cutting radial depth. However, since full immersion milling is more vulnerable to chatter vibrations, when variation of the coefficients under different radial immersions are the same and the contact area ($\dot{A}_c$) is relative large, half radial immersions may be the best practical choice for performing the calibration.

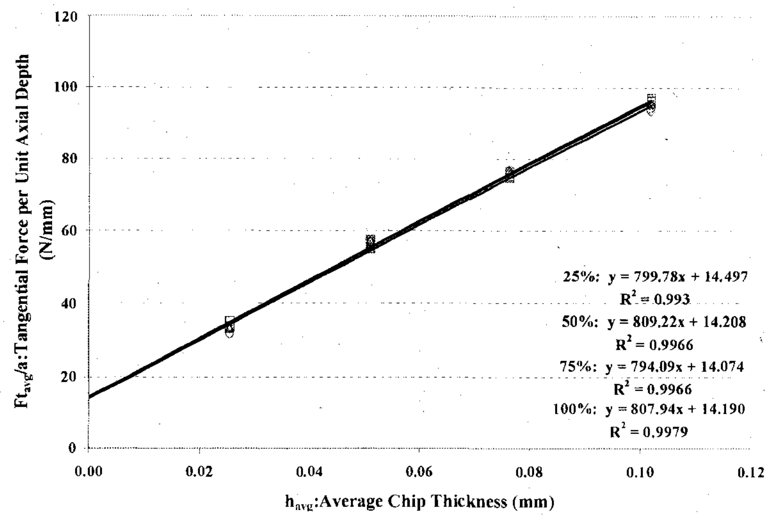

Figure 3-3. K_{TC}&K_{TE} vs. Radial Depth (Experiment C3 - one flute carbide cutter)

Table 3-2. Variation of K_{TC} (N/mm^2) and K_{TE} (N/mm) with radial depth

	Immersion (D)				Average	Standard Deviation	Coeff of Variation
	100%	75%	50%	25%			
Ktc	807.94	794.09	809.22	799.78	802.76	6.18	.0077
Kte	14.19	14.07	14.21	14.50	14.24	0.16	.011

The standard deviations of K_{TC} & K_{TE} under various cutting conditions are listed in **Tables 3-1** and **3-2**, which indicate that changing cutting parameters, e.g. cutting speed, feedrate and cutting depth, did not appear to have a significant influence on the cutting coefficients in this instance. The insensitivity of the coefficients to non-wear related effects is essential to establish the reliability of the proposed method. If the coefficients are affected by other non-wear related factors then it becomes impossible to accurately relate the tool wear state to the coefficient changes.

3.4 Influences of Helix Angle on K_{TC} & K_{TE}

Helical ball end mill (BEM) cutters are widely used in machining sculptured surfaces, whose helix angle gradually increases from zero at the tip to a constant value in the cylindrical part. If the cutting edge is broken into small increments, the tangential force model coefficients may be different at each location.

In order to find the relationship between the helix angle and the cutting coefficients, Experiment C4 was conducted with up-milling on an AISI 6061 aluminum thin plate, thickness = 3.175 mm, and an AISI 6061 aluminum block, thickness = 50.8 mm as shown in **Figure 3-4**. Each calibration was performed by making a "cleaning cut" and then stepping over 5.08 mm. Four different feedrates were run and power was recorded for each test condition.

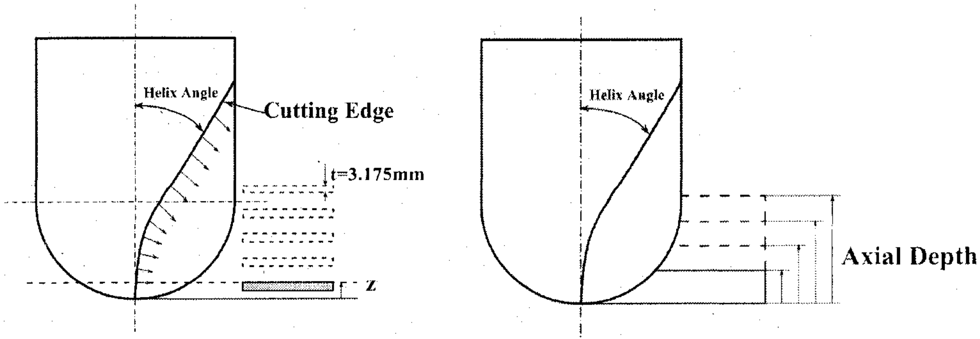

(a) Calibrated with thin plate **(b) Calibrated with block**

Figure 3-4. Calibration using a 19.05 mm 2 flute BEM

3.4.1 Calibration with Aluminum Thin Plate

The calibration of a HSS BEM cutter, D = 19.05 mm, was repeated four times on the aluminum thin plate at the cutter axial positions z = {3.81, 5.08, 6.35, 7.62, 8.89, 10.16, 11.43, 12.7} mm and feedrate f = {0.01, 0.02, 0.03, 0.04} mm/tooth with same cutting depths. The cutting power was measured by the spindle power sensor. The material removal rate $\dot{Q}$ and the contact area rate $\dot{A}_c$ are calculated as shown in Appendix E. It is assumed that the helix angle, α, linearly increases from zero degrees at the bottom of the hemisphere to a constant, e.g. 30-degree. Therefore, the equivalent helix angle can be calculated as follows listed in **Table 3-3**:

Table 3-3. Equivalent helix angle at different cutting position

Cutting Position (z: mm)	3.81	5.08	6.35	7.62	8.89	10.16	11.43	12.7
Equivalent helix angle (degree)	5.00	11.00	15.00	19.00	23.00	26.00	28.00	30.00

The values of K_{TC} & K_{TE} at the different axial sections, i.e. the different helix angle, are plotted in **Figure 3-5**. It shows that the values of K_{TC} stay approximately constant except at the very tip of the tool, where there is roughly a 20% increase. The deviations of K_{TE} are normal variations and do not exhibit any trend with helix angle.

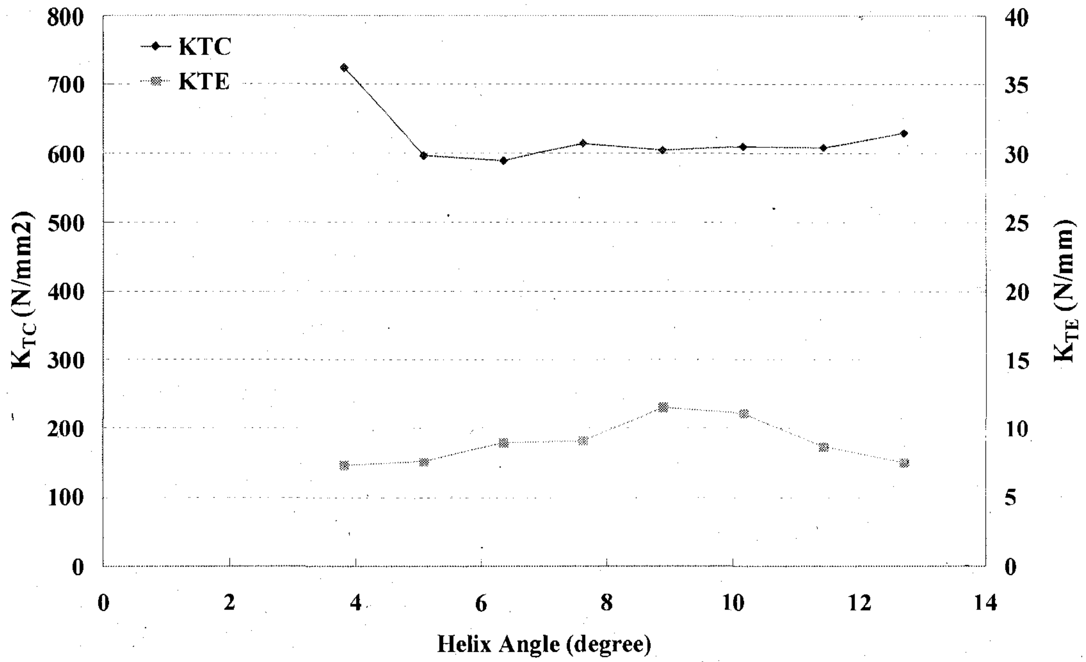

Figure 3-5. Distribution of K_{TC} & K_{TE} of BEM calibrated with the aluminum thin plate

3.4.2 Calibration with Aluminum Block

The same calibration procedure was repeated four times on the aluminum block at eight axial depths a = {3.81, 5.08, 6.35, 7.62, 8.89, 10.16, 11.43, 12.7} mm. The values of K_{TC} & K_{TE} at the different axial depths are plotted in **Figure 3-6** along with the values from the thin plate calibration for comparison. The estimated values of the cutting power for the aluminum block experiment are calculated using the mean values of K_{TC} & K_{TE} obtained from the thin plate calibration and the corresponding values of $\dot{Q}$, $\dot{A}_c$, The comparison between estimated and measured values of cutting power is plotted in **Figure 3-7**. The deviations of cutting power under four feedrates are listed in **Tables 3-4**, which shows a maximum 12% deviation between the estimated and measured cutting power.

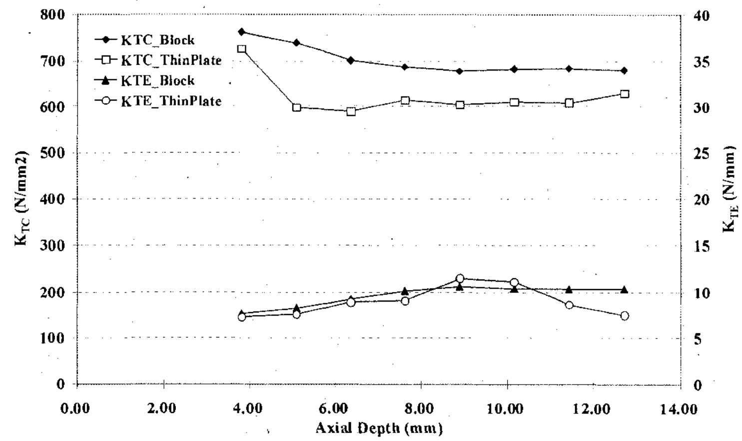

Figure 3-6. Distribution of K_{TC} & K_{TE} of BEM calibrated with the aluminum block

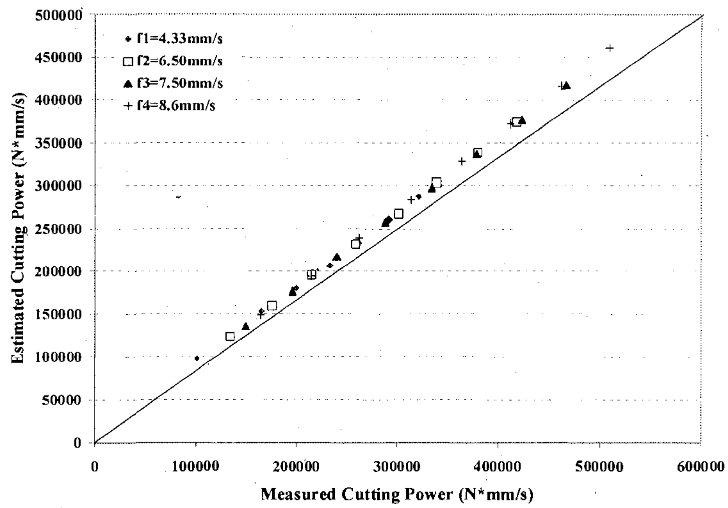

Figure 3-7. Estimated vs. experimental values of cutting power on the aluminum block

Table 3-4. Comparison of the estimated and experimental cutting power

Axial Depth (mm)	3.8	5.1	6.4	7.6	8.9	10.2	11.4	12.7
P1_est (N*mm/s)	97427	125316	152723	179844	206809	233737	260655	287574
P2_est	123369	160062	196273	232198	267967	303699	339422	375144
P3_est	135804	176746	217207	257381	297400	337382	377354	417326
P4_est	148929	194270	239130	283703	328121	372502	416873	461244
P1_exp (N*mm/s)	101707	133163	165318	200094	232773	261608	291666	321199
P2_exp	133862	175279	214774	258113	300928	338675	379917	418013
P3_exp	149765	196250	240113	288171	334131	378694	423431	467119
P4_exp	164444	214424	261783	313685	363839	412246	462052	509410
Error (%)	-4.4	-6.3	-8.2	-11.3	-12.6	-11.9	-11.9	-11.7
	-8.5	-9.5	-9.4	-11.2	-12.3	-11.5	-11.9	-11.4
	-10.3	-11.0	-10.5	-12.0	-12.4	-12.2	-12.2	-11.9
	-10.4	-10.4	-9.5	-10.6	-10.9	-10.7	-10.8	-10.4

3.5 *Influences of Flank Wear on K_{TC} & K_{TE}*

In the milling process, flank wear proceeds smoothly for moderate cutting conditions, however the intermittent cutting forces and temperature variation that occur when the tool enters and exits the cutting zone, cause periodic expansion and contraction of the tool, leading to chipping of the cutting edges. Power has long been known to increase linearly with the wear land in turning [13], and it is confirmed to be true in milling by our results.

Figure 3-8 shows the change of K_{TC} & K_{TE} vs. the average flank-wear width VB in Experiments W1 and W2. It shows that K_{TE} has a generally linear relationship with flank wear (VB), while K_{TC} is roughly constant as flank wear increases.

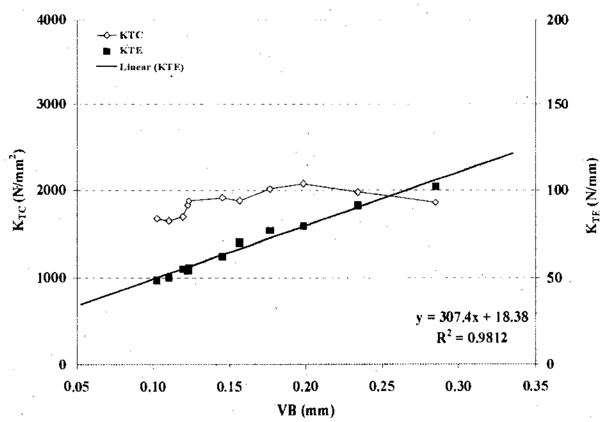

(a) Experiment W1

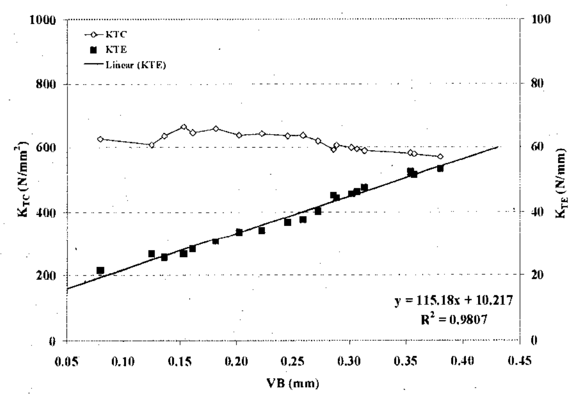

(b) Experiment W2

Figure 3-8. Influences of flank wear on K_{TC} & K_{TE}

3.6 Influences of chipping on K_{TC} & K_{TE}

The occurrence of chipping changes the geometry of the cutting edge and makes the actual rake angle more negative [17]. Meanwhile, the shear stress and normal stress on the tool-chip interface increase due to cracks. Worn tools obtained from Sandvik were calibrated (Appendix A). Thus, the cumulative effect of chipping on coefficients is that K_{TC} increases with the size of the chipping magnitude, as shown in **Figure 3-9**, while no such relationship exists for K_{TE}. In the real cutting, tiny chips were generated along the cutting edge after numbers of passes, which caused a very small change in K_{TC}. When the tool life is near the end, large scale chipping resulted in a dramatic increase of K_{TC}.

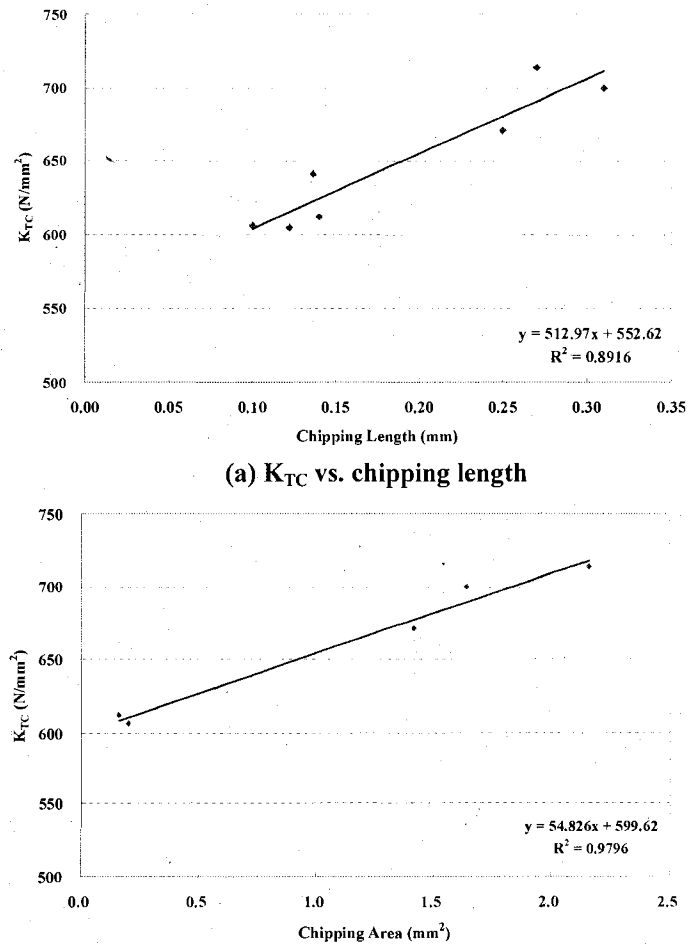

(a) K_{TC} vs. chipping length

(b) K_{TC} vs. chipping size

Figure 3-9. Effects of chipping on K_{TC}

3.7 Summary

A number of calibration experiments were conducted to investigate the characteristics of K_{TC} & K_{TE}. It was found that K_{TC} & K_{TE} satisfy all requirements of indicators of tool wear. The change of feedrates, cutting speeds and immersion depths have no effect on K_{TC} & K_{TE}, therefore the threshold of coefficients can be used in a wide range of cutting conditions. K_{TC} is not affected by flank wear, but it increases with chipping size. K_{TE} has a direct relation with cutting power and linearly increases with flank wear. The effect of helix angle on K_{TC} & K_{TE} was briefly studied using a ball-end mill, which shows that K_{TC} stays roughly constant at the large helix sections and K_{TE} does not seem to depend on the helix angle. The independence of K_{TE} on helix angle is of great importance since this is the coefficient that correlates most closely with flank wear. This observation also makes sense since there is no obvious reason that the edge rubbing should depend on the helix angle. The variation of KTC with helix angle also makes sense but needs to be further studied.

Chapter 4

WEAR EXPERIMENT RESULTS

The influences of the cutting process on tangential force model coefficients have been thoroughly investigated. However, little work has been done on the effect of wear characteristics on cutting coefficients during milling. In this chapter, a study was undertaken to investigate the wear behavior and mechanism of cutting coefficients during the flat end milling of AISI-1018 steel using HSS cutters, uncoated Carbide cutters, and coated carbide inserts at various cutting conditions. The effects of cutting parameters on the tangential force model coefficient while wearing the tool are discussed. Due to the diversity of tool material and micro-structure, the wear progression of each type of tool was somewhat different: (i) Coated Insert: flank wear and almost no chipping (ii) HSS: flank wear and a little bit of chipping; (iii) Carbide: flank wear, a significant amount of chipping and groove wear. It has been found that the cutting speed has the greatest effect on tool life, i.e. higher cutting speed results in more rapid flank. Feedrate and depth of cut also affect tool life to a lesser degree. The experimental results show that the cutting coefficients exhibit a common pattern for all cutting conditions and tool materials: K_{TC} stays roughly constant till near the end of the tool life, where chipping and groove wear were large enough to change tool geometry, while K_{TE} gradually increased with the increase of cutting distance and tool flank wear.

4.1 Coated Carbide Insert

The types of commercial coated carbide inserts used in the tool wear experiments TI1-TI4 (see Table 2-1) were Sandvik R390-11 T3 08M-PM and RA390-016O16L-11L. Although two inserts can be used in the milling cutter, only one was used in our tests to avoid the runout issue. In this series of tests, the cutting speed was set to 125 or 200 m/min, feed was 0.04 or 0.08 mm/tooth, and the radial and axial depth were kept to 3.05 and 5.08 mm, respectively. Cutting coefficients were calibrated periodically while wearing the tool and the wear flank faces were examined using an optical measurement inspection system (Mitutoyo) and an LCD capturing microscope (ESPA D3).

4.1.1 Flank Wear

Due to its general characteristics, i.e. low friction coefficient, high hardness, good temperature properties and good adhesion to the substrate, the Titanium nitride coating (gold in color) enhances the lubricity of the tool, improves the oxidation resistance of the tool, protects the tool against diffusion wear and reduces the temperature variation in the tool, rendering it less susceptible to cracking, and therefore greatly improves the life of carbide tools. The flank wear rate is much lower than in uncoated tools, and the chipping is significantly prevented at sharp edges. Therefore, the coated tool predominantly experienced flank wear throughout the entire cutting process, as shown in **Figure 4-1(a)**. After the coating has been removed by the chip adhesion at low speeds, cracks weakened the tool edge and caused chipping to occur. This was followed by the formation of surface fracture at the cracks which would contribute to form a large fracture surface, as shown in **Figure 4-1(b)**.

(a) Flank wear

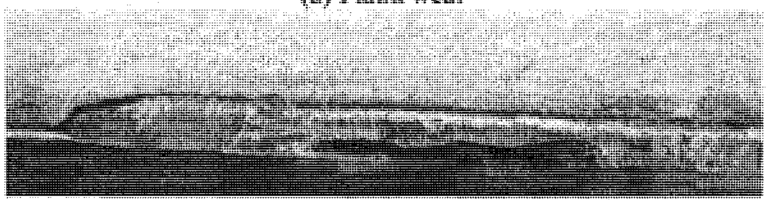

(b) Flank wear with chipping

Figure 4-1. Micrographs of the flank face of the coated inserts

(a) TI1

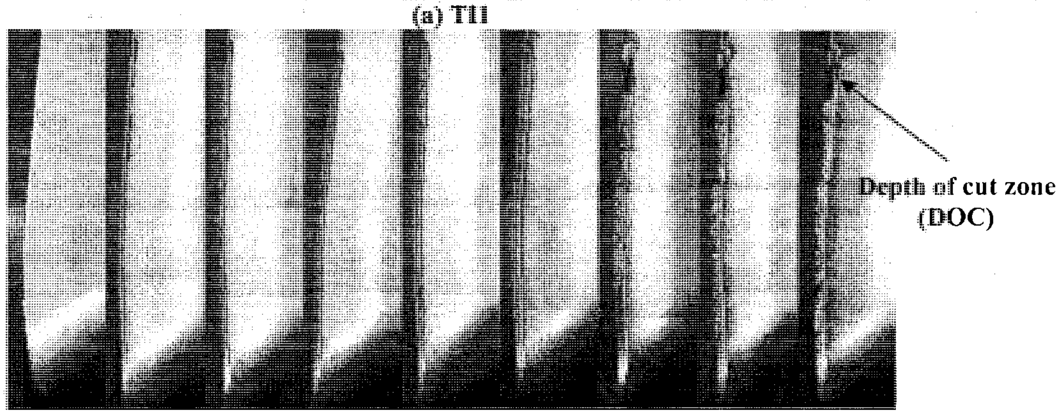

(b) TI4

Figure 4-2. Wear progression of coated carbide insert

The wear progression of the coated carbide insert in milling is illustrated in **Figure 4-2**. According to ISO 8688-2:1989 (E) [33], the recommended tool life criterion for uniform wear is flank wear of 0.3 mm. For this study, a flank wear criteria of 0.2 mm was selected to reduce test time.

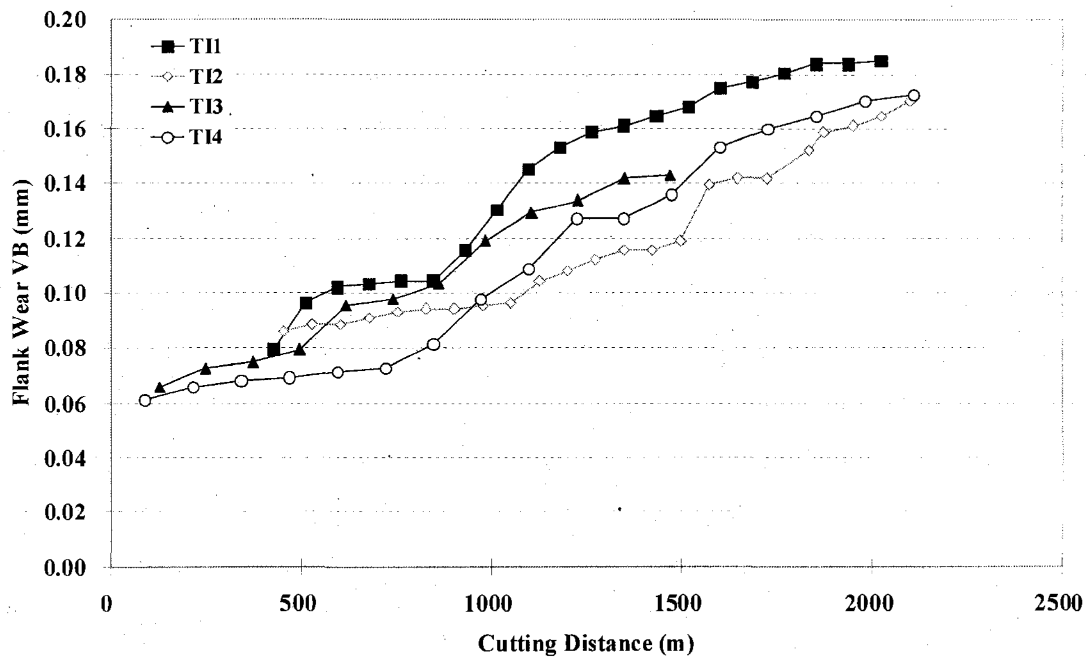

Figure 4-3. Flank wear progressions of coated carbide inserts

The highest flank-wear width was observed at the flank face near the depth of cut zone in **Figure 4-2**. **Figure 4-3** shows the change in the flank-wear width (*V*B) with cutting distance in machining AISI-1018 steel with flood coolant at different cutting conditions. It was found that increasing the feed from 0.04 to 0.08 mm/tooth (TI1 vs. TI2) and increasing the cutting speed from 125 to 200 m/min with constant feed (TI1 vs. TI3) produces a longer tool life (see **Table 2-1** for cutting conditions). The wear rate increased at lower cutting speeds and feed due to the development of BUE edge, and the coating was worn off by it. The experimental results show that the tool life in TI4 (Down milling) is somewhat longer than in TI1 (Up milling). The exit angle in TI1 is 68.9°.and the exit angle for TI4 is 180° which confirms the conclusions discussed in Section *1.2.3*. It is important to note that wear tests are highly variable and multiple tests are required to draw conclusions.

4.1.2 K_{TC} & K_{TE}

Figure 4-4 shows the change in K_{TC} & K_{TE} with cutting distance. The common pattern in the graphs shows that K_{TC} stays roughly constant in milling, while K_{TE} gradually increased with flank wear. Comparing **Figure 4-4** and **4-3**, it can be concluded that K_{TE} linearly increases with flank wear. The ratio of K_{TE} vs. VB, i.e. the slope, is affected by the wear modes.

Experiments TI1 ~ TI3 have almost the same wear progression, i.e. a gradually increasing flank wear with slight chipping, while larger chipping occurs in Experiment TI4. The variation of the flank wear obtained for a given cutting condition is between 5 and 8% from the mean value It was found that TI1 ~ TI3 have the identical ratio of K_{TE} vs. VB, while the ratio of TI4 (the slope of the trend) is much higher. Since K_{TE} is directly related to the cutting power, the higher ratio of K_{TE} vs. VB of the down mill immersion cutting indicates that chipping deteriorated the tool condition and consumed more energy to remove material. **Figure 4-4** further proves that the significant change of K_{TC} only occurs when the size of chipping exceeds a critical value.

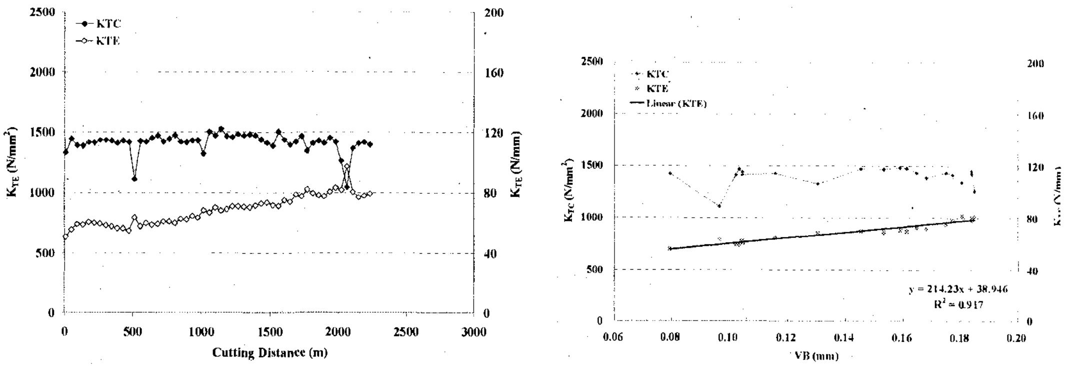

(a) Experiment TI1 (f=0.18m/min, 2500rpm, Upmill)

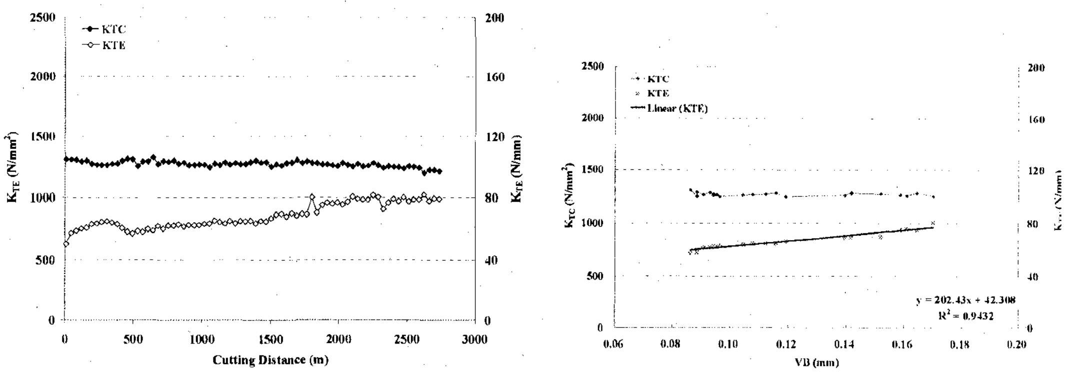

(b) Experiment TI2 (f=0.38m/min, 2500rpm, Upmill)

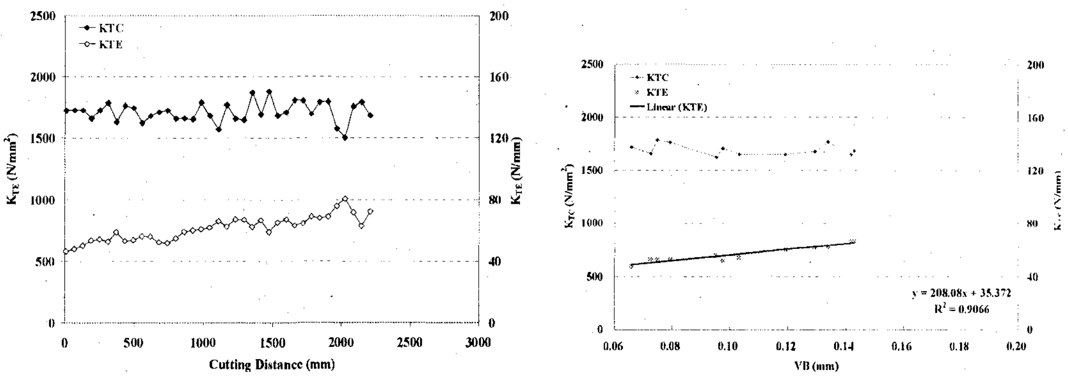

(c) Experiment TI3 (f=0.29m/min, 4000rpm, Upmill)

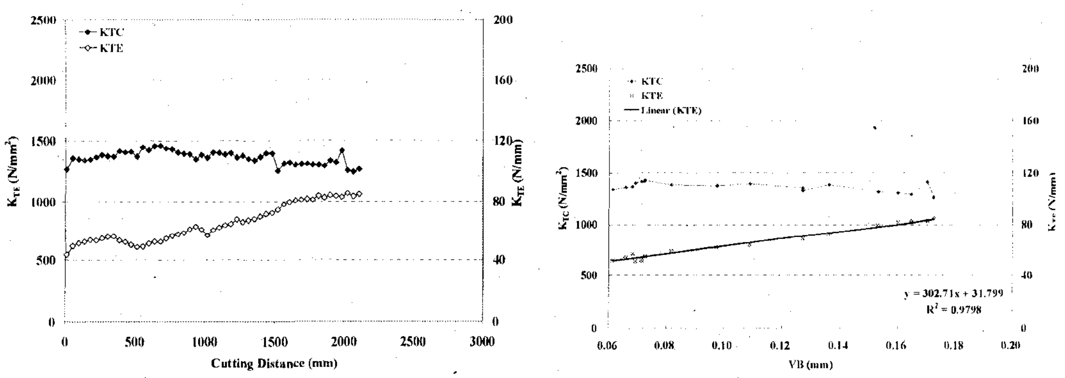

(d) Experiment TI4 (f=0.18m/min, 2500rpm, Downmill)

Figure 4-4. Trends of K_{TC} & K_{TE} while wearing coated carbide inserts

4.2 High Speed Steel Cutter

Tool wear experiments TH1 ~ TH3 (see **Table 2-1**) were conducted at cutting speeds of 35 and 50 m/min with the application of an emulsified water-based coolant (Superedge 6759 Castrol) flooding over the whole cutting section. The axial and radial cutting depths were kept constant at 3.05 mm and 6.35 mm, respectively. The HSS end mills used in this work had one flute and a helix angle of 30-degree.

4.2.1 Flank Wear

Due to its low hardness and low wear resistance, HSS cutters exhibit a much higher wear rate (see in **Figure 4-5**) than coated carbide inserts (see in **Figure 4-3**). Since HSS cutters were used close to their limits of yield and fracture stresses, abrasive wear dominates the flank and crater wear of the HSS tool edge seen in **Figure 4-6**. The grooved pattern is a combination of the rubbing action of hard particles in the work material, and the protection against scratching offered by the hard phases in the tool material. Chipping can occur but is a rather scarce event.

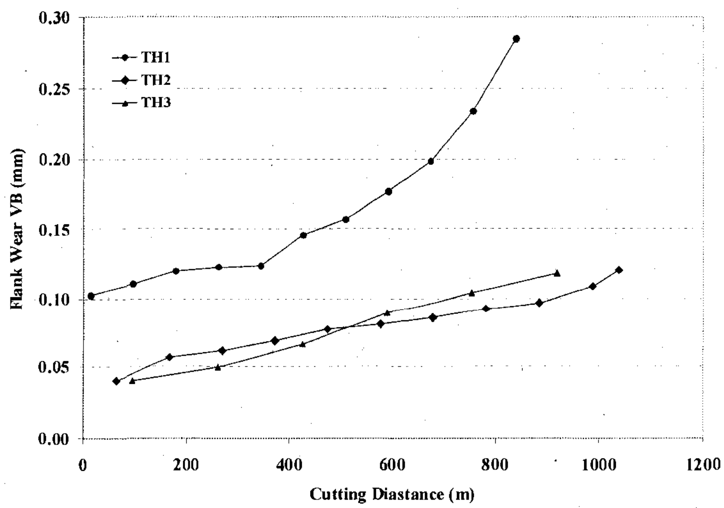

Figure 4-5. Flank wear progression of HSS cutter

When cutting speed and feed are low (e.g. TH1), BUE is a common occurrence on the tip of the cutting edge. When the BUE reached a critical size, it broke away from the cutting edge and part of it smears on the surface of workpiece. Previous studies [19] have shown that BUE decreases as (a) cutting speed increases, (b) chip thickness decreases, (c) rake angle increases, (d) tip radius of the tool decreases. **Figure 4-5** confirms the above statement at this specified cutting condition.

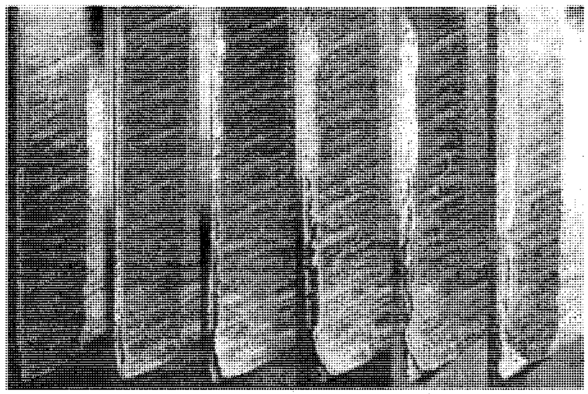

(a) TH1

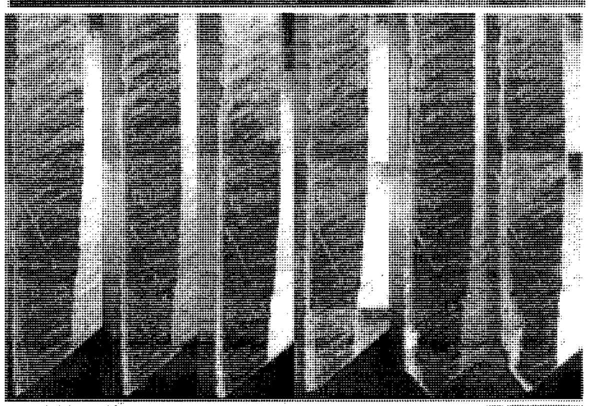

(b) TH2

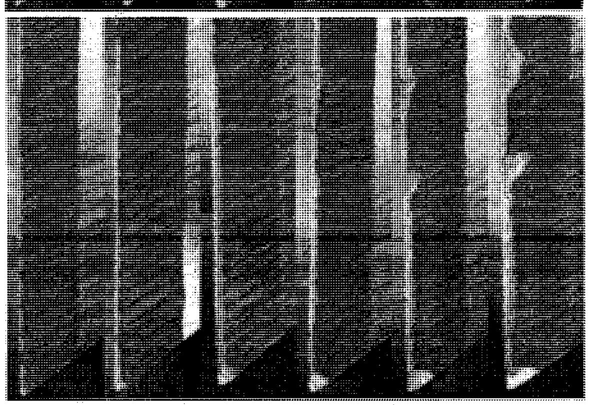

(c) TH3

Figure 4-6. Wear progression of HSS cutters

4.2.2 K_{TC} & K_{TE}

The poor wear performance of HSS made calibration more difficult. The tool wore much more quickly near the end of its life, thus the cutting power increase of a worn tool in a specified distance is higher than that of a sharp tool, and the power separation in **Figure 4-7** is enlarged. Therefore, K_{TC} tends to increase. In order to eliminate this undesired phenomenon, the cutting distance during calibration should be minimized.

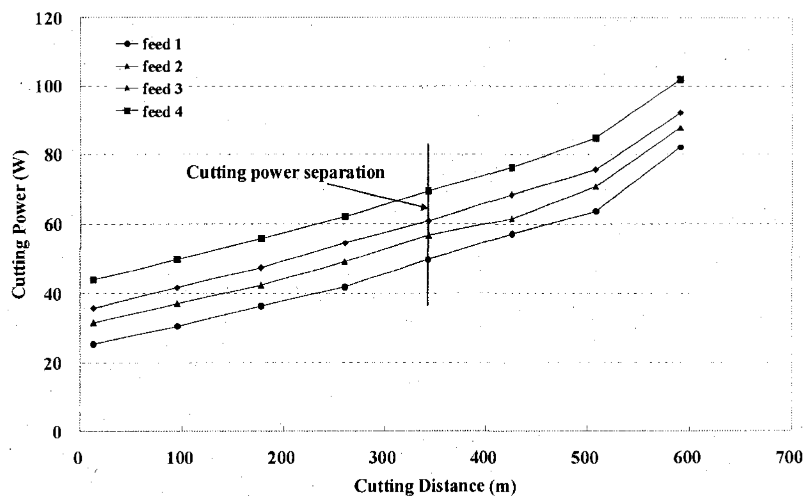

Figure 4-7. Cutting power progression of HSS (TC1)

Figure 4-8 shows the changes of K_{TC} & K_{TE} with cutting distance for HSS cutters, which exhibit the same pattern as the coated carbide inserts. It shows that with an increase in the flank wear, K_{TE} increases, except the higher ratio of K_{TE} vs. VB due to HSS cutter's low wear performance. Because of the development of BUE in Experiment TH1, the K_{TE} value level in TH1 is much higher than those of TH2 and TH3 which indicates that BUE aggravated the tool wear and consequently created small chipping with higher cutting energy requirements. Thus, the increased rate of K_{TE} or the ratio of K_{TE} vs. VB in Experiment TH1 is highest, and a slight increase in K_{TC} was also observed.

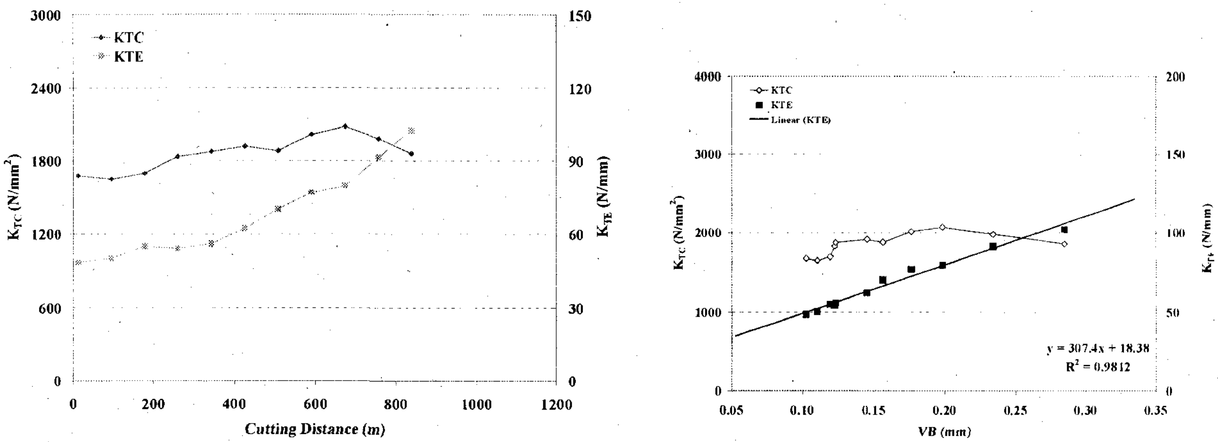

(a) Experiment TH1 (f=0.04m/min, 880rpm)

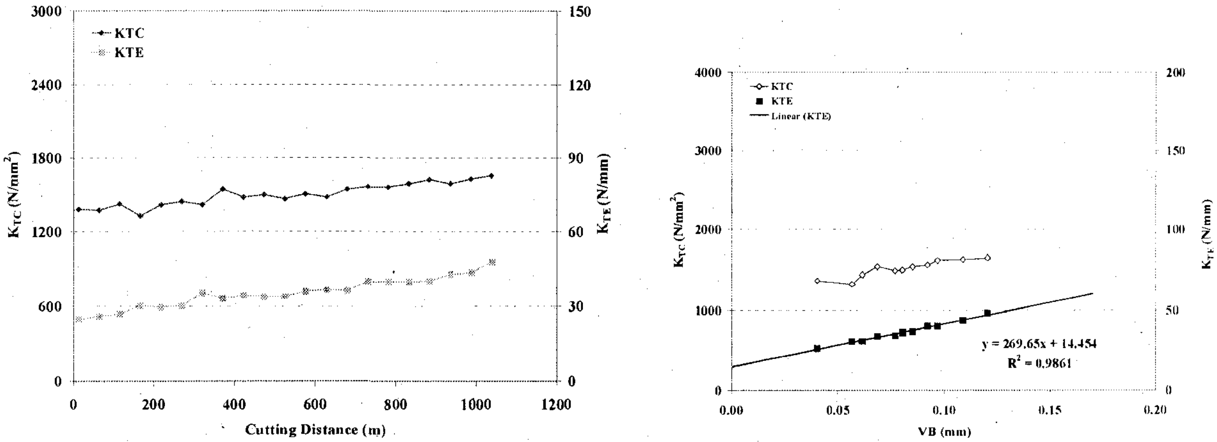

(a) Experiment TH2 (f=0.06m/min, 880rpm)

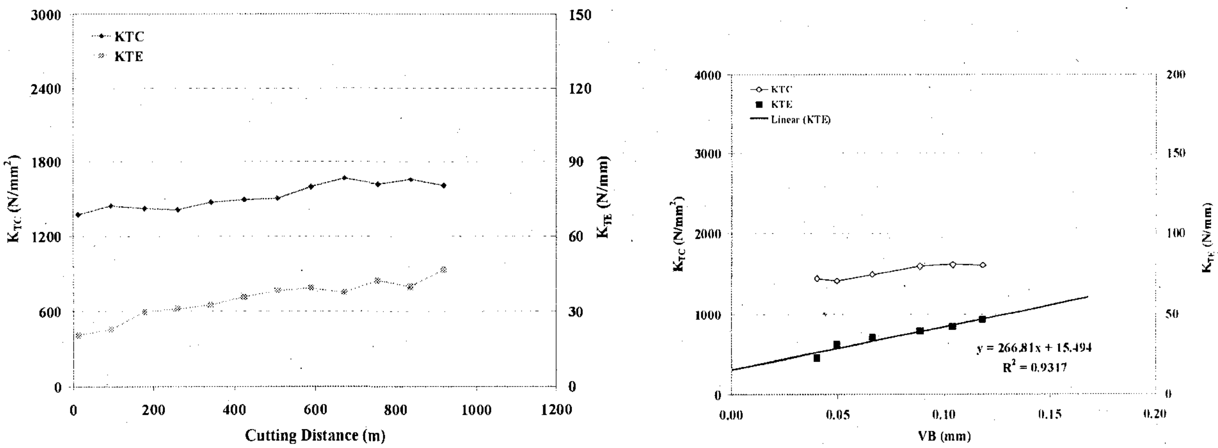

(a) Experiment TH3 (f=0.05m/min, 1100rpm)

Figure 4-8. Trends of K_{TC} & K_{TE} while wearing HSS cutter

4.3 Carbide Cutter

Because of their high hardness over a wide range of temperatures, high elastic modulus, high thermal conductivity and low thermal expansion, carbide tools are among the most important, versatile and cost-effective choice for a wide range of cutting applications [20]. Experimental work was conducted in order to study the effect of tool wear on the change of K_{TC} & K_{TE}. The commercial carbide cutters used in tool wear experiments TC1- TC4 were Kennametal HEC500S2. The axial depth of cut was kept constant at 3.05 mm.

4.3.1 Chipping and breakage of the cutting edge

The carbide cutter used to mill AISI-1018 at all cutting conditions showed evidence of chipping and deep grooves, as shown in **Figure 4-9**, and the worst wear location was found at the depth of cut zone. The existence of stress variation, cycle mechanical impact and burrs at the cutting edge generated during machining coupled with the brittleness of tool materials accelerated the development of chipping, flaking, and fracture of the carbide cutters. Honed edges combined with a cutting edge radius preparation may increase the chipping resistance.

At the initial stages of cutting, the wear at the flank face and the nose was uniform, and fine-scale chipping was detected in a discrete manner along the cutting edge after 100m of the surface cutting distance, **Figure 4-9(a)**. As cutting continued, the chipped areas developed to a large scale by overlapping on each other and groove wear was initiated at the chipping region, **Figure 4-9(b, c).** Flank wear was not the dominant wear mode. The tool failed catastrophically due to excessive fracture from 800 to 1000m of the surface cutting distance at various cutting conditions, **Figure 4-9(d)**.

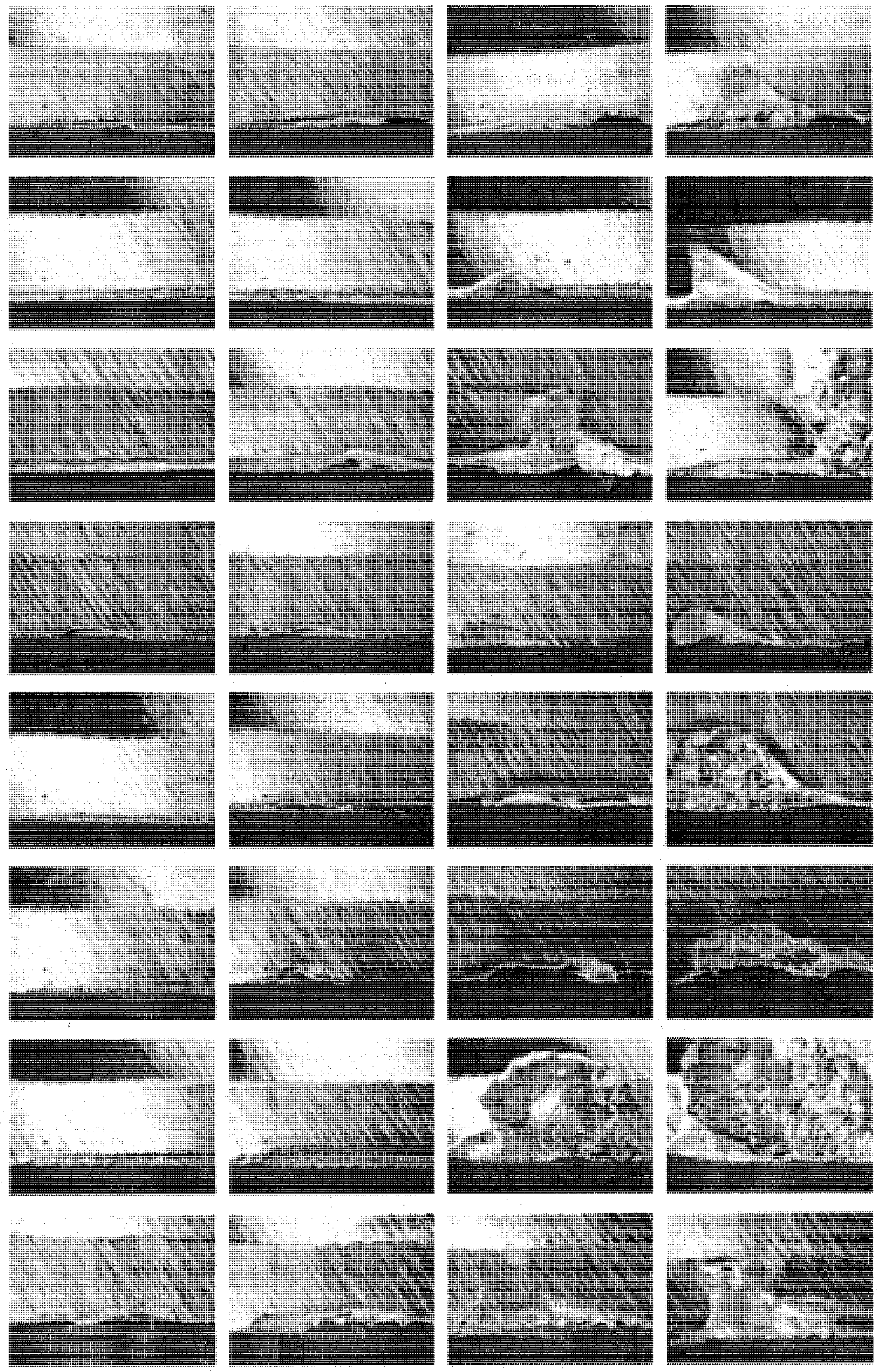

(i) TC1
(ii) TC2
(iii) TC3
(v) TC4
(iv) TC5
(vi) TC6
(vii) TC7
(viii) TC8

(a) (b) (c) (d)

Figure 4-9. Wear progression of carbide cutters

Figure 4-10 shows that the higher feedrate accelerated the development of chipping (TC1 vs. TC2), This is probably because the greater cutting temperature and stresses generated on the flank face caused the yield strength of the tools to reduce. Therefore, we conclude that decreasing the feedrate has an inverse effect on chipping (TC1 vs. TC3). As shown in **Figure 1-11**, increasing or decreasing cutting speeds (TC4/TC5) will cause the low flank wear rate, which may be due to the frequent occurrences of Built-Up Edge in Experiment TC1. Because of the application of flood coolant amplifying the temperature variation of cutting tool between entry and exit cycle, an evident trend from the results was the poor tool life experienced when milling under wet environments at the high cutting speeds employed (TC1 vs. TC6). Thus, it's better to use carbide cutters in dry environment rather than with the application of coolant.

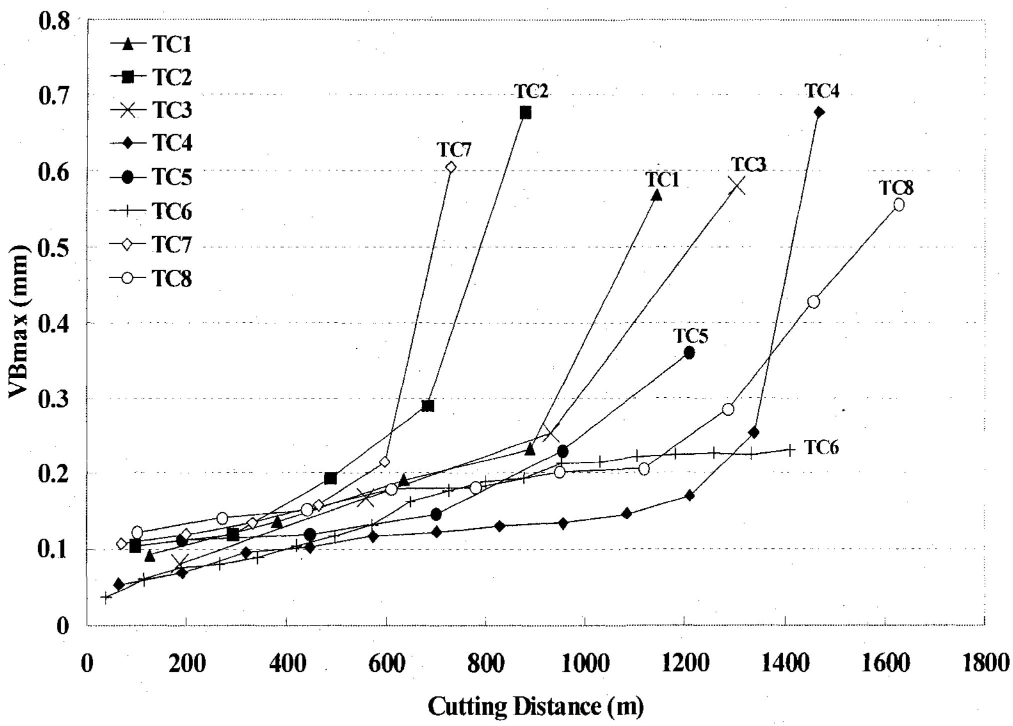

Figure 4-10. Flank wear (VBmax) progression of carbide cutters

4.3.2 K_{TC} & K_{TE} for Carbide Cutters

The procedure for online calibration tests of K_{TC} & K_{TE} was performed in a short distance to avoid any significant amount of wear occurring during the calibration. The model coefficients are clearly affected by tool wear, but their response is different.

4.3.2.1 Influences of Tool Wear on K_{TC}

As shown in **Figure 4-11(a)**, the tool life of carbide tools is unlike the wear progression of coated carbide inserts or HSS tools, and may be divided into three stages: (1) gradual wear, (2) rapid wear and (3) fracture. K_{TC} expresses different characteristics within these stages. Since flank wear or slight chipping is the dominant wear mode within the first two stages, the cutting surface is in a relatively intact condition and the power levels remain generally equidistant from each other while gradually increasing, as shown in points (1) of **Figure 4-11(b)** and therefore K_{TC} remains roughly constant. When the tool is near the end of its life, large chipping or groove wear occurs on the cutting edge, as shown at point (2) of **Figure 4-11(b)**, which changes the geometry of the cutting edge and makes the actual rake angle more negative [18]. Then, the power levels begin to dramatically vary over time, which will be consequently reflected in a large change in K_{TC}. Therefore, for the experiments that we conducted, the tool life may statistically be divided into two stages: (1) Stable K_{TC} stage; (2) Unstable K_{TC} stage. Results were consistent under various cutting conditions, as shown in **Figure 4-11**, thereby K_{TC} is sensitive to tool wear modes and stages, which can be used as a qualitative indicator to discern the tool status.

It was confirmed by the following wear tests based on carbide tools cutting AISI-1018 steel.

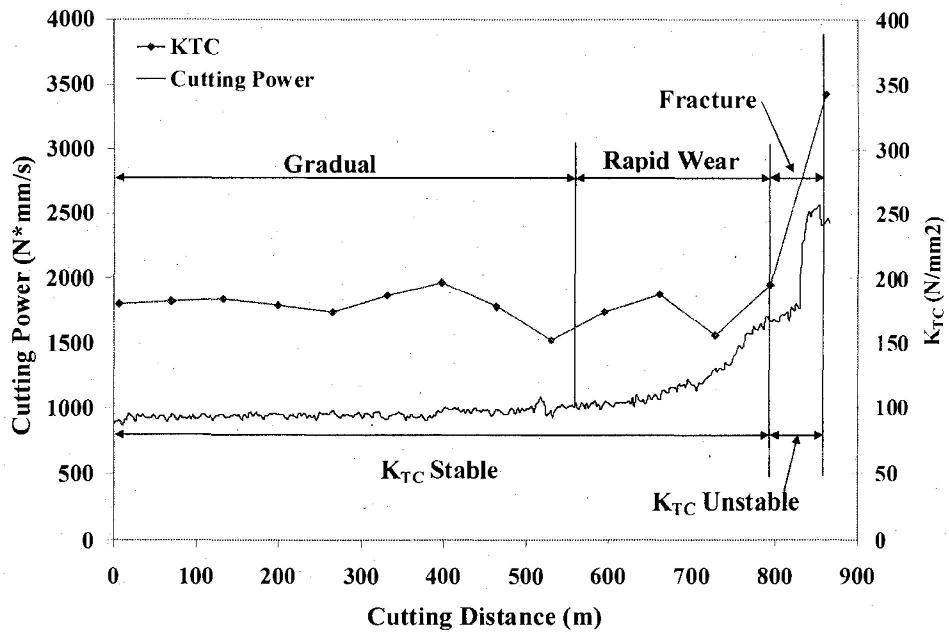

(a) Tool Wear Stages

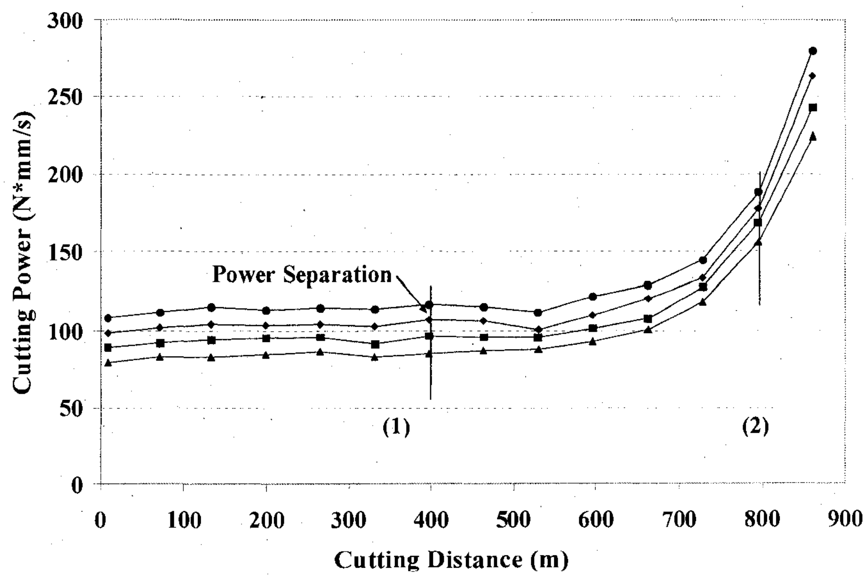

(b) The four curves correspond to four different feedrates, and the separation between the curves determines the slope of the line shown in Figure 1, i.e. K_{TC}

Figure 4-11. Characteristics of K_{TC} within different tool life stages – Experiment TC3

4.3.2.2 Influences of Tool Wear on K_{TE}

K_{TE} of carbide cutters was found to increase proportionally with flank wear, even if the dominant wear mechanism of carbide is completely different from that of insert or HSS cutters. The results shown in **Figure 4-12** illustrates that as the cutting power changes, K_{TE} will follow a similar pattern. With increasing flank wear VB, there was a similar increase in cutting power for all of our wear experiments. The cutting power plots changed very little during the gradual wear phase, but increased significantly during the rapid wear phase and then fluctuated during the fracture phase. This phenomenon is accurately reflected in the trends of K_{TE}. Since K_{TE} has almost the same beginning values for all nominal cutters, we can eliminate the effect of the fluctuation of tare power on the final results. The changing cutting conditions only affect the rate of K_{TE} change in each experiment.

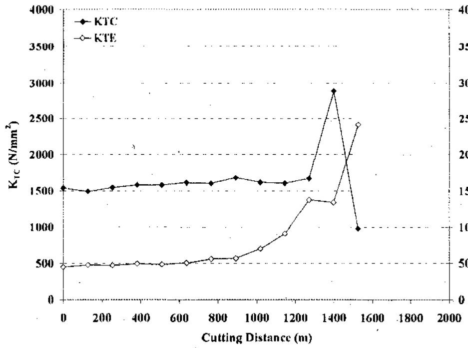

(i) Experiment TC1

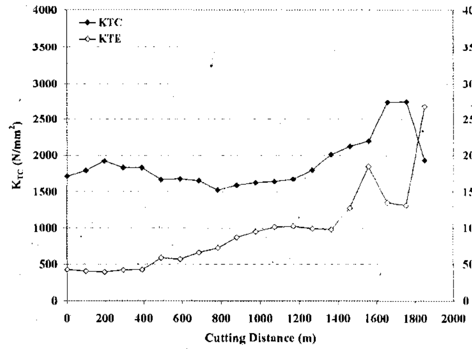

(ii) Experiment TC2

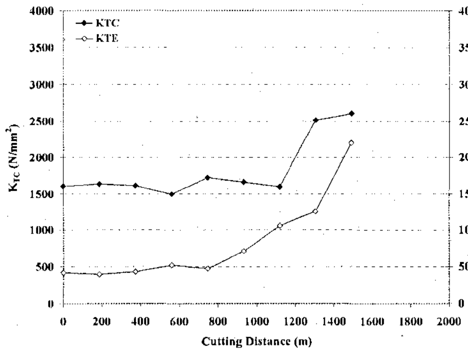

(iii) Experiment TC3

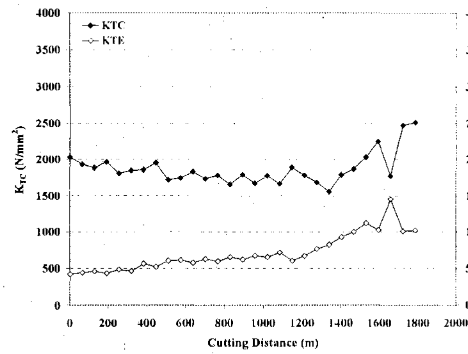

(iv) Experiment TC4

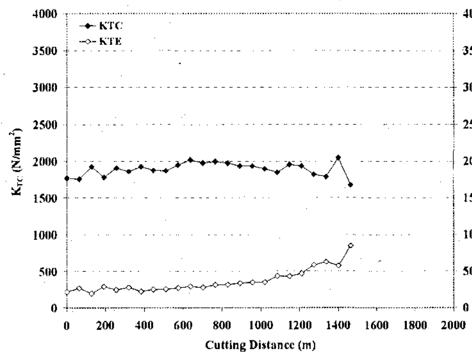

(v) Experiment TC5

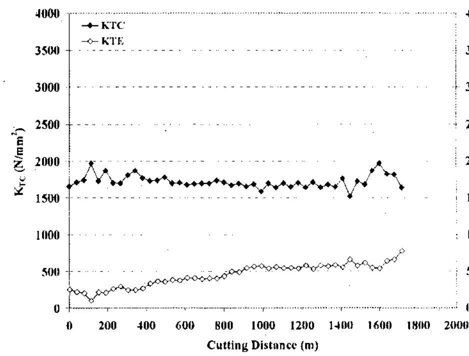

(vi) Experiment TC6

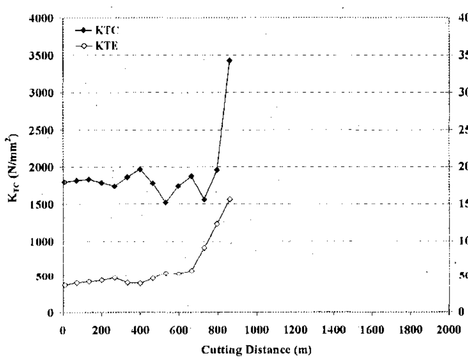

(vii) Experiment TC7

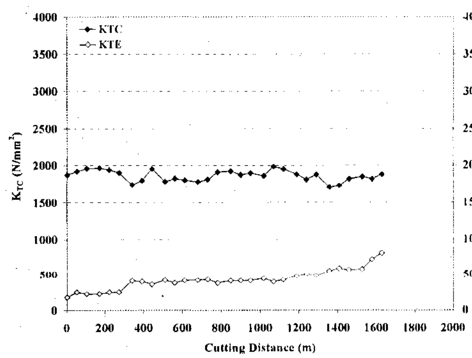

(viii) Experiment TC8

Figure 4-12. Trends of K_{TC}&K_{TE} in wear experiments

4.4 Tool Calibration of Worn Tools Obtained from Industry

A number of cutters were obtained from Turbocam, a local company that makes blisk type parts. These cutters were considered to be "worn out" and no longer fit for service. The purpose of these tests were to see if the calibration method could be applied to tools obtained from industry and help to determine what constitutes a "worn out" tool. The actual usage of the tools is unknown. Six worn cutters (6.35 mm HSS flat end mill) with four flutes and 30-degree helix angle were calibrated on a AISI-6061 aluminum thin plate, thickness h = 3.175mm, at five different sections, axial positions z = {4.32, 8.89, 13.97, 19.05, 22.86} mm.

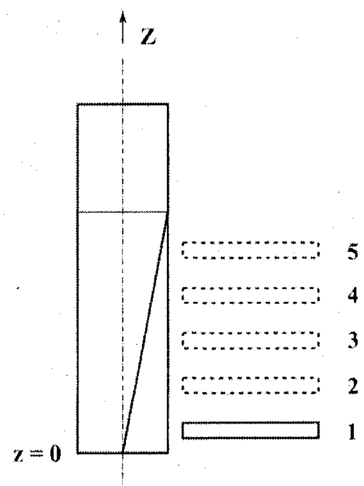

Figure 4-13. Tool calibration method - TurboCam

Because these tools were used for variable axial depth cuts, the wear status of each section is different. **Figure 4-14** shows that K_{TC} stays roughly constant at all sections, while K_{TE} decreases from the tip (z = 0 mm) to the top (z = 25.4 mm), which indicates that the tip is the most worn place along the cutting edge. **Table 4-1** shows the increase of K_{TE} and cutting power of the worn tools compared to a sharp tool. For this instance, a minimal 21-percent increase of cutting power corresponds to a 93-percent increase of K_{TE} at the tip of Tool 1. Therefore, it is feasible to set a threshold of K_{TE} for replacing tools, which satisfies the combined requirements of productivity, quality and energy consumption.

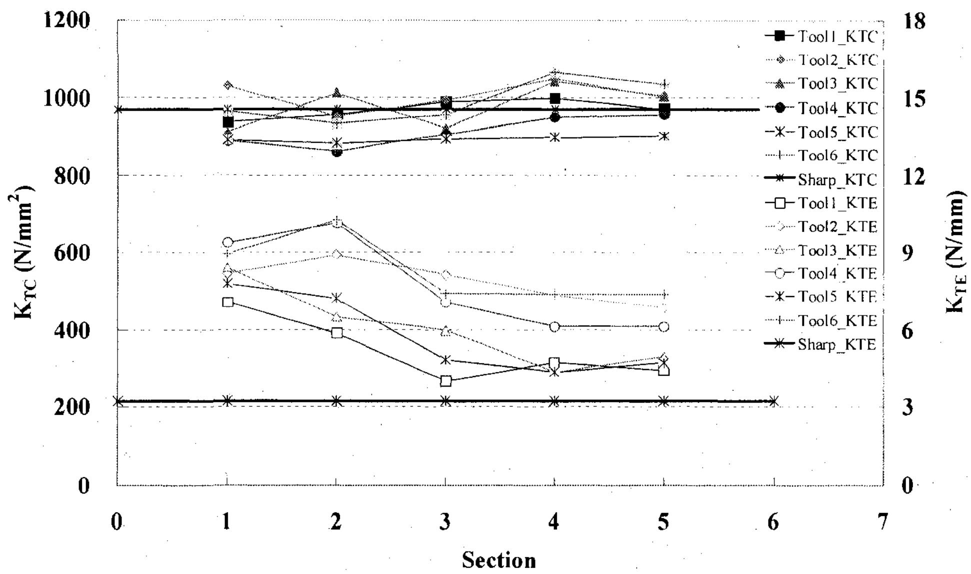

Figure 4-14. Distribution of KTC & KTE for tools from Turbocam

Table 4-1. Increase of K_{TE} and cutting power at the tool tip

Increase	Tool 1	Tool 2	Tool 3	Tool 4	Tool 5	Tool 6
K_{TE} (%)	93	122	129	156	112	144
POWER (%)	21	33	44	44	29	41

4.5 Summary

The characteristics of K_{TC}&K_{TE} were observed to be consistent for all cutters used in wear tests. K_{TC} stays roughly constant untill near the end of the tool life, while K_{TE} gradually increases with the increase of cutting distance and the tool flank wear. This phenomenon is confirmed by the tools from Turbocam, which are used in real cuts and have different wear status. Therefore, a new approach can be developed by using a constant K_{TC} and the direct relation between K_{TE} and the cutting power.

Chapter 5

TOOL WEAR ESTIMATION

According to the results of calibration and tool wear experiments, K_{TC} & K_{TE} satisfy all requirements of the tool wear indicator: (a) they are insensitive to cutting conditions, (b) high correlation to tool wear - K_{TC} stays roughly constant until near the end of the tool life, while K_{TE} gradually increases with the increase of cutting distance and tool flank wear, (c) no off-line calibration is required, (d) the power signals were simply measured by a non-invasive, inexpensive power sensor. Thus, the method using K_{TC} &r K_{TE} as the measures of tool wear is a simple and reliable way to monitor the tool wear during machining. Moreover, since K_{TC} & K_{TE} are insensitive to cutting conditions, the major limitation of conventional TCM systems, i.e. "if any process variables are changed during cutting, the threshold of the signal feature will vary greatly and the system must be retrained" [31], is minimized. This result was proved to be valid over a wide variety of cutting conditions.

5.1 Defining a worn tool

Since the definition of a worn tool is highly dependent on the task that the tool is performing, e.g. (e.g. roughing vs. finishing), defining the limits for K_{TC} or K_{TE} must be task dependent. **Figure 5-1** illustrates how the wear limit might be defined for a specific task. An increase of 40% in K_{TE} (70 N/mm) is used to set a limit for changing the tool and an 80% increase (90 N/mm) defines a completely worn tool. Generally, the limitations on the coefficients should satisfy the following prerequisites: (1) K_{TC} is within the stable area and(2) K_{TE} is below the value where fracture occurs.

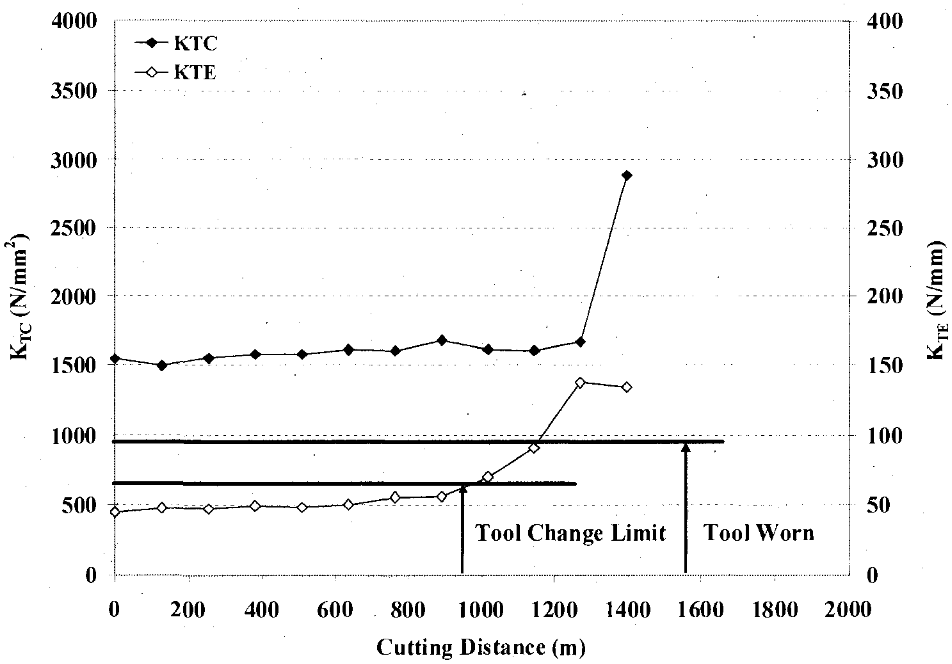

Figure 5-1. Tool wear limits of the tool wear

Figure 5-2 shows micrographs of the tool edge at K_{TE} values of 70 N/mm (lower limit) and 90 N/mm (upper limit) for the carbide tool wear experiments TC1 ~ TC8 listed in **Table 2-1**. Even if chipping on the cutting edge resulted in a sudden loss of tool material and gave a wide dispersion of tool life, carbide tool failure occurred at almost the same coefficients values. In general, chipping or notch wear began to spread or the flank wear VB exceeded 0.2mm at K_{TE}≈70 N/mm, as shown in **Figure 4-8**, which might be defined as the tool change limit, K_{TE} (L_c). When K_{TE} is larger than 90 N/mm, there is a sharp power increase of approximately 25~30% and groove or notch fracture occurs, which can be defined as the tool worn limit, K_{TE} (L_w).

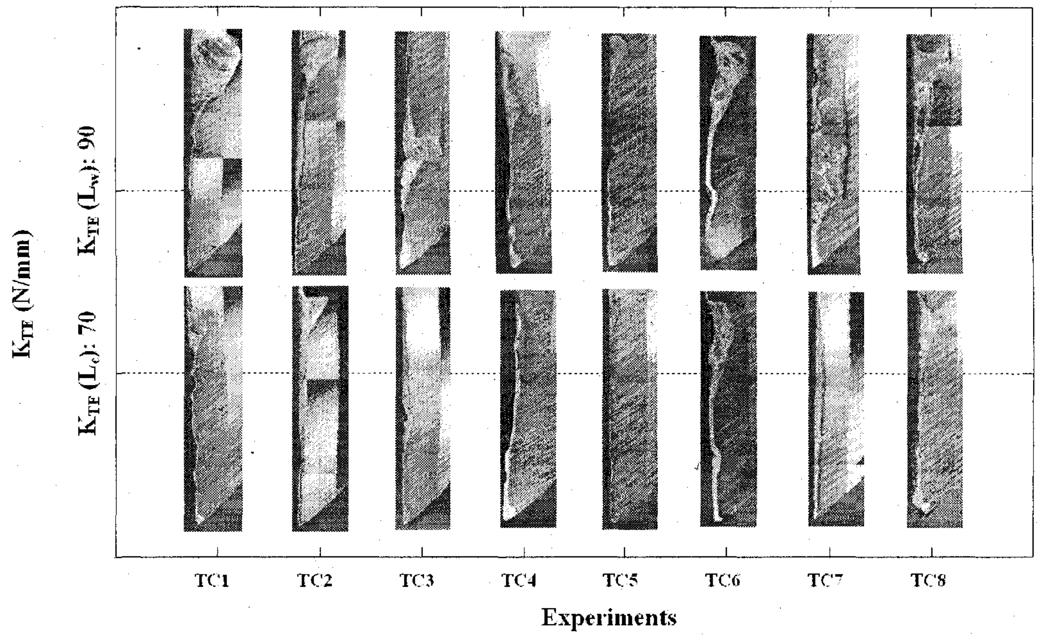

Figure 5-2. Values of K_{TE} for the tool change and worn alarm

Tool life is measured in cutting distance (m) defined as the distance the cutting edge moves while in contact with the workpiece. **Table 2-1** shows the comparison of the tool life, as defined by the 40% and 80% K_{TE} increase criteria. The results are quite interesting and yield some unexpected results. For example, Experiment TC2 shows a decrease in tool life compared to TC1, which is expected since the average chip thickness is increased. However, Experiment TC3 should enjoy a longer life since the chip thickness is lower than Experiment TC1, but it doesn't. Other surprises include a longer tool life than expected when not using coolant (Experiment TC6) and a very short tool life when the radial immersion is decreased (Experiment TC7).

Tool life in milling is a complex phenomenon, highly dependent on the impact of entry and exit, thermal cycling, chip thickness and surface speed. The process is also somewhat stochastic and subject to statistical variation. Models which attempt to predict tool life are therefore inaccurate. In-process estimation is therefore a superior strategy for maximizing tool life.

5.2 In-process estimation of tool wear status

The characteristics of K_{TC} and K_{TE} as measured during this specific set of experiments were that K_{TC} was roughly constant during the first two wear phases and K_{TE} increases proportionately with flank wear. These observations provide a simple and reliable method for online estimation of the tool condition. Therefore, during the first phase of the wear we may substitute the average value of K_{TC} obtained from all eight wear tests into **Equation 2-5** (see **Table 5-1**). It can then be rearranged to estimate the instantaneous value of K_{TE} by simply measuring power for the known material removal rate and contact area rate. This eliminates the need for the two variable regression used to generally calibrate the cutting model coefficients. **Equation 5-1** uses power to estimate tool wear but is superior to simply relying on power increase since it normalizes the wear for the current volumetric removal rate and contact area.

$$K_{TE}(t) = \frac{P_c(t) - \dot{Q} \cdot K_{TC}}{\dot{A}_c} \tag{5-1}$$

Table 5-1. Standard deviation of K_{TC} within stable stage

	Experiment								Average	Standard Deviation	Coeff of Variation
	TC1	TC2	TC3	TC4	TC5	TC6	TC7	TC8			
Ktc	1644.86	1881.08	1828.94	1871.89	1893.30	1726.40	1905.32	1857.35	1826.14	86.37	0.047

The remaining life of a tool can be evaluated by a life remaining ratio (L_r), which is calculated by:

$$L_r = \frac{K_{TE}(L_w) - K_{TE}(t)}{K_{TE}(L_w) - K_{TE}(0)} \tag{5-2}$$

where $K_{TE}(L_w)$ = 80 N/mm as an example, and Lr is a dimensionless ratio equal to one when the tool is new and approaches zero as the tool is worn out. **Figure 5-3** illustrates the procedure of monitoring tool status based on this method. The TCM system would automatically change the tool when the life remaining ratio is zero, i.e. the instantaneous value of K_{TE} reaches the tool worn limit.

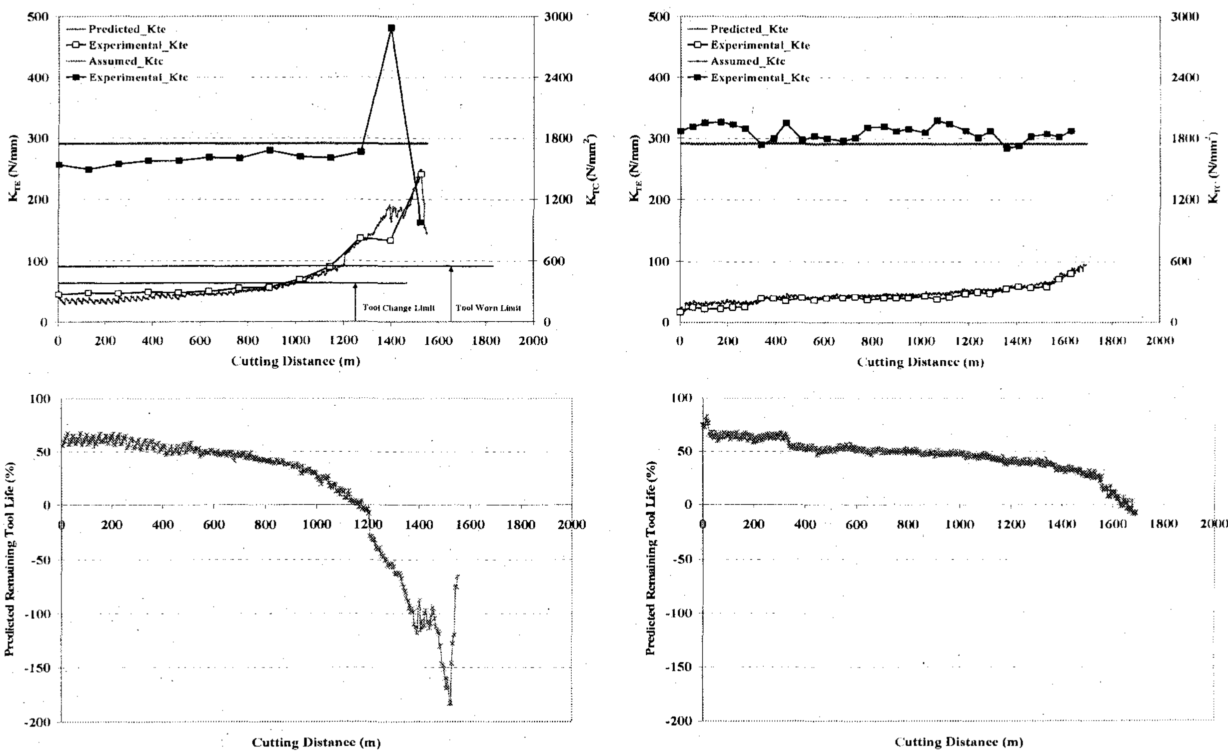

(a) Experiment TC1 **(b) Experiment TC8**

Figure 5-3. Tool wear online estimation by tracking cutting force coefficients

As discussed previously, the major limitation of the conventional TCM systems is that changing process variables greatly affect the worn signal threshold and the system must be retrained. This limitation is minimized by the cutting force coefficients method. To test the performance of our method in the presence of changing process conditions, we conducted a wear experiment at five different conditions with up-milling on an AISI-1018 steel block (12.7 mm HSS flat end mill cutter). Stage (1) provided a baseline, and then one or two variables were changed in each stage. The conditions for each stage are listed in **Table 5-2**.

Table 5-2. Parameters of cutting stages

Stage	Cutting Speed (m/min)	Feedrate (m/min)	Axial Depth (mm)	Radial Depth (mm)
1	35	0.038	3.05	6.350
2	35	0.064	3.05	6.350
3	35	0.038	2.03	6.350
4	35	0.051	3.05	6.350
5	35	0.051	3.05	3.175
6	46	0.046	3.05	6.350

Figure 5-4(a) shows that the conventional signal thresholds, e.g. power, force, and etc., are very sensitive to the change of cutting parameters. In this instance, different power threshold limits must be set for each condition, which greatly increases the complexity of the TCM system. Unlike conventional TCM systems which rely on a simple power threshold, the cutting model coefficients method can work with a wide variety of cutting conditions as shown in **Figure 5-4(b)**.

5.3 Summary

The new cutting force coefficients method is confirmed to be valid in a wide range of cutting conditions. The output from the inexpensive and non-invasive power sensor is input into Equation 5.1 to estimate Kte thereby greatly improving the usage and convenience of a TCM system.

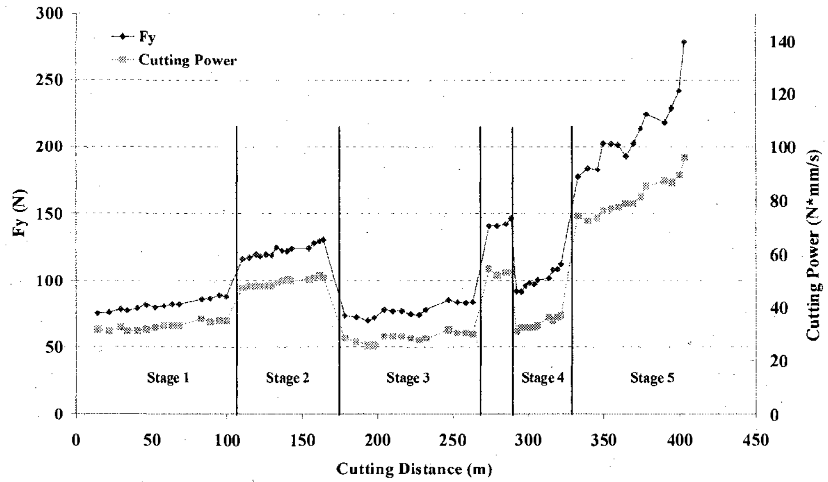

(a) Cutting power and force progression

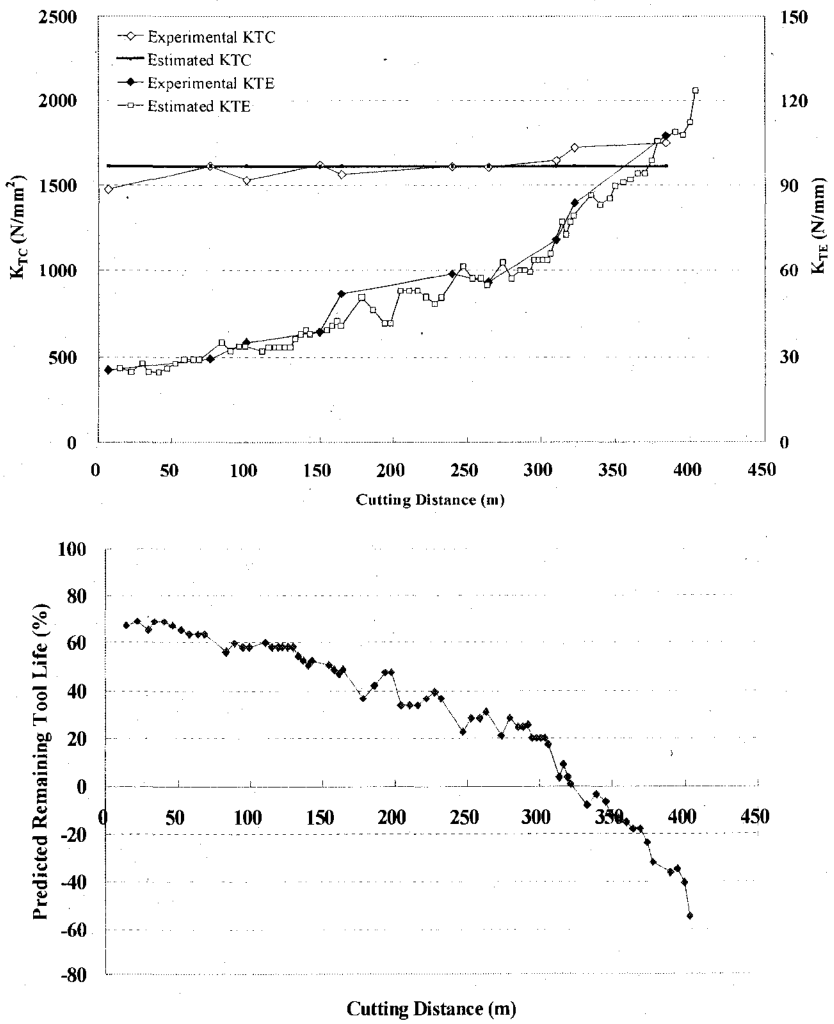

(b) K_{TC} & K_{TE} and tool wear prediction

Figure 5-4. Tool wear monitoring with varied cutting conditions

Chapter 6

RADIAL COEFFICIENTS AND VIBRATION

Tool wear monitoring methods are classified into direct and indirect methods. Direct methods observe the tool wear with optical instruments and indirect methods measure physical phenomena that are correlated with the tool wear. Examples of indirect methods include cutting force, temperature, vibration, spindle motor current, acoustic emission and surface roughness. In this chapter, the radial force model coefficients and vibration methods are investigated. The results indicate that both of these methods can be accurately correlated with tool wear in a specified cutting process, but they are not superior to the tangential force model coefficients method due to their inherent limitation, especially when the cutting conditions are variable.

6.1 Radial Coefficients

As introduced in Section 2-3, the radial coefficients, K_{RC} & K_{RE}, can be calibrated with **Equation 2-9** using the average cutting forces in the X and Y direction using a Kistler dynamometer and the tangential force coefficients calculated from the average cutting power, simultaneously. **Figure 6-1** shows the tangential and radial coefficients from Experiments TC1 ~TC4. K_{RC} & K_{RE} proportionally increased with K_{TC} & K_{TE} during the gradual wear stage, while the rate of increase of K_{RE} increased much faster than K_{TE} toward the end of tool life.

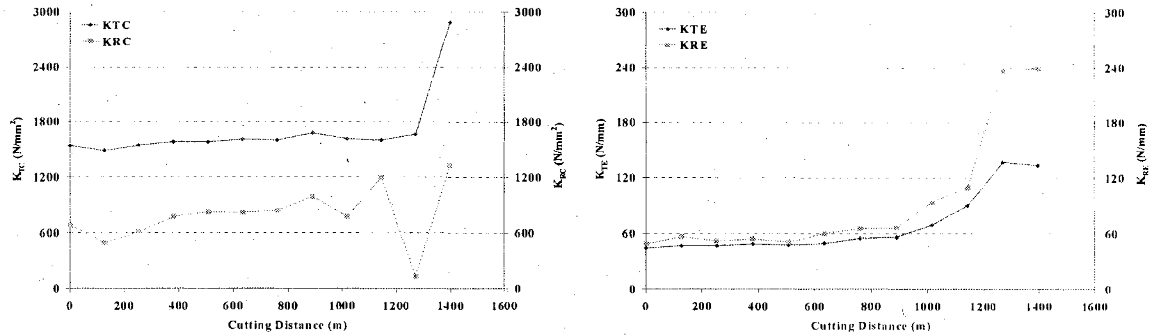

(a) TC1

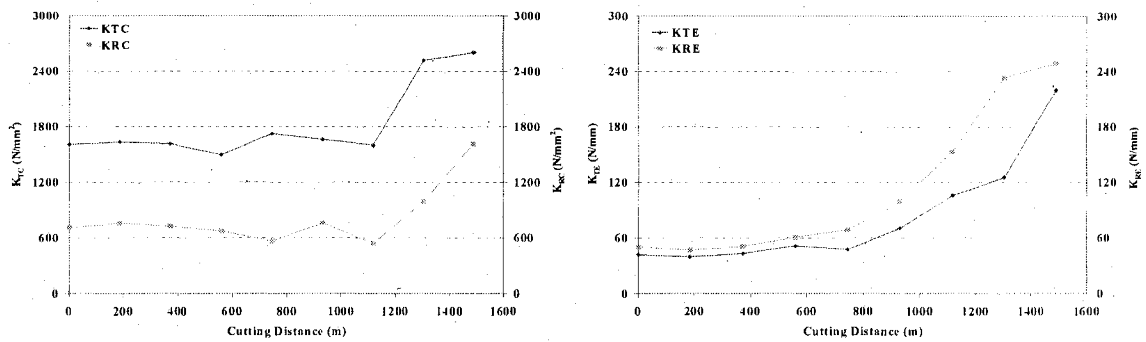

(b) TC2

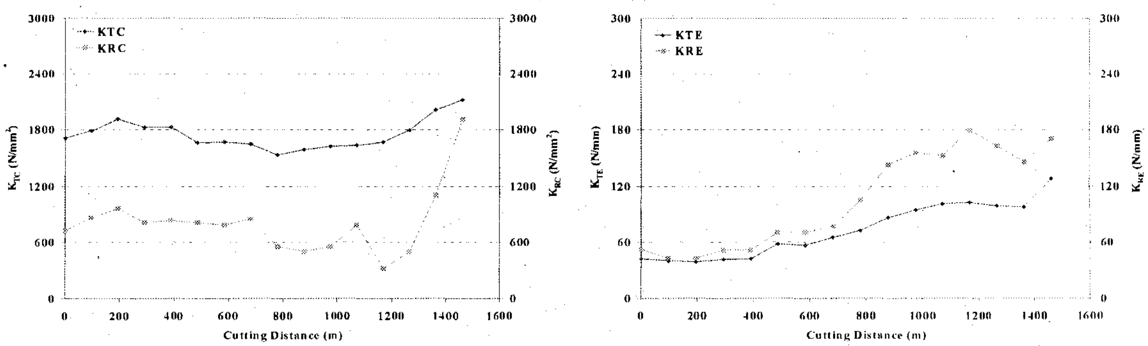

(c) TC3

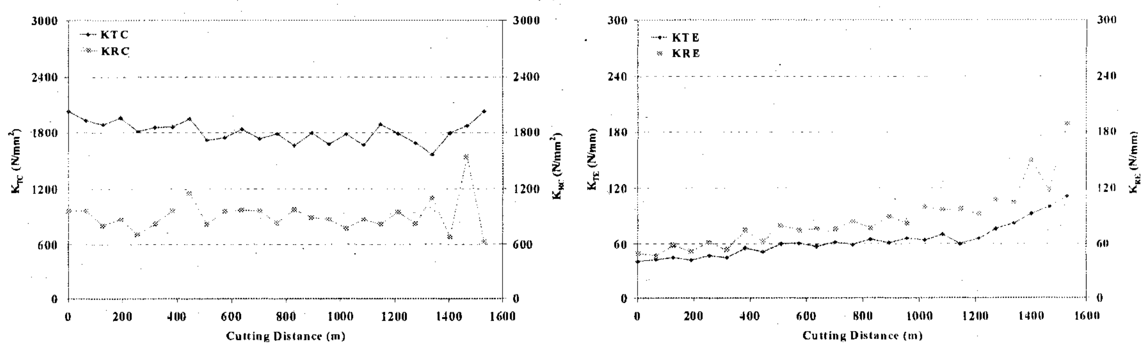

(c) TC4

Figure 6-1 Radial coefficients and Tangential coefficients vs. Cutting Distance

Since K_{RC} & K_{RE} present nearly the same patterns as K_{TC} & K_{TE}, they can be used as the indicators of tool wear. **Figure 6-2** shows that the values of K_{RC} & K_{RE} are about 0.5 and 1.2~1.6 times of K_{TC} & K_{TE}, respectively.

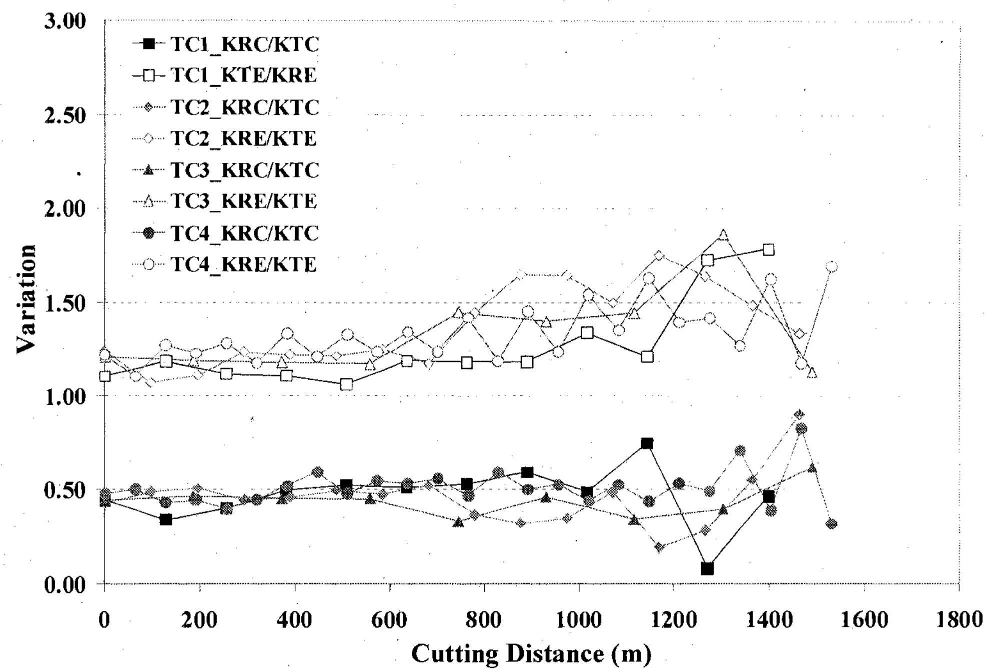

Figure 6-2 Ratios of K_{RC}/K_{TC} and K_{RE}/K_{TE}

It is noted that since the calibration of K_{RC} & K_{RE} is based on the values of the average cutting force and K_{TC} & K_{TE}, the cumulative error of measurements will significantly affect the final results. Moreover, in order to measure the cutting force, it is necessary to use an expensive dynamometer limiting the use of this method.

6.2 Vibration

The advantages of vibration measurement include ease of implementation and the fact that no modifications to the machine tool or the work piece fixture are required [28]. Vibration monitoring is mainly used to detect tool condition, surface quality, and dimensional deviations and chatter phenomenon in machining applications. The previous study [29] showed that the vibration amplitude increases with the progression of tool wear. In this study, the "smart tool" embedding vibration sensor [27] and the contact microphone were used to investigate the relationship between vibration and the tool wear. The sensor configuration is shown in **Figure 6-3**.

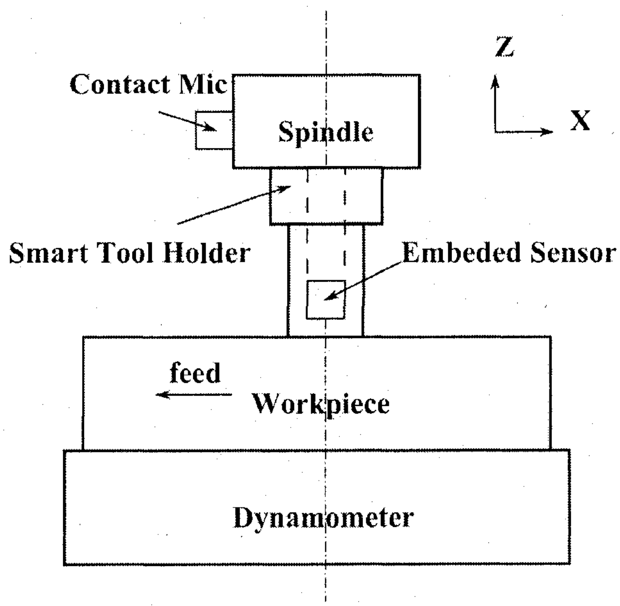

Figure 6-3. Vibration sensor configuration

6.2.1 Smart Tool

A Hosiden, KUB2823 Electret Condenser Microphone was integrated into the "Smart Tool". It has a frequency range of 50 Hz -15000 Hz and a sensitivity of -45Db/Pa. The vibration data was continuously collected by the Electret Condenser Microphones, and transferred to a PC with Bluetooth, and recorded at 20000 Hz.

Since only one insert was used in this study, the tooth passing frequency (TPF) is same as the spindle rotating frequency, 41.7 Hz. The dominant frequency components in the vibration spectrum graph, **Figure 6-4**, are around the spindle frequency and their harmonics. It was observed that the intensity of the vibration energy was concentrated at several frequencies, i.e. the first to fourteenth harmonic of spindle frequency, and the amplitude of vibration signals increased as the flank wear and cutting distance increased.

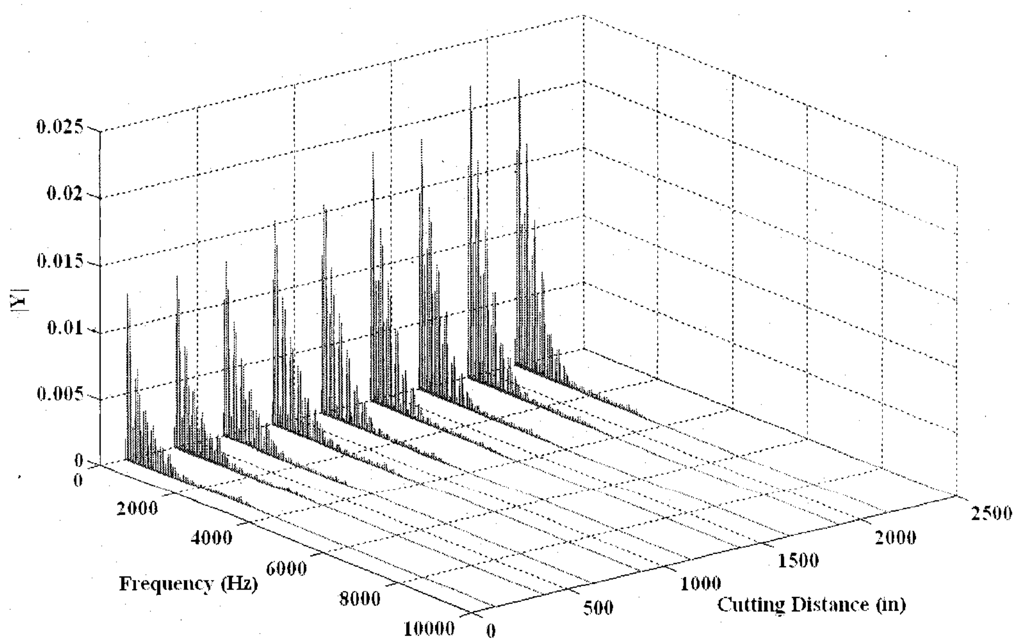

Figure 6-4. FFT progression in Experiment T11 – Smart Tool

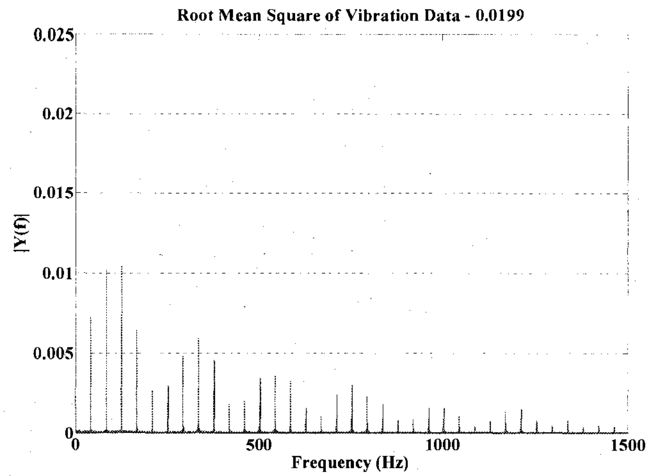

(a) Sharp tool

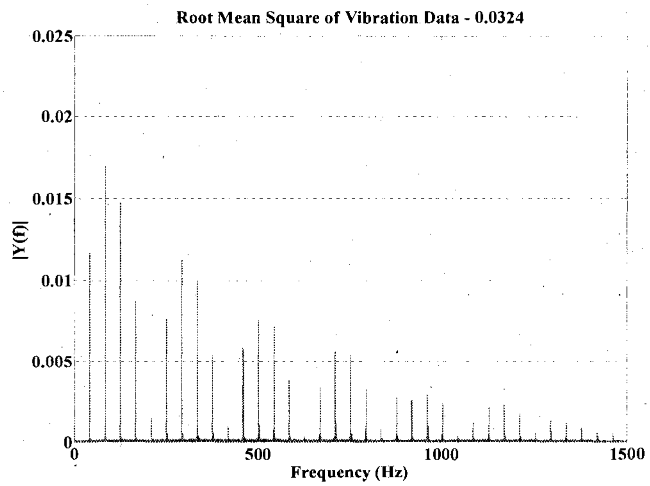

(b) 50% worn tool

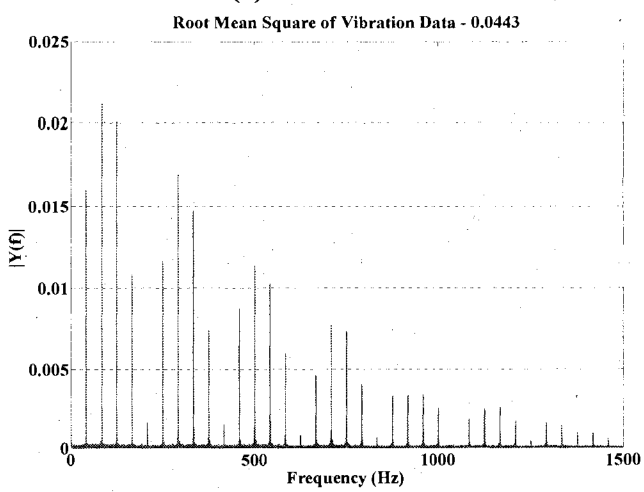

(b) 100% worn tool

Figure 6-5. Vibration spectrum at different wear conditions– Smart Tool

Figure 6-5 shows details of an FFT analysis at three tool conditions, sharp, 50% worn and 100% worn. The dominant peak frequency occurred at the second and third harmonic of spindle frequency, 83.4 and 125.1 Hz. It was found that the magnitude of spindle frequency and its harmonics spectrum increased significantly with increasing flank wear, and the increase amplitude is almost proportional to flank wear, e.g. the amplitude of the first harmonic of spindle frequency increased from 0.0075 (sharp) to 0.012 (50% worn), then to 0.0165 (100% worn). The increment is 0.0045 between sharp and 50% worn, and is also 0.0045 between 50% and 100%. The relationship of vibration amplitude to cutting distance is plotted in **Figures 6-6** and **6-7**.

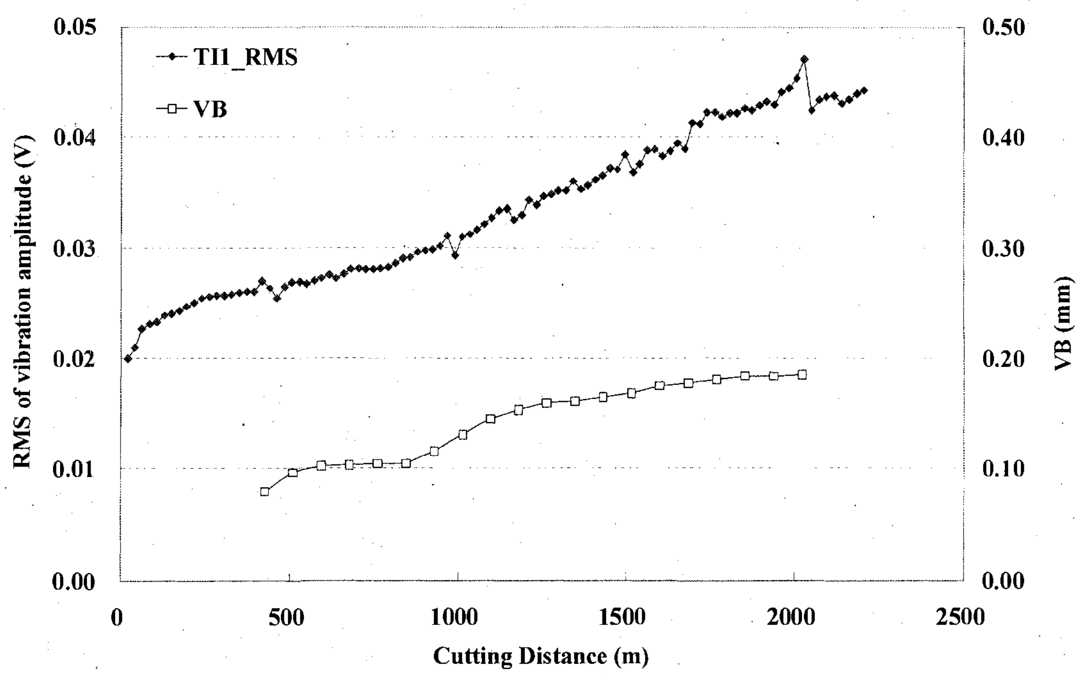

Figure 6-6. RMS of vibration amplitude vs. flank wear (VB) – Smart Tool

Figure 6-6 shows that as tool flank wear increases, the root mean square of vibration amplitude gradually increases. This confirms a previous study showing that the increase in flank wear caused the tool-workpiece contact area to increase such that additional energy was required to cut the part leading to an increase in the noise and vibration emanating from the contact area [30].

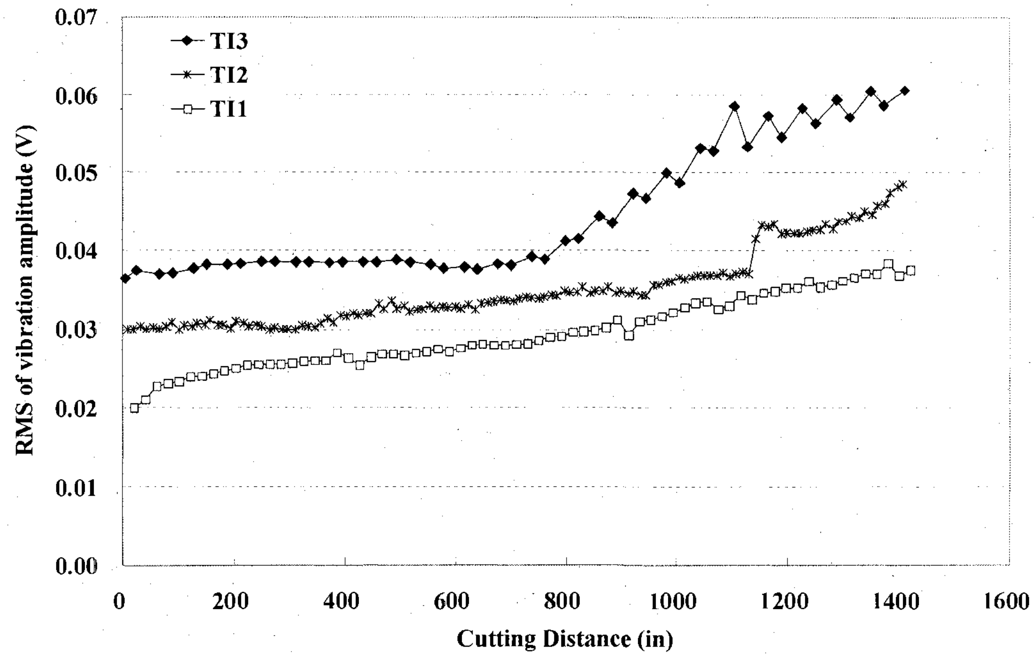

Figure 6-7. RMS of vibration amplitude vs. cutting speed/feedrate – Smart Tool

The root mean square of vibration signals is presented in **Figure 6-7** for different cutting speeds and feedrates. In general, vibration increased with feedrate (TI1 vs. TI2) and with cutting speed (TI1 vs. TI3). The increase in vibration magnitude was much higher with cutting speed, confirming that the cutting speed has the greater effect on vibration signals than the feedrate.

6.2.2 Contact Microphone

An AKG C411 L contact microphone was used to measure vibration in the X cutting direction. It has a range of 10Hz to 18,000Hz and a sensitivity of 1mv/msec-2. The results obtained show that this sensor is almost the same as the "smart tool". There appears to be more scatter in the contact mic measurements but it is difficult to make a fair comparison since the data came from different experiments. Further research would be required with simultaneous experimental data from identical sensors on the spindle and inside the tool. The superiority of a sensor inside the tool would need to be clearly established in order to justify the expense of modifying each tool.

Figure 6-8 presents the progression of the RMS vibration amplitude and flank wear in TI4 as the tool wears. It shows that the signal amplitude of the contact microphone increased with increasing flank wear.

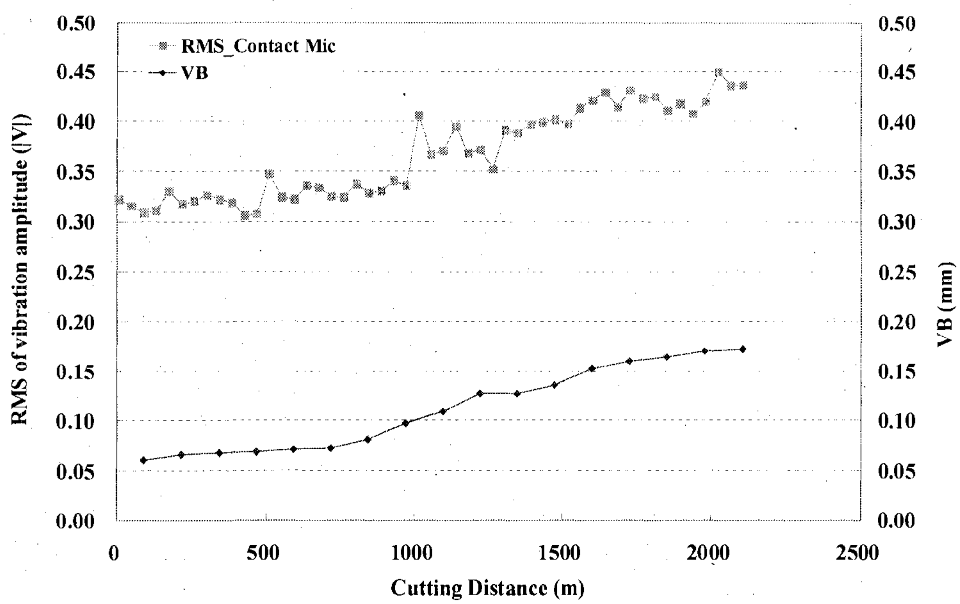

Figure 6-8. RMS of vibration amplitude vs. flank wear (VB) – Contact Mic

The FFT progression of vibration measured by the contact microphone was plotted in **Figure 6-9**, which shows the same increasing trend of FFT amplitude as that of the

"Smart Tool". The dominant peak frequency is located at around the spindle frequency, which is different from "Smart Tool" and should be further investigated.

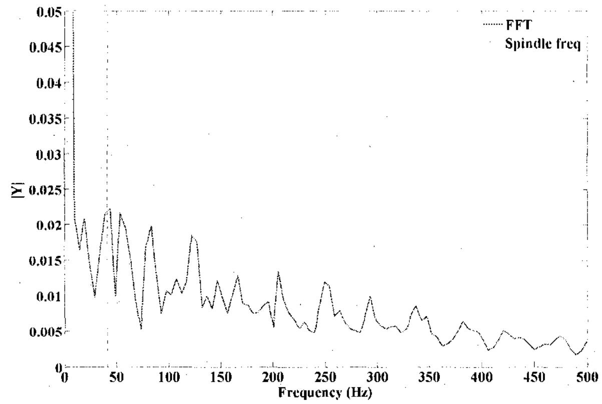

(a) Sharp tool

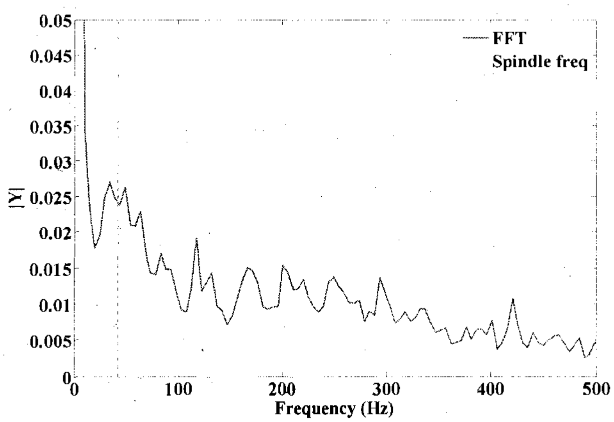

(b) 50% worn tool

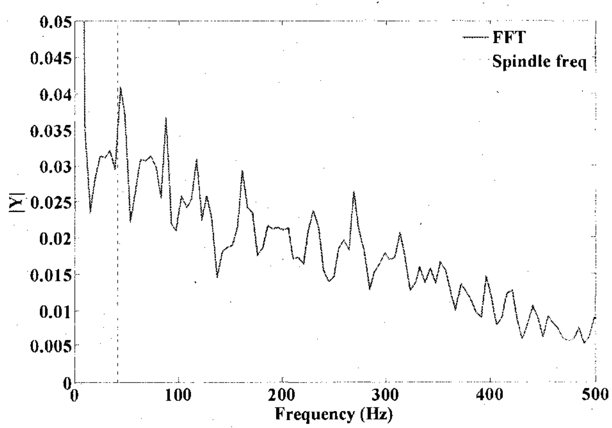

(c) 100% worn tool

Figure 6-9. FFT progression in Experiment TI4 – Contact Mic

6.2.3 Worn Edge Detection using Vibration Signal

In order to investigate the effect of a worn tooth on K_{TC} & K_{TE} of a tool with three teeth, one up milling experiment was conducted on AISI-6061 aluminum block with the same Sandvik insert and shank, R390-11 T3 08M-PM and RA390-016O16L-11L, with (1) 3 sharp inserts; (2) 2 sharp and 1 worn inserts; (3) only 1 worn insert. In this test, the cutting speed was set to 175 m/min, feed of the wear stage was f = {0.25, 0.38, 0.51, 0.64, 0.76} mm/min, and the radial and axial depths were constant at 3.05 and 5.08 mm, respectively.

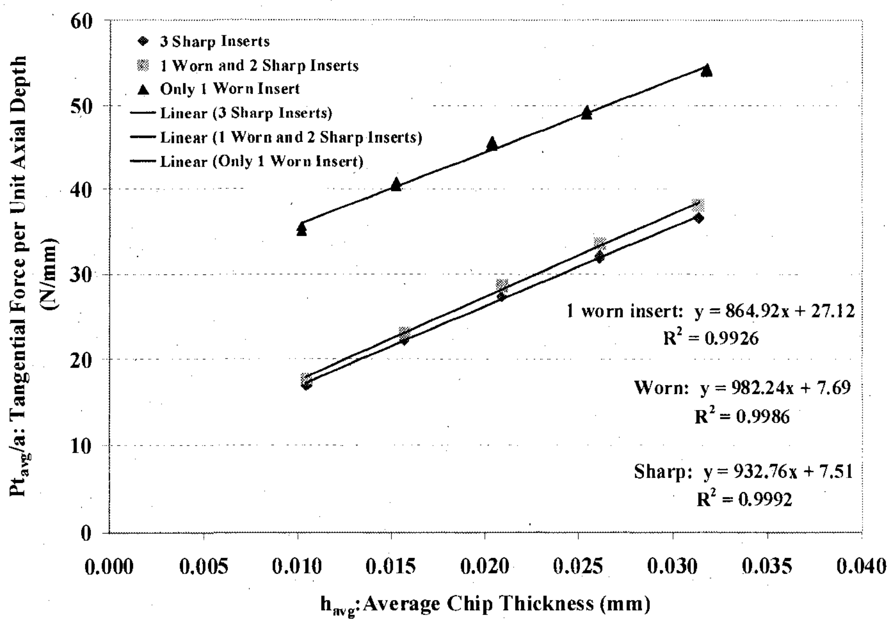

Figure 6-10. K_{TC} & K_{TE} of different worn edge conditions

The upper curve in **Figure 6-10** is for a single worn tooth. The plot at the bottom is for a tool with three sharp teeth and the line just above that is with one worn tooth and two sharp teeth. The graph clearly indicates that it would be difficult to use power to diagnose a single worn tooth when the rest of the teeth are still sharp, see **Table 6-1**. While both K_{TC} & K_{TE} increase with a single worn tooth on a multiple tooth tool, the increase is very small compared to the single worn tooth case. The 261% change dwarfs the 2-5% change when one tooth is dull and two are sharp.

Table 6-1. Variation of K_{TC} & K_{TE} for different worn conditions

	3 Sharp	1 Worn 2 sharp (%)	1 Worn (%)
K_{TC}	932.24	982.4 (+5.4%)	864.92 (-7.2%)
K_{TE}	7.51	7.69 (+2.4%)	27.12 (+261%)

Figures 6-11 and **6-12** show that there is no significant difference in power between a tool with three sharp inserts and a tool with one worn and two sharp inserts. For cutting force, Fy, the amplitude of the first harmonic of spindle frequency decreases, while the amplitude of the second harmonic of spindle frequency increases. For the contact mic the amplitude of the first harmonic of spindle frequency decreases, while the amplitude of the second harmonic of spindle frequency also decreases. Thus, FFT of Fy and contact mic can be used to detect a worn tooth in a multi-teeth insert cutter.

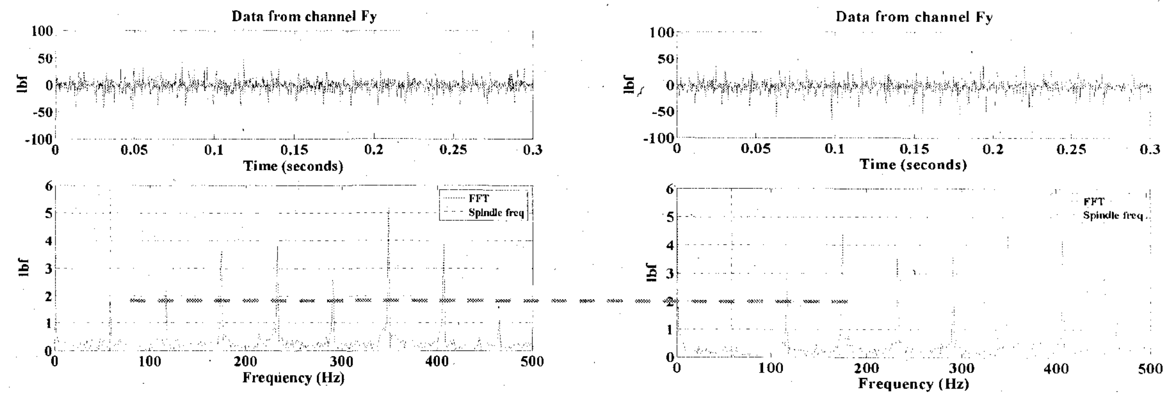

(a) Fy

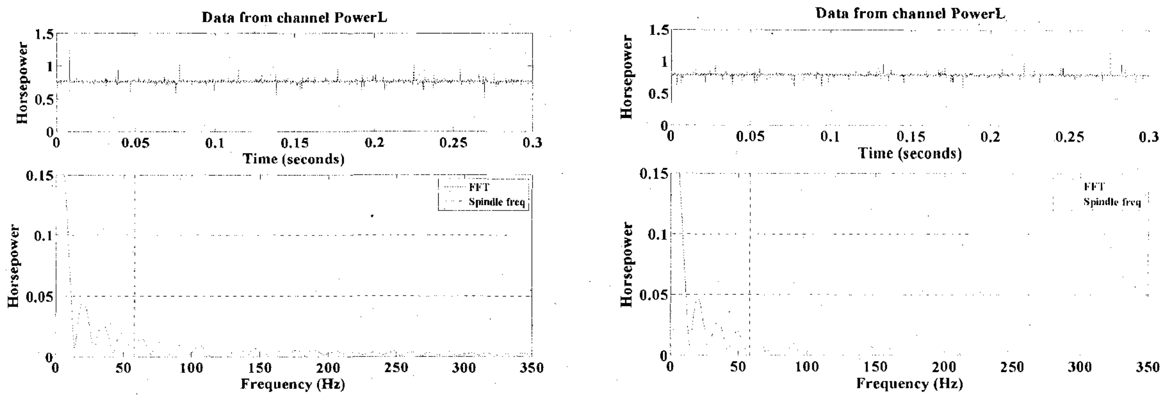

(b) Cutting power

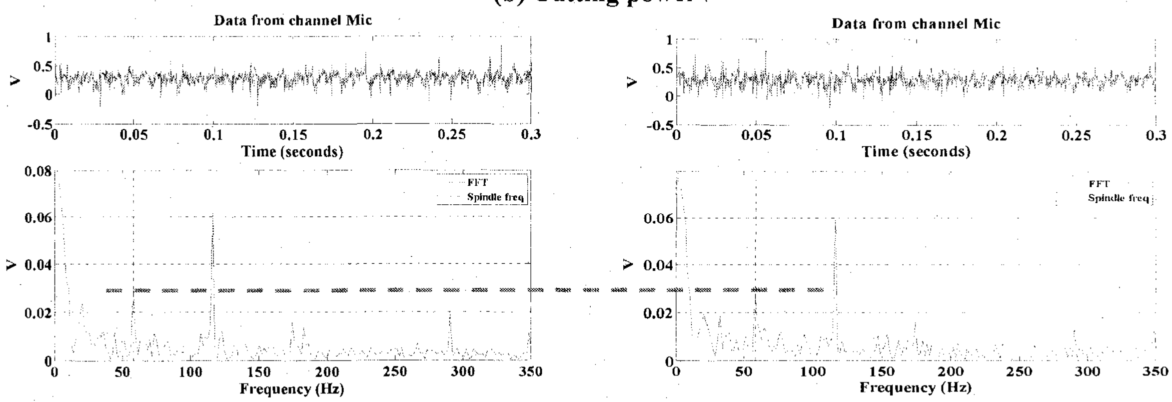

(c) Contact mic

3 sharp inserts | 1 worn and 2 sharp inserts

Figure 6-11. FFT of cutting force, power and contact microphone signals at f = 0.51 mm/min

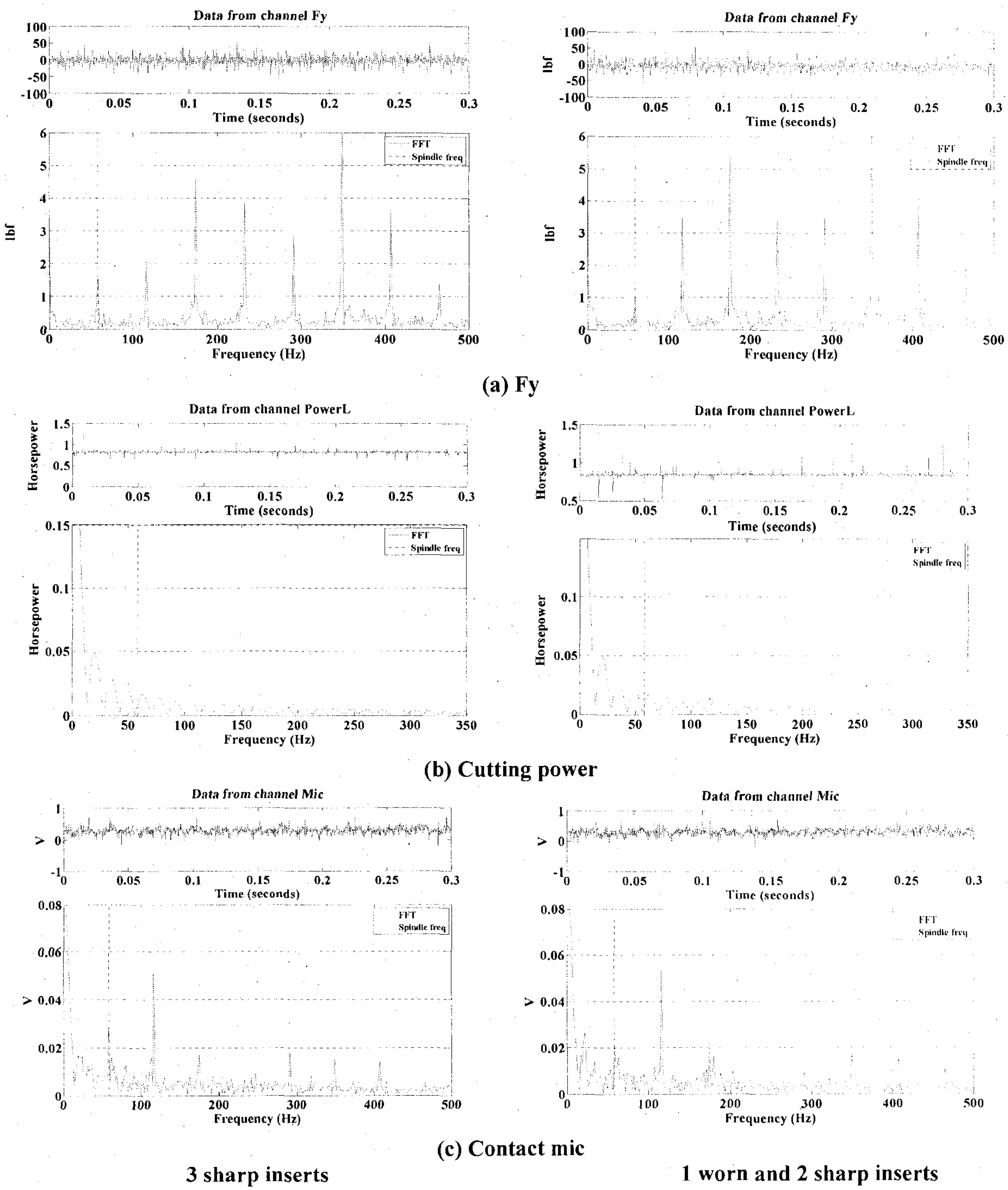

Figure 6-12. FFT of cutting force, power and contact microphone signals at f = 0.64 mm/min

6.3 Summary

The radial force coefficients, K_{RC} & K_{RE}, are proven to be proportional to the tangential force coefficients, K_{TC} & K_{TE}. Unlike the previous reported results [12] that both K_{RC} and K_{RE} are about 0.3 times K_{TC} and K_{TE}, the experimental results show that K_{RE} is larger than K_{TE} and increased at a greater rate near the end of the tool life. The vibration method has advantages over the coefficient method in detecting slight tool wear because the change of the cutting power is not large enough to be distinguished. The root mean square of the vibration amplitude has a direct relation with flank wear, and the FFT of the vibration signals increase with cutting distance and flank wear. Both vibration methods are sensitive to changes in the cutting conditions.

Chapter 7

CONCLUSION AND FUTURE WORK

7.1 Conclusion

In this thesis, tool wear monitoring techniques for the end milling process are proposed. The first approach involves using cutting force coefficients to estimate tool wear. The other approach uses the relationship between flank wear and vibration signals to track tool wear. The experimental results of this series of tests using three kinds of cutters, i.e. an uncoated carbide flank end mill cutter, a coated carbide insert and a HSS flank end mill cutter, on AISI-6061 aluminum and AISI-1018 steel show that both cutting coefficients and vibration can be used as reliable indicators of tool wear.

7.1.1 Tangential Force Model Coefficients

Various calibration experiments were conducted to investigate the feasibility of using the tangential force model coefficients, K_{TC} and K_{TE}, as indicators of tool wear. The experimental results proved that K_{TC} and K_{TE} satisfy all requirements:

- Insensitive to cutting conditions – The changes in cutting conditions have little effect on K_{TC}, and K_{TE}. The variations of K_{TC} at four different radial immersions (100%, 75%, 50%, 25%), eight different cutting speeds (1000, 1500, 2000, 2500, 3000, 3500, 4000, 4500, 5000 rpm) and eleven different feedrates (0.15, 0.2, 0.3, 0.43, 0.55, 0.67, 0.76, 0.89, 1.02, 1.14, 1.27 m/min) were less than 2 percent. But, changes in the tool geometry (e.g.

helix angle, rake angle, etc.) does have a significant influence on K_{TC} and K_{TE}. Calibrations on a BEM cutter confirmed that K_{TC} decreased as the helix angle increased.

- Highly sensitive to tool wear – K_{TE} linearly increases with the flank wear area (VB), and therefore has the potential to predict tool flank wear without in-process calibration. K_{TC} was found to be almost constant with the progression of the flank wear under different cutting conditions, but was affected by edge chipping or macro fractures. Large chipping or fractures change the geometry of the cutting edge, and consequently cause K_{TC} to dramatically change near the end of tool life. K_{TC} is suitable to discern the tool wear stages.

- Consistency – K_{TC} and K_{TE} express similar characteristics for all of the wear tests and are not affected by tool materials and variations in the cutting conditions, e.g. spindle speed, feedrate, coolant/no coolant, up or down milling: K_{TC} stayed relatively constant within the stable life stage, and K_{TE} increased proportionally with tool flank wear.

Therefore, a cutting force coefficient method was proposed to continuously monitor tool wear that is universal for all cutting conditions. Since a non-invasive power sensor was used in this method and a universal threshold can be used for most practical cuts, this method may be both simple and convenient for monitoring tool wear and more accurate than existing TCM systems which typically relay on only a power measurement.

7.1.2 Vibration Signals

The relationship between vibration and tool wear was investigated during end milling. It is well known that the vibration amplitude increases with tool wear. In this study, FFT amplitude of the vibration signals were in agreement with this common expectation. The increase in amplitude of the peak frequencies with increasing wear was more obvious at the first to fourth harmonics of spindle frequency. Comparing the change in flank wear and vibration amplitude, it is clear that flank wear (VB) has a critical role in the progression of vibration.

Although the vibration method has its inherent disadvantage in monitoring tool wear, i.e. greatly affected by cutting conditions, it is very useful in wear detection of slight cutting conditions, where the change of tool wear is not large enough to be detected by the power threshold method.

7.2 Future Work

7.2.1 Effects of Tool Geometry and Material on Coefficients

This series of experiments were carried out mostly with 30-degree helical end mills with three kinds of tool material in AISI-6061 aluminum and AISI-1018 steel. More experiments should be done with other types of tools to investigate the effect of tool geometries on tangential force coefficients, e.g. helix angle, rake angle, and dimension. It is expected that tool material has no effect on K_{TC} & K_{TE} such that tools with the same geometries but different tool material will provide similar coefficients. The percent change in KTE for a given wear state may also depend on the material being cut and this needs to be studied.

7.2.2 Effect of Cutting Environment on Tool Wear

High-speed machining generates high cutting temperatures in the tool-chip interface, which rapidly decreases tool life due to the increased temperature. Improvements in productivity greatly depend on the effectiveness of the cooling/lubrication environment. In this study, the life of carbide tools without coolant is much longer than expected, which indicates that finding the optimal cooling/lubrication environment is a critical issue to improve tool life, and is worthy of further research.

7.2.3 Coefficients and Surface Finish

It is well known that tool wear has a great effect on surface finish. Our experimental results show that chipping and macro fractures cause changes in K_{TC}. If there is a direct relation between coefficients and surface finish, the new cutting force coefficient method combined with vibration measurement should be able to predict surface finish.

7.2.4 Vibration

More experiments would be performed with simultaneous experimental data from identical sensors on the spindle and inside the tool. The superiorities of a sensor inside the tool would need to be clearly established, e.g. the sensitivity of the vibration signals and the effect of the measuring direction.

REFERENCES

1 Prickett, P. W. and C. Johns, (1999), "An overview of approaches to end milling tool monitoring", International Journal of Machine Tools and Manufacture, Vol. 39, pp. 105-122.

2 Rehorn, A. G., J. Jiangand, and P. E. Orban, (2004), "State-of-the-art methods and results in tool condition monitoring: a review," International Journal of Advanced Manufacturing Technology, DOI 10.1007/s00170-004-2038-2.

3 Y. Altintas (1992), "Prediction of cutting forces and tool breakage in milling from feed drive current measurements", ASME Journal of Engineering Industry 114 386–392.

4 X. Li, H.X. Li, X.P. Guan, R. Du, "Fuzzy estimation of feed-cutting force from current measurement—a case study on intelligent tool wear condition monitoring", IEEE Transactions on SMC (Part C) 34 (2004) 506–512.

5 Kim S, Klamecki BE, "Milling cutter wear monitoring using spindle shaft vibration", J Manuf Sci E-T ASME 1997;119:118–9.

6 Waschkies, E., "Tool wear monitoring at turning", Trans. ASME,J. Engng for Industry, 1994, 116, 521–524.

7 Carolan, T. A., Wilkinson, P., Hand, D. P., Barton, J. S., Jones, J. D. C. and Reuben, R. L. "Assessment of tool wear in milling using acoustic emission detected by a fibre-optic interferometer", Trans. ASME, J. Mfg Sci. Engng, 1996, 118, 428–433.

8 Xu, Min, Robert B. Jerard and Barry K. Fussell, "Energy Based Cutting Force Model Calibration for Milling", Comput.-Aided Des. Appl., 2007, Vol. 4, Nos. 1-4, p 341-351.

9 Robert B. Jerard, Barry K. Fussell, Bennett Desfosses, Min Xu, Bryan Javorek, Yanjun Cui, Jeffrey Nichols, Raed Hassan, Chris Suprock, (2008), "Model - Sensor – Information Technology Integration for Machine Tools", NSF Engineering Research and Innovation Conference, , Knoxville, Tennessee

10 Novak, H. Wiklund, "On-line prediction of the tool life", Annals CIRP 45/1 (1996) 93–96.

11 Ryabov, K. Mori, N. Kasashima, "In-process direct monitoring method milling tool failures using a laser sensor", Annals CIRP 45/1 (1996) 97-100.

12 Altintas, Y., (2000), "Manufacturing Automation: Metal Cutting Mechanics, Machine Tool Mechanics, Machine Tool Vibrations, and CNC Design", Cambridge University Press, ISBN 0-521-65973-6.

13 Jerard, R. B., B. K. Fussell, M. Xu, C. Yalcin, (2006), "Process Simulation and Feedrate Selection for Three-axis Sculptured Surface Machining", International Journal of Manufacturing Research, 1(2), pp. 136-156.

14 M. Laszlo, P. Janos, "Step towards intelligent manufacturing: modeling and monitoring of manufacturing processes through artificial neural networks", Annals CIRP 42/1 (1993) 485–488.

15 K. Jemielniak, O. Otman, "Catastrophic tool failure detection based on acoustic emission signal analysis", Annals CIRP 47/1 (1998) 31–34.

16 D.A. Dornfeld, M.F. Devries, "Neural network sensor fusion for tool condition monitoring", Annals CIRP 39/1 (1990) 101–105.

17 T.J. Ko, D.W. Cho, J.M. Lee, "Fuzzy pattern recognition for tool wear monitoring in diamond turning", Annals CIRP 41/1 (1992) 125–128.

18 J. Gu, G. Barber, S. Tung, R.-J. Gu, "Tool life and wear mechanism of uncoated and coated milling tools", Wear 225 (1999) 273–284.

19 Serope Kalpakjian, Steven R. Schmid, 2008, "Manufacturing Processes for Engineering Materials", 5th Edition, Pearson Education, Inc

20 George Tlusty, "Manufacturing Processes and Equipment", Prentice-Hall, 1999.

21 N. Liu, C. Han, H. Yang, Y. Xu, M. Shi, S. Chao, F. Xie, "The milling performances of TiC-based cermet tools with TiN nanopowders addition against normalized medium carbon steel AISI1045", Wear 258 (2005) 1688–1695

22 Shaw, M.C., Thurman, A.L., and Ahlgren, H.J., (1966). J.Engng.Ind.88.142

23 E.M. Trent, P.K. Wright, "Metal Cutting", fourth ed., Butterworth-Heinemann, Oxford, 2000.

24 T.H.C. Childs, K. Maekawa, P. Maulik, 'Effects of coolant on temperature distribution in metal machining", Mater. Sci. Technol. 4 (1988) 1006–1019.

25 S.B. Billatos, N. Basaly, "Design and analysis of fluidless cooling devices for high speed machining", ASME Conference Design Engineering and Technical, Boston, Main, USA, 1995, pp. 779–807

26 Joël RECH, "CUTTING EDGE PREPARATION AND SURFACE ISSUES", HSS Forum's International Conference « Smart solutions for metal cutting », Aachen, 2-3 February 2005

27 Suprock, C.A., Fussell, B.K, Jerard, R.B., Hassan, R.Z., (2008) "A Low Cost Wireless Tool Tip Vibration Sensor for Milling", ASME MSEC 2008, MSEC_ICMP2008-72492

28 Metha, N. K., Pandey, P. C. and Chafcravarti, G., 1983, "An Investigation of Tool Wear and Vibration Spectrum in Milling," *Wear,* Vol. 91, pp. 219-234.

29 Steinhauz, G., Braun, S., and Lenz, E., 1984, "Automated Vibration Based Tool Wear Monitoring: Application to Face Milling," *Proceedings of ASME International Computers in Engineering Conference,* pp. 401-406.

30 R.Y. Chiou, S.Y. Liang, "Analysis of acoustic emission in chatter vibration with tool wear effect in turning", International Journal of Machine Tools and Manufacture 40 (2000) 927 - 941.

31 Jones, J., Y. Wu, "Cutting tool's power consumption measured", US Patent, US 5 587 931. 1996

32 "Tool life testing in milling - Part 2: End milling", ISO 8688-2:1989, American National Standards Institute

33 Predator Software, http://www.predator-software.com, accessed Oct. 10, 2008.

APPENDIX A: Tool Wear Experiment Setup Procedure

1. Select the cutter type, the number of flute, cutting speed and sampling revolutions.

Example:

RPM	2500
Diameter (in)	0.5
Flute	1
Sampling Revolutions	30

2. Select radial depth (the entry and exit angle)

Example:

	slot	3/4down	1/2 Down	1/4 Down	Center
$\Delta\Phi$ (Φ_{exit}-Φ_{entry})	3.1416	2.0944	1.5708	1.0472	0.6515
The radial depth (b)	0.5	0.375	0.25	0.125	0.2

3. Select average chip-thickness to calculate feedrate

$$f = h_{avg} \cdot \left(\frac{r \cdot \omega \cdot n \cdot \Delta\phi}{b} \right)$$

Example:

	Feedrate (in/min)				
havg (in)	slot	3/4down	1/2 Down	1/4 Down	Center
0.00040	1.57	1.40	1.57	2.09	0.81
0.00060	2.36	2.09	2.36	3.14	1.22
0.00080	3.14	2.79	3.14	4.19	1.63

The chip-thickness ranges for different materials:

	Average chip-thickness (in)	
Tool Material	Aluminum	Steel
HSS	0.001~0.0025	0.005~0.0012
Carbide	0.001~0.004	0.008~0.002
1. At least four different feedrates should be used in a calibration.		
2. Each feedrate should be repeated at least twice.		

4. Calculate calibration cutting distances

Since the wear rate of cutters, especially HSS cutter, is very high when tool wear experiments are conducted with high cutting speed on steel blocks, the calibration procedure should be operated within a distance as short as possible to avoid the unwanted wear. Two elements will be considered to design this cutting distance: (1) power sensor time constant; (2) sampling revolution.

4.1 Power Sensor Time Constant

The time constant is defined as the time for a power sensor to vary its output value by 68% of the total difference between its initial power and its final power when it is subjected to a power step function. As Figure A-1 shows, the time constant of the power sensor, T_c, in our machine is about 0.5s.

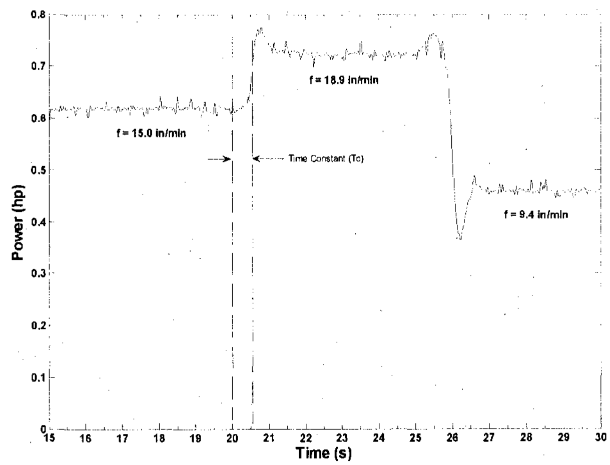

Figure A-1. The power sensor signals

4.2 Calibration Cutting Distance

If the sampling revolution, r_s, is equal to 30, the calibration cutting distance of each feedrate, L, is calculated as following:

- Waiting time - $T_w = 3 \times T_c$
- Measure time - $T_m = r_s/\omega$

$$L = 2.2 \cdot \max(T_w, \quad T_m) \cdot f$$

Example:

havg (in)	Section	Feedrate	safety distance	measure distance	length
0.0004	1	0.603	0.010	0.021	0.045
0.0006	2	0.904	0.015	0.031	0.068
0.0008	3	1.205	0.020	0.041	0.090

In order to get reliable results, the calibration of each feedrate should be repeated at least twice, but the total calibration cutting distance should be less than 3 inches for carbide tools, and 1.8 inches for HSS tools.

5. Experiments Preparation

- Since the cross-section of workpiece is not perfectly square, the top surface should be finished to prevent the measured cutting power fluctuating from one side to another side.
- The dynamometer must be reset every five minutes to avoid zero drift.
- The maximal cantilever of the thin plate should be less than 20 times of its thickness to avoid resonance.
- It takes about 10 minutes to warm the CNC machine and stabilize tare power before any tests can be run.

APPENDIX B: KISTLER Dynamometer Calibrating Procedure

1. Install KISTLER dynamometer

   (a) Remove all blocks on the KISTLER dynamometer;

   (b) Use the edge finder to make the x/y axes of KISTLER dynamometer parallel with the x/y axes of FADAL CNC.

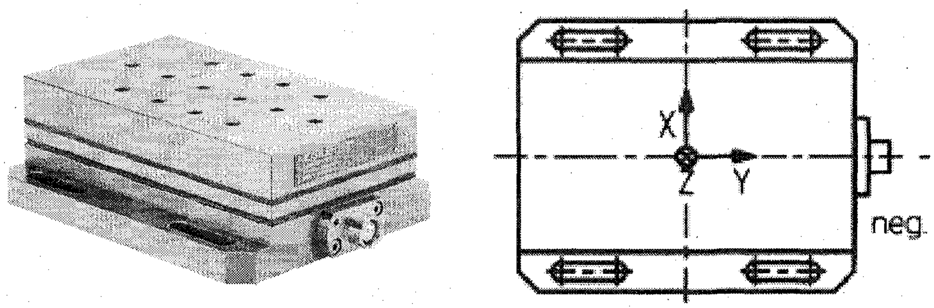

Figure B-1. Direction of KISTLER dynamometer

2. Measure force with VC Performance

   Optimize > Data Acquisition: set sampling rate = 20 Hz; sampling time = 5 s.

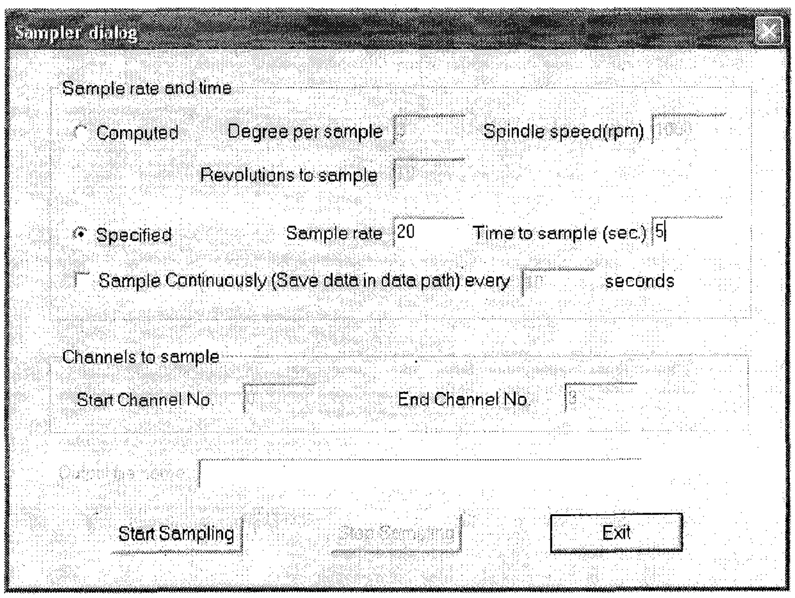

Figure B-2. Data sampling screen

3. Force Calibration

(a) Fx – use the spindle to push the spring scale against the dynamometer at the center point of its left side with various specified forces, as shown in Figure B-3.

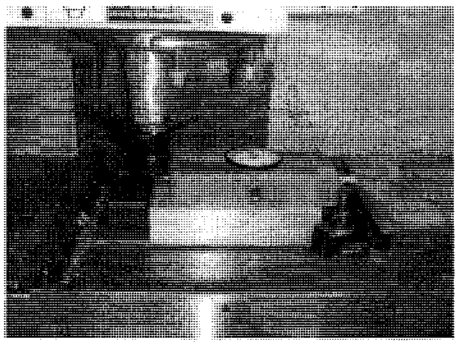

Figure B-3. X-direction loading

Fx INPUT(lb)	OUTPUT1	OUTPUT2	OUTPUT3	Average (lb)
10	10.7770	11.3559	10.9650	11.0326
20	21.4403	21.6526	21.3587	21.4839
30	31.7210	32.1082	31.7540	31.8611
40	41.6679	41.2857	41.8475	41.6004
50	52.2201	51.8874	51.6691	51.9255
60	61.9022	61.1680	62.8952	61.9885
75	77.5204	76.6531	76.0449	76.7395
90	91.4218	90.6490	90.6857	90.9188

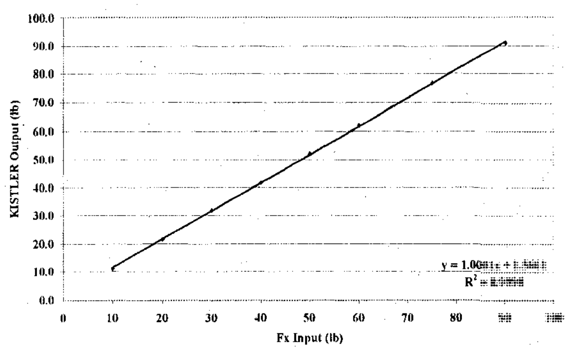

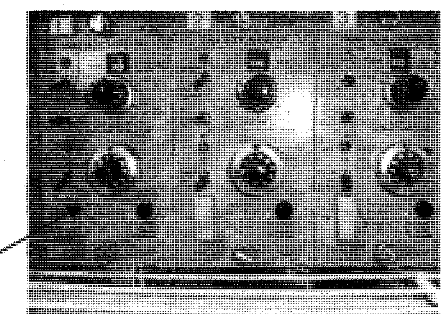

$$\frac{N_{ideal}}{1} = \frac{N_{current}}{K}$$ N: sensitivity of amplifier;

K: ratio of input and output force (slope)

(b) Fy – the same procedure as Fx

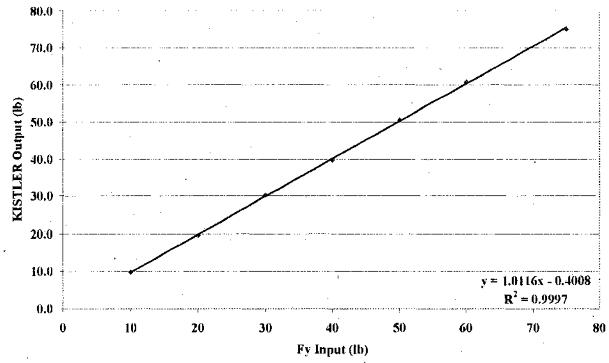

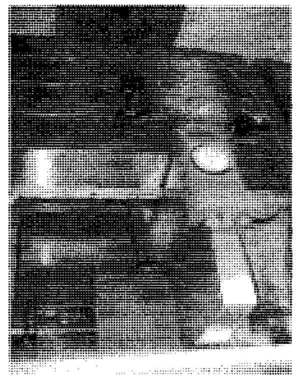

(c) Fz – Calibrate Fz by loading several steel blocks on the dynamometer.

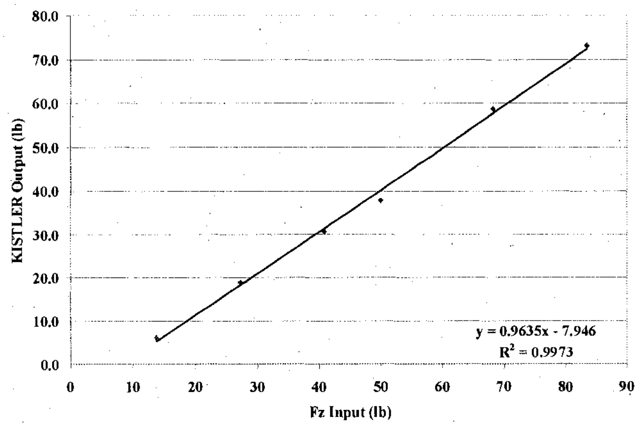

$$N_{ideal} = \frac{N_{current}}{K} = \frac{3.69}{0.9635} = 3.83$$

4. Measure force without loading for 5 minutes to check the situation of zero drift of the dynamometer.

APPENDIX C: Experiment Results

1.1 Experiment C1

RPM	RD (mm)	AD (mm)	Feedrate (mm/min)	Q_dot (mm^3/s)	Ac_dot (mm^2/s)	Power (N*mm/s)	P/Ac (N/mm)	Q/Ac (mm)
3819	12.7	5.08	2.5	2.731	215.04	458692.8	34.5	0.0127
3819	12.7	5.08	3.4	3.642	215.04	506832.2	37.9	0.0169
3819	12.7	5.08	5.1	5.462	215.04	585641.0	44.4	0.0254
3819	12.7	5.08	7.1	7.647	215.04	686391.3	52.2	0.0356
3819	12.7	5.08	9.1	9.832	215.04	793653.0	60.1	0.0457
3819	12.7	5.08	11.2	12.017	215.04	895163.8	67.5	0.0559
3819	12.7	5.08	12.7	13.656	215.04	909265.1	71.3	0.0635
3819	12.7	5.08	14.8	15.932	215.04	1017887.1	79.9	0.0741
3819	12.7	5.08	16.9	18.208	215.04	1132661.1	88.5	0.0847
3819	12.7	5.08	19.1	20.484	215.04	1247298.9	97.6	0.0953
3819	12.7	5.08	21.2	22.760	215.04	1357457.3	106.3	0.1058

1.2 Experiment C3

RPM	RD (mm)	AD (mm)	Feedrate (mm/min)	Q_dot (mm^3/s)	Ac_dot (mm^2/s)	Power (N*mm/s)	P/Ac (N/mm)	Q/Ac (mm)
3000	12.7	5.08	1.99	2.1	84.4	177550.8	34.0	0.025
3000	12.7	5.08	3.99	4.3	84.4	287995.9	56.5	0.051
3000	12.7	5.08	5.99	6.4	84.4	386557.5	75.4	0.076
3000	12.7	5.08	7.98	8.6	84.4	487915.3	96.2	0.102
3000	9.525	5.08	1.77	1.4	56.3	111144.0	33.0	0.025
3000	9.525	5.08	3.55	2.9	56.3	185939.1	56.0	0.051
3000	9.525	5.08	5.32	4.3	56.3	251646.9	75.2	0.076
3000	9.525	5.08	7.10	5.7	56.3	315257.6	93.9	0.102
3000	6.35	5.08	1.99	1.1	42.2	84581.3	33.3	0.025
3000	6.35	5.08	3.99	2.1	42.2	139104.8	56.4	0.051
3000	6.35	5.08	5.99	3.2	42.2	192230.2	76.3	0.076
3000	6.35	5.08	7.98	4.3	42.2	241860.6	95.5	0.102
3000	3.175	5.08	2.66	0.7	28.2	53824.5	31.8	0.025
3000	3.175	5.08	5.32	1.4	28.2	97163.6	57.1	0.051
3000	3.175	5.08	7.98	2.1	28.2	126522.4	75.9	0.076
3000	3.175	5.08	10.64	2.9	28.2	159376.3	94.7	0.102

1.3 Experiment C2

RPM	RD (mm)	AD (mm)	Feedrate (mm/min)	Q_dot (mm^3/s)	Ac_dot (mm^2/s)	Power (N*mm/s)	P/Ac (N/mm)	Q/Ac (mm)
1500	6.35	5.08	1.00	0.5371	21.1	37048.0	30.6	0.025
1500	6.35	5.08	1.99	1.0720	21.1	65707.8	52.4	0.051
1500	6.35	5.08	2.99	1.6091	21.1	92270.5	74.2	0.076
1500	6.35	5.08	3.99	2.1463	21.1	111144.0	89.8	0.102
2000	6.35	5.08	1.33	0.7147	28.1	48931.3	30.1	0.025
2000	6.35	5.08	2.66	1.4293	28.1	85280.3	51.4	0.051
2000	6.35	5.08	3.99	2.1463	28.1	118134.2	71.8	0.076
2000	6.35	5.08	5.32	2.8609	28.1	149590.1	88.9	0.102
2500	6.35	5.08	1.66	0.8945	35.2	61513.7	29.5	0.025
2500	6.35	5.08	2.49	1.3406	35.2	88076.4	40.3	0.038
2500	6.35	5.08	3.32	1.7866	35.2	107648.9	51.6	0.051
2500	6.35	5.08	4.99	2.6811	35.2	153784.2	71.9	0.076
2500	6.35	5.08	6.65	3.5756	35.2	182444.0	86.7	0.102
3000	6.35	5.08	1.99	1.0720	42.2	83183.3	32.4	0.025
3000	6.35	5.08	2.99	1.6091	42.2	109047.0	43.2	0.038
3000	6.35	5.08	3.99	2.1463	42.2	138405.8	54.6	0.051
3000	6.35	5.08	5.99	3.2182	42.2	186638.1	73.7	0.076
3000	6.35	5.08	7.98	4.2902	42.2	230676.3	91.2	0.102
3500	6.35	5.08	2.33	1.2518	49.2	94367.6	31.9	0.025
3500	6.35	5.08	4.66	2.5036	49.2	157279.3	52.9	0.051
3500	6.35	5.08	5.99	3.2182	49.2	198521.4	66.9	0.065
3500	6.35	5.08	6.98	3.7531	49.2	231375.3	78.2	0.076
3500	6.35	5.08	9.31	5.0049	49.2	271219.4	91.0	0.102
4000	6.35	5.08	2.66	1.4293	56.3	104852.9	32.0	0.025
4000	6.35	5.08	3.99	2.1463	56.3	155881.3	42.9	0.038
4000	6.35	5.08	5.32	2.8609	56.3	176152.8	52.4	0.051
4000	6.35	5.08	7.98	4.2902	56.3	245355.7	72.3	0.076
4500	6.35	5.08	2.99	1.6091	63.3	121629.3	31.7	0.025
4500	6.35	5.08	4.49	2.4125	63.3	161473.4	42.3	0.038
4500	6.35	5.08	5.99	3.2182	63.3	232074.3	55.9	0.051
4500	6.35	5.08	8.98	4.8274	63.3	275413.5	71.8	0.076
5000	6.35	5.08	3.32	1.7866	70.3	139104.8	33.0	0.025
5000	6.35	5.08	4.99	2.6811	70.3	183143.0	43.6	0.038
5000	6.35	5.08	6.65	3.5756	70.3	227181.2	53.8	0.051
5000	6.35	5.08	8.31	4.4700	70.3	267025.3	63.2	0.064

1.4 Experiment C4

(a) Calibration with the aluminum thin plate

			Feedrate	4.33mm/s	6.5 mm/s	7.5mm /s	8.67mm/s
Axial Position (mm)	Helix Angle	Ac_dot (mm^2/s)		Q_dot (mm^4/s)			
				68.83	104.19	121.26	138.95
3.81	5	3658.90	havg (mm)	0.0188	0.0285	0.0331	0.0380
			P/Ac (N/mm)	21.1	27.6	31.3	35.0
5.08	11	3186.83	havg (mm)	0.0216	0.0327	0.0381	0.0436
			P/Ac (N/mm)	20.5	26.9	30.4	33.5
6.35	15	2970.32	havg (mm)	0.0232	0.0351	0.0408	0.0468
			P/Ac (N/mm)	22.6	29.5	33.2	36.4
7.62	19	2846.77	havg (mm)	0.0242	0.0366	0.0426	0.0488
			P/Ac (N/mm)	23.9	31.5	35.5	38.9
8.89	23	2774.83	havg (mm)	0.0248	0.0375	0.0437	0.0501
			P/Ac (N/mm)	26.5	34.1	38.1	41.7
10.16	26	2752.77	havg (mm)	0.0250	0.0379	0.0441	0.0505
			P/Ac (N/mm)	26.4	34.0	38.2	41.8
11.43	28	2735.09	havg (mm)	0.0252	0.0381	0.0443	0.0508
			P/Ac (N/mm)	24.0	31.7	35.8	39.6
12.7	30	2735.09	havg (mm)	0.0252	0.0381	0.0443	0.0508
			P/Ac (N/mm)	23.3	31.4	35.7	39.2

KTC (N/mm^2)	KTE (N/mm)	z position (mm)
725.62	7.26	3.81
596.49	7.53	5.08
589.66	8.92	6.35
614.19	9.08	7.62
604.21	11.51	8.89
609.89	11.13	10.16
609.04	8.66	11.43
628.47	7.51	12.70

(b) Calibration with the aluminum block

Axial Depth (mm)	Helix Angle (degree)	Ac_dot (mm^2/s)	Feedrate	4.33mm/s	6.5 mm/s	7.5mm /s	8.67mm/s
			Q_dot	81.45	123.14	143.13	164.22
			havg (mm)	0.0156	0.0236	0.0274	0.0314
3.81	5	5224.56	P/Ac (N/mm)	19.5	25.6	28.7	31.5
			Q_dot	109.0	164.8	191.6	219.8
			havg (mm)	0.0170	0.0256	0.0298	0.0342
5.08	11	6426.95	P/Ac (N/mm)	20.7	27.3	30.5	33.4
			Q_dot	136.5	206.5	240.1	275.4
			havg (mm)	0.0180	0.0273	0.0317	0.0364
6.35	15	7575.59	P/Ac (N/mm)	21.8	28.4	31.7	34.6
			Q_dot	164.0	248.2	288.7	331.0
			havg (mm)	0.0189	0.0286	0.0332	0.0381
7.62	19	8692.17	P/Ac (N/mm)	23.0	29.7	33.2	36.1
			Q_dot	191.6	289.9	337.2	386.5
			havg (mm)	0.0196	0.0296	0.0344	0.0395
8.89	23	9791.39	P/Ac (N/mm)	23.8	30.7	34.1	37.2
			Q_dot	219.1	331.5	385.7	442.1
			havg (mm)	0.0201	0.0305	0.0354	0.0406
10.16	26	10886.49	P/Ac (N/mm)	24.0	31.1	34.8	37.9
			Q_dot	246.6	373.2	434.2	497.7
			havg (mm)	0.0206	0.0312	0.0362	0.0415
11.43	28	11980.48	P/Ac (N/mm)	24.3	31.7	35.3	38.6
			Q_dot	274.2	414.9	482.7	553.3
			havg (mm)	0.0210	0.0317	0.0369	0.0423
12.7	30	13074.48	P/Ac (N/mm)	24.6	32.0	35.7	39.0

KTC (N/mm^2)	KTE (N/mm)	Axial Depth (mm)
762.52	7.63	3.81
739.63	8.26	5.08
700.78	9.25	6.35
686.62	10.11	7.62
677.11	10.61	8.89
681.82	10.37	10.16
683.66	10.36	11.43
679.98	10.38	12.70

APPENDIX D: Experiment reference index

The experiment index is in reference to table 2-1 in *Section 2-4*. All the raw data can be found in the computer in the DML know as Fadal at extension: \\Fadal\experimental data\Data\Yanjun

Experiment	File Extensions
C1	2007_06_01_Calibration_Slot&Center_VariedFeedrate
C2	2008_08_22_Calibration_CuttingSpeed
C3	2008_03_17_Calibration\3000RPM_HALF_1(2)
C4	2008_07_28_ThinPlate_BEM\2008_08_01_BEM
W1	2008_06_03_WearTest
W2	2008_06_19_FlankWear
TC1	2008_01_07_WearTest
TC2	2008_01_09_WearTest
TC3	2008_01_10_WearTest
TC4	2008_01_25_WearTest
TC5	2008_01_28_WearTest
TC6	2008_02_06_WearTest
TC7	2008_02_28_WearTest_1
TC8	2008_03_10_WearTest
TH1	2008_06_03_WearTest
TH2	2008_08_13_WearTest_HSS
TH3	2008_08_14_WearTest_HSS
TI1	2008_06_09_Insert_WearTest
TI2	2008_07_15_WearTest_Insert
TI3	2008_07_21_WearTest_Insert
TI4	2008_09_05_WearTest_Insert

APPENDIX E: Code for BEM cutters calibration

- Calculate K_{TC} and K_{TE} for ball-end mill cutters.
- It is only valid for the **upmill** calibration on the aluminum **thin plate**.

```
% Use least square fit to calibrate Ktc, Kte and Ptare
% Author: YANJUN CUI Min Xu
% Date  : 2008.12.02
% Output:

function CalibrateBEMKtcKteWithJerardModel1
Close all;
clear;

% user needs to modify these variables corresponding to the test
D = 0.75;          % tool diameter
Nt = 2;       % number of teeth
bSIUnits = 1;  % use SI units? 1 --- Yes, 0 --- No
sWorkPieceMaterial = '6061';   % work piece material
sToolType = 'HSS FEM';  % tool type
R = D/2;
% load motor efficiency data
load Efficiency_RPM
Dimensions = size( Efficiency_RPM );
iNum = Dimensions(1);

% read the data file, user need to modify the data file name to what they
% are trying to use
[fileName,PathName,FilterIndex] = uigetfile('*.lst', 'Please choose a move info list file to calibrate with');
if( fileName == 0 )
  return;
end;
fname = sprintf('%s%s', PathName, fileName);

DataPoints = textread(fname, '',  'headerlines', 1); % 21 columns of data, skip the first headerline
Dimensions = size(DataPoints);
NumToStart = 1;  % start data index
NumToEnd = Dimensions(1); % end data index
iNumPointsUsed = NumToEnd - NumToStart + 1;

AD = DataPoints(NumToStart:NumToEnd,11);    % axial depth
Feed = DataPoints(NumToStart:NumToEnd,14);  % feed rate, unit: inch/min
w = DataPoints(NumToStart:NumToEnd,7);  % spindle speed, unit: rpm
Pe = DataPoints(NumToStart:NumToEnd,20); % Measured power, unit: HP


for i = 1:(NumToEnd-NumToStart+1)
% get motor efficiency based on spindle speed
for iCount = iNum:-1:1
  if( w(i) > Efficiency_RPM(iCount, 2) )
    n(i) = Efficiency_RPM(iCount, 1);  % motor efficiency
    break;
  end;
```

```
end;

if( w(i) < Efficiency_RPM(1, 2) )
   n(i) = Efficiency_RPM(1, 1);   % motor efficiency
end;
P_Msd(i, 1) = Pe(i, 1)*6600*n(i);  % cutting power, unit: inch.lbf/sec
end;

% Zmin ---- Z minimal value (start from the too tip), unit: in
% Zmax ---- Z maximal value (start from the too tip), unit: in
% For the ball part, Z value is between 0 and D/2
% Valid Y value should be between -D/2 and D/2
% e.g. for a center cut of radial depth of D/4, Ymin is -D/8, Ymax is D/8
%        for a slot cut, Ymin is -D/2, Ymax is D/2
%        for up mill cut, Ymax is D/2
%        for down mill cut, Ymin is -D/2

prompt = {'slot - 0; upmill - 1; downmill - 2; center - 3:', 'Enter Workpiece Thickness:'};
dlg_title = 'Input for BEM Cutting Parameters';
num_lines = 1;
def = {'1', '0.125'};
answer = inputdlg(prompt,dlg_title,num_lines,def);
Cut_type  = str2num(answer{1});
     H  = str2num(answer{2}); %Workpiece Thickness

if ( H > R)
   prompt = {'Enter Radial Depth:'};
   dlg_title = 'Input for BEM Cutting Parameters';
   num_lines = 1;
   def = {'0.2'};
   answer = inputdlg(prompt,dlg_title,num_lines,def);
   RD = str2num(answer{1}); %Radial depth
else
   prompt = {'Enter Radial Depth:', 'Enter z position'};
   dlg_title = 'Input for BEM Cutting Parameters';
   num_lines = 1;
   def = {'0.2','0.15'};
   answer = inputdlg(prompt,dlg_title,num_lines,def);
   RD = str2num(answer{1}); %Radial depth
   AD = str2num(answer{2}); %Radial depth
end
AD = mean(AD);

% only available for upmill cuts
 if (AD < R)
    [CA, MR] =BEMCuttingGeometry(R, RD, AD,H );
 else
   if (AD<R+H)
      AD = R;
      [CA, MR] =BEMCuttingGeometry(R, RD, AD,H );
      CA = CA + R*acos((R-RD)/R)*(AD-R);
      MR = MR + RD*(AD-R);
   else
      CA = R*acos((R-RD)/R)*H;
      MR = RD*H;
```

```
    end
end

MRR = MR.*Feed;
Ac_dot = CA.*ones(Dimensions,1)*Nt.*w/60;
Q_dot  = MR.*ones(Dimensions,1).*Feed/60;

% tao = 60./w;
% Q_dot = MRR/60 ;              % MRR, unit: in^3/sec
% Ac_dot = CA*Nt./tao;            % Average Contact Area of one revolution, unit: in^2/sec
A=[Q_dot Ac_dot];
B=A'*A;
Kt=inv(B)*A'*P_Msd;
%Kt=inv(A'*A)*A'*P_Msd;
Ktc = Kt(1);
Kte = Kt(2);
P_Est = Ktc*Q_dot + Kte*Ac_dot;

% calculate deviation
Dev_P = P_Est - P_Msd;
Err_P = Dev_P./P_Msd*100;
Abs_Err_P = abs( Err_P );
Max_Err_P = max(Abs_Err_P);
Stdev_P = std(Dev_P);

figure(1);
sTitle = sprintf('Calibration results of %.4f" tool, %d flutes, %s, with %s, w=%drpm, Ktc=%.1flbf/in^2,
Kte=%.2flbf/in', D, Nt, sToolType, sWorkPieceMaterial, w(1), Ktc, Kte);

% use SI units
if( bSIUnits == 1)
    P_Msd = P_Msd * 0.113;
    P_Est = P_Est * 0.113;
    Dev_P = Dev_P * 0.113;
    Stdev_P = Stdev_P * 0.113;
end;

subplot(2,2,1);
plot(P_Msd,'-*');
hold on;
plot(P_Est, '-o');
if( bSIUnits == 1)
    ylabel('Power (W)');
else
    ylabel('Power (in.lbf/sec)');
end;
legend('Actual Power', 'Estimated Power');
title( sTitle, 'fontweight', 'bold', 'fontsize', 12);
subplot(2,2,2);
plot(Dev_P,'-o');
if( bSIUnits == 1)
    ylabel('Dev\_P (W)');
    string = sprintf('Standard deviation = %.1f W', Stdev_P);
else
    ylabel('Dev\_P (in.lbf/sec)');
```

```
  string = sprintf('Standard deviation = %.2f in.lbf/sec', Stdev_P);
end;
text(2, -0.02, string);
subplot(2,2,3);
plot(Err_P,'-o');
%axis([1,NumToEnd,0,max(Err_P)]);
ylabel('Err\_P(%)');
subplot(2,2,4);
maxx=ceil(max(P_Msd)/0.5)/2;
minx=floor(min(P_Msd)/0.5)/2;
plot(P_Msd, P_Est,'*', P_Msd, P_Msd, '-');
grid on
if( bSIUnits == 1)
  xlabel('Actual Power (W)');
  ylabel('Estimated Power (W)');
else
  xlabel('Actual Power (in.lbf/sec)');
  ylabel('Estimated Power (in.lbf/sec)');
end;

% set the page size and paper orientation for printing
set(gcf, 'PaperType', 'usletter');
set(gcf, 'PaperUnits', 'inches');
set(gcf, 'PaperOrientation', 'Landscape');
set(gcf, 'PaperPosition', [.25 .25 20 12]);

% save the model paramters for later use
outp = fopen('FEMModelParameters.dat', 'at');
fprintf(outp, '%.4f\t%d\t%d\t%.4f\t%.1f\t%.2f\t%s\n', D, Nt, max(w), max(AD), Ktc, Kte,fname);
fclose(outp);

outp = fopen('BEMAc_dot.dat', 'at');
fprintf(outp, '%.4f\t\t%s\n', mean(Ac_dot),fname);
fclose(outp);

outp = fopen('BEMQ_dot.dat', 'at');
fprintf(outp, '%.4f\t\n%s\n', Q_dot, fname);
fclose(outp);
% end of file

function [CA, MR] =BEMCuttingGeometry(R, RD, AD,H )
  r1 = (R^2-(R-AD+H)^2)^0.5;
  r2 = (R^2-(R-AD)^2)^0.5;

  theta1 = acos((R-AD+H)/R);
  theta2 = acos((R-AD)/R);

  s = R*(theta2 - theta1);
  Ravg = (r1 + r2)/2;
  beta = acos((Ravg - RD)/Ravg);
  CA = s*Ravg*beta;
  MR = RD*H;
```

APPENDIX F: Code for Smart Tool vibration Data Analysis

```
function [spec,freqs]=VibrationAnalisis()


close all;
clear all;

Fs = 20000;             % Sampling frequency

[fileName,PathName,FilterIndex] = uigetfile('*.mat', 'Please choose vibration data with');
if( fileName == 0 )
   return;
end;
fname = sprintf('%s%s', PathName, fileName);
OriginalData = load (fname);
OriginalData = OriginalData.y;
sTitle = sprintf('%s',fname);

for i = 1:4

figure('position',[10 50 1100 800]);
plot(OriginalData);
title( sTitle, 'fontweight', 'bold', 'fontsize', 12);

[x] = ginput(2);


close all;

data = OriginalData(x(1):x(2));


L = length(data);    % Length of your signal in # samples (ex; 10 seconds at 20kHz)
%
NFFT = 2^nextpow2(L); %a high resolution on frequencies, minimum is 2^nextpow2(L)
data = double(data) .* hamming(L);
Y = fft(data,NFFT)/L;
freqs = Fs/2*linspace(0,1,NFFT/2);

% spec=2*abs(Y(1:NFFT/2));
% Plot single-sided amplitude spectrum.
% semilogy(freqs,spec)
% title('Single-Sided Amplitude Spectrum')
% xlabel('Frequency (Hz)')
% ylabel('|Y(f)|')

%the signal power spectrum amplitude
[P_data,F_data] = pwelch(data,2^12,2^11,2^12,20000);

%root mean square of vibration data
data_rms = sqrt(mean(data.^2));
```

```
%%%%%%%%%%%%%%%%%%%%%%%%%%%%%%%%%%%%%%%%%%%%%%%%%%%%%%%
%
figure;
sTitle = sprintf('Root Mean Square of Vibration Data - %.4f',data_rms);

% Plot single-sided amplitude spectrum.
% subplot(2,1,1);

plot(freqs,2*abs(Y(1:NFFT/2))) ;
title( sTitle, 'fontweight', 'bold', 'fontsize', 12);
xlabel('Frequency (Hz)');
ylabel('|Y(f)|');
axis([0 500 0 0.025]);
set(gca,'YGrid','on')

% subplot(2,1,2);
% plot(F_data,P_data,'r');
% xlabel('Frequency (Hz)');
% ylabel('Signal Power: |Y(f)|^2');
% % axis([0 500 0 0.00005]);
% set(gca,'YGrid','on')

% save the model paramters for later use
outp = fopen('RMSVibrationData.dat', 'at');
if (i==1)
   fprintf(outp, '%s\n', fname);
end
fprintf(outp, '%.4f\n', data_rms);
fclose(outp);

i = i+1;
% close all;
end
sprintf(fname)
```